Theses and Dissertations

2017

Method for the Prediction of the Energy Harvested by Vibrational Piezoelectric Devices Applied to Civil Infrastructure

Julia Tesser Tomasi
Lehigh University

Follow this and additional works at: http://preserve.lehigh.edu/etd

⚙ Part of the Structural Engineering Commons

METHOD FOR THE PREDICTION OF THE ENERGY HARVESTED BY

VIBRATIONAL PIEZOELECTRIC DEVICES APPLIED TO CIVIL INFRASTRUCTURE

By

Julia Tesser Tomasi

A Thesis

Presented to the Graduate and Research Committee

of Lehigh University

in Candidacy for the Degree of

Master of Science

in

Structural Engineering

Lehigh University

December 2016

This thesis is accepted and approved in partial fulfillment of the requirements for the Master of Science.

_____

Date

_____

Thesis Advisor: Dr. Paolo Bocchini

_____

Chairperson of Department: Dr. Panos Diplas

iii

Acknowledgments

I would the like to thank CAPES, for the scholarship through the Ciencias sem Fronteiras program, also known as Brazilian Scientific Mobility Program.

I would like to thank the adviser of this work, Dr. Paolo Bocchini, for his guidance, professionalism, objectivity and patience through it.

I would like to thank some of the professionals I met in the United States, being those Professors, Physicians or Structural Engineers, as Dr. Richard Decker, Dr. Cristie Cunningham, Abby Sheneman, Tom and Marguerite Pinto.

I would like to thank my fellow colleagues in Dr. Bocchini`s research group at Lehigh University, especially Aman, Vasileios and Amirali, for always being available to help.

I would like to thank the amazing friends I met in Lehigh during these years, especially Aniket, Patricia, Radja, Sila, Tim and Fernando, without whom I would not have made it all the way to the conclusion of this work.

I would like to thank also my friends in Brazil, especially Leo, Joyce, Zaiden and Marina, who were able to bring brightness into this experience even from far.

I would like to thank my grandparents and family for all the prayers and support.

And always and forever, I would like to thank my dear parents, Isabel and Giancarlo, for living with the distance during these two years and supporting me in every single moment and every step on the way.

Table of contents

vi

viii

List of tables

List of figures

xi

xii

xiv

xv

Abstract

Piezoelectric devices have had specific applications in the energy harvesting industry for several years. The simplicity of these generators is making them attractive for researchers in a wide range of engineering applications. The goal of this work is to develop a rigorous procedure to quantify the electrical energy generation potential from piezoelectric devices, considering the coupled problem involving random wind loads, structural vibration, electro-mechanics and energy collection. With that in mind, a finite element model of a piezoelectric device is developed to determine the energy that can be harvested from the vibration in a sample bridge structure. The load considered to act on the bridge and, consequently, on the device is the wind, modeled by the Kaimal Spectrum. The analysis is performed in a probabilistic fashion, using Monte Carlo simulation and considering a large set of wind load samples generated by spectral representation. The harvester device is a cantilever beam constituted of a rubber core with piezoelectric layers, at the top and bottom, which is modeled using the Finite Element Method (FEM). The output obtained from the finite element model is the electrical potential. The beam is attached to a one-loop simple electrical circuit where the total energy generated and supplied to a resistor is computed. The results can be used to obtain the variation of average voltage and power supplied to an electric system and thus, for a given application, help to design the energy management system. The research on the theoretical FE model provides a method for an efficient and practical harvesting from bridges or other structures exposed to wind loads by a piezoelectric harvester device fixed on it.

1 Introduction

Current energy resources are not infinite. With the ever growing increase in population, demand of energy is also increasing continuously. Non-renewable sources are the most used form of energy source currently, but renewable sources are starting to become applicable, being sustainable and abundant. With this idea in mind, several works have been developed in the last few years trying to find new projects, new approaches and new solutions to supply the expanding energy demand. From all ambient energy sources, the most common are light, wind, thermal and vibration. Vibration energy, which is clean, ubiquitous and renewable, has attracted worldwide researchers in disciplines ranging from mechanical, civil, material and electrical to aeronautical and it has been, since its first emergence, one of the foci for energy harvesting, namely, vibration energy harvesting [4]. This thesis can be identified as one of these several works, using a structural engineering background, to analyze an energy harvester device.

The term *energy harvester* is defined in [1] as the generator device undergoing vibrations due to a specific form of excitation. The functioning of the harvester element consists of a beam located on a vibrating host structure, where the strain induced by the dynamic load results in an alternating voltage output across their electrodes. This area of research has intrigued both academia and industry and, within this field, one of the most studied harvesting processes is the use of the piezoelectric effect to convert ambient vibrations into useful electrical energy.

This work is motivated by the personal interest and concern about the future in energy demand of the world and, especially, on supplying it in a sustainable way which allows new generations to maintain the same life quality that (some people) of this generation are pleased

2

to enjoy. As pointed out in [2], in recent decades, a new and truly global impact of humankind`s energy consumption has overshadowed the long-standing and still significant consequences associated with traditional pollution, resource extraction, and energy-enabled development. That impact is the global climate change, brought about largely by the emissions from fossil fuel combustion. Climate change is a problem that knows no national or even continental boundaries. It will affect all of humanity – although not all equally. It will not have the civilization-ending impact of an all-out nuclear war or major asteroid hit, but climate change will greatly stress an already overcrowded, divided and combative world.

Wolfson [2] brings up also the fact that it makes little sense to become enthusiastic about one specific renewable energy source if it cannot make a quantitatively significant contribution to humankind's total energy supply, with an important analysis of the assessment of environmental impacts too. Hence, the initial idea for this work stemmed from a manuscript by Lu et al. [3], which discusses the idea of harvesting energy with a micro piezoelectric power generator, from the air load in a ventilation duct. The original contribution consists in transitioning this idea to a much bigger scale. The device evaluated in [3] is shown in Figure 1. Additional references for the use of piezoelectric elements for energy harvesting can be found in [6], [8], [9], among many others, in which different approaches and areas of engineering are investigated.
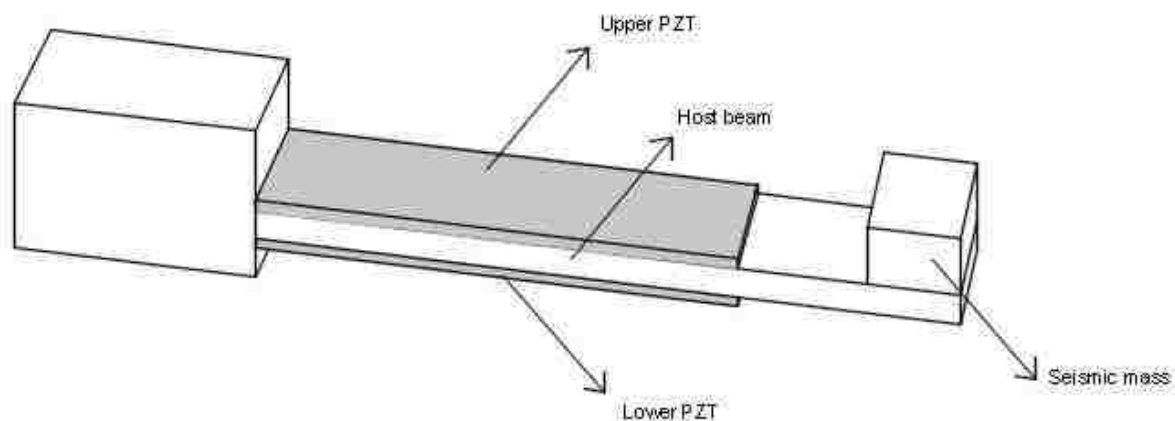
Figure 1: Device evaluated in reference paper. (Adapted from [3])

It is important to mention also the connection of this thesis with other undergoing research at the Advanced Technology for Large Structural Systems (ATLSS) at Lehigh University, in terms of possible applications to resilience of systems. In fact, generating energy locally on the bridge, in case of power outages due to problems in a city power-grid, would keep the systems on the bridge functional (e.g., traffic lights, lights, sensors, etc), as well as being a possible preparedness strategy to be considered for the enhanced disaster response [5].

The aim of this thesis is to develop a rigorous procedure to quantify the electrical energy generation potential from piezoelectric devices, considering the coupled problem involving random wind loads, structural vibrations, electro-mechanics and energy collection. Here a method is studied to apply the approach of civil engineering in the energy harvesting scenario. A wind load is modeled using Kaimal Spectrum and simulated generating samples, using Monte Carlo Simulation (MCS), which brings a probabilistic perspective into the study. This load is considered to be applied to a device connected to a cantilever beam, modeled using the Finite Element software Abaqus, which allows the consideration of both mechanical and piezoelectric

4

properties in the problem. The electrical potential output is extracted from the software and applied to a simple one-loop circuit for quantification. A general schematic summarizing the work is presented in Figure 2.
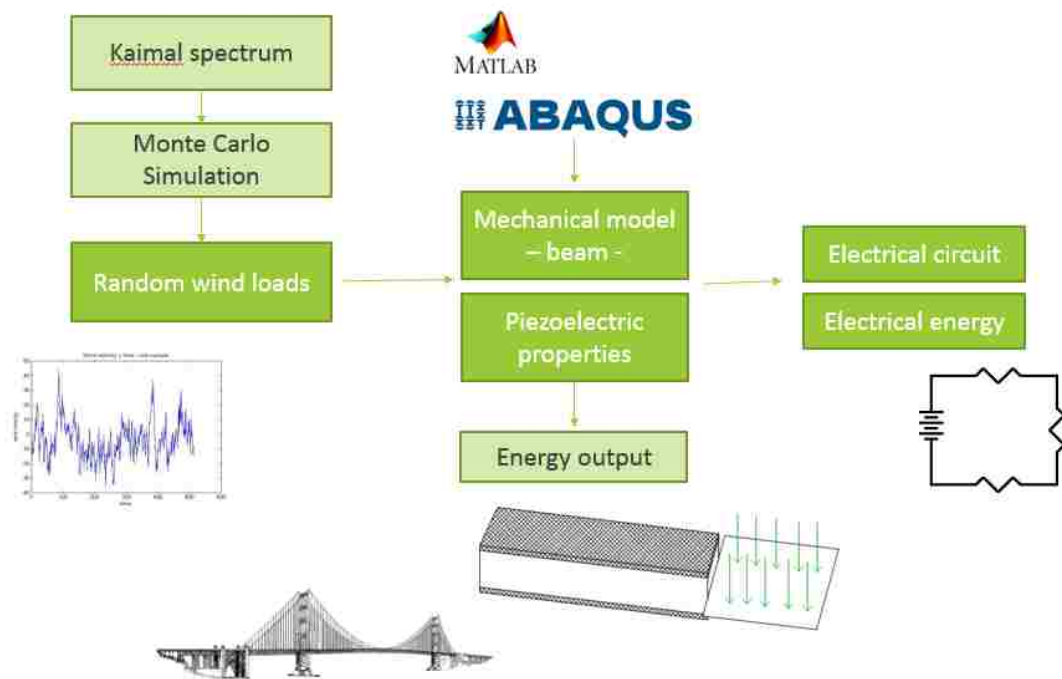
Figure 2: General pictorial representation of the thesis outline. The first part summarizes the Kaimal Spectrum representation and sample generation with MCS combined for the random wind loads model, where a sample is graphically shown; the second part illustrates the beam and piezoelectric device working together, with the use of Matlab and Abaqus software packages; at last, the device is connected to an circuit where the electrical energy output is quantified analytically.

Following Figure 2, the general representation of the harvester device is displayed in Figure 3, in order to provide a general idea of the configuration and dimensions that are being considered.

5
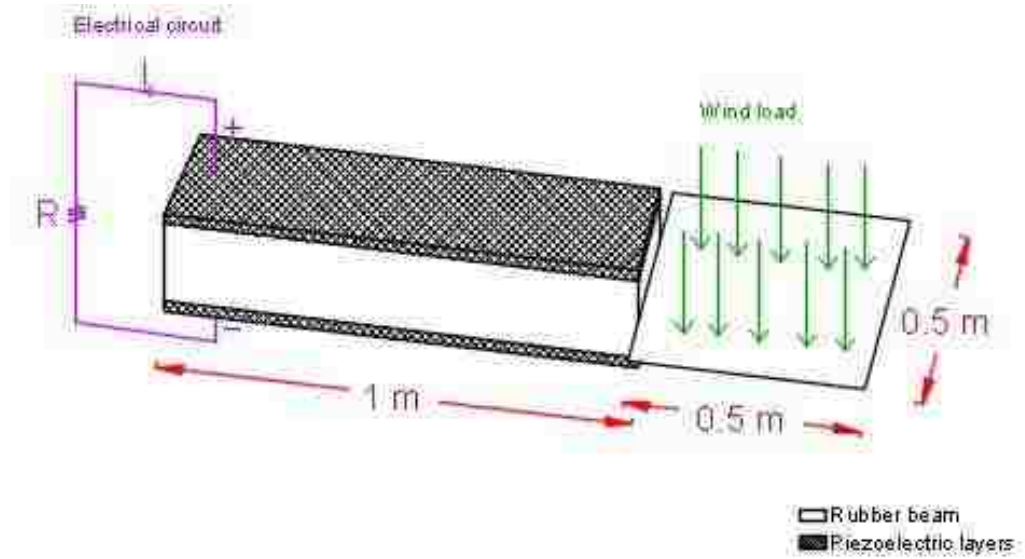
Figure 3: Harvester device: Rubber beam with piezoelectric layers and load receptor plate

The thesis is organized as follows: Chapter 2 describes the load receptor device. Chapter 3 details the wind load. Chapter 4 outlines the theory and definitions about piezoelectric devices. Chapter 5 discusses the study on the use of piezoelectric elements in Abaqus. Chapter 6 shows the FEM analysis of the harvester beam, for static and dynamic load cases, both with Abaqus alone and with Abaqus and Matlab combined. Chapter 7 shows the electrical circuit used for quantification of the data. Finally, the conclusion and further work possibilities are elucidated.

6

2   Description of the device

2.1   Concept

A random load representing the wind is considered to be applied to a load receptor mechanical device (plate), which is connected to a structure composed of a rubber beam and two piezoelectric layers, one on the top and one on the bottom of the rubber component. Figure 4 shows the geometry of the device. Several designs and properties were considered possible for this schematic structure and, through hand calculations, the dimensions presented here were chosen.
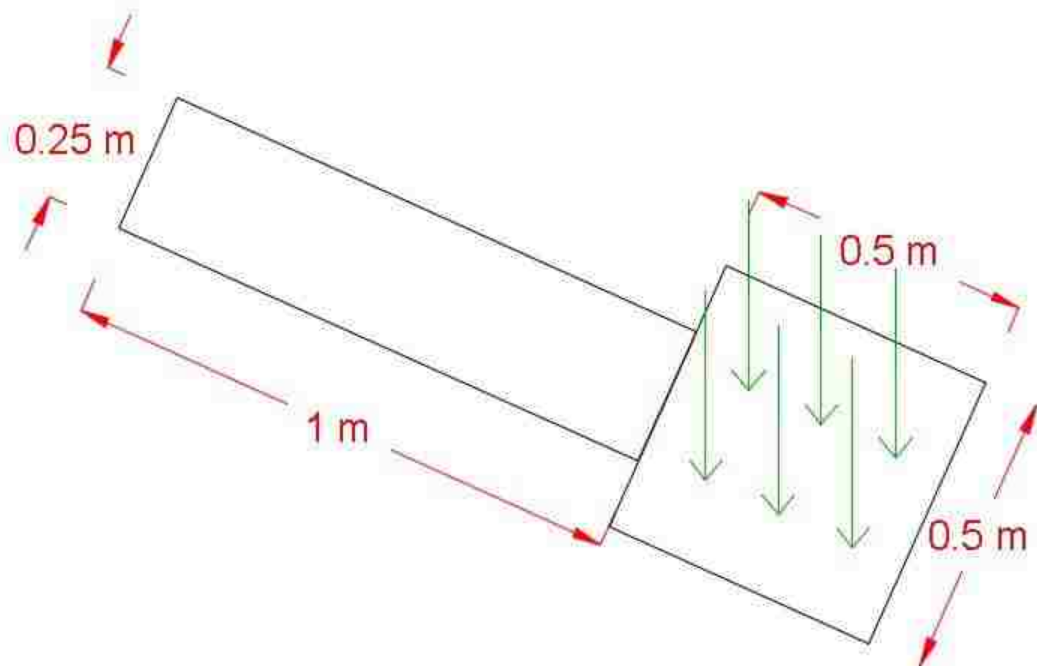
Figure 4: Sketch of the mechanical device to receive the wind load – top view

7

Based on some initial hand calculations, which were verified later in the process, the considered dynamic wind load showed an approximated mean value of pressure of 92.41 Pa, which is the value applied as an equivalent static load for the preliminary design. This value is the mean value of all the probabilistic wind loads, stored in matrix F_k, considering only their absolute values and it is obtained using Equation 5, exposed and detailed in Chapter 3.

Taking that into consideration, the dimension of the plate had to be chosen in order for the beam structure to present a significant value for tip displacement, but they could not be too large, in a way that the plate would be disproportionate to the beam.

The chosen plate is 50 cm by 50 cm, which gives the results showed in Table 1:

Table 1: Characterization of static load and moment applied to the beam device

	Description	Calculation	Value	Unit
Q_w	Pressure	$-$	92.41	Pa
A	Area of plate	$0.5 \; x \; 0.5$	0.25	m^2
P	Force on the plate	$0.25 \; x \; 92.41$	23.10	N
d	Distance of P to beam	$-$	0.25	m
M	Moment caused by the plate	$23.10 \; x \; 0.25$	5.78	Nm

8

2.2   Representation

The load receptor device itself is not modeled in this work, and it can be considered a part of design refinement, which is the goal for a future phase of the work. For the scope of this thesis, internal stresses in the load receptor device (i.e., the plate) are not deemed important. Therefore, for all subsequent analyses the plate is not modeled, and only the force and moment that it applies to the beam are considered, as shown in Figure 5:
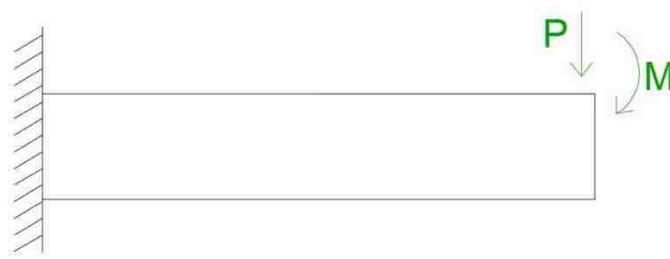
Figure 5: Sketch representing the analyzed beam

Considering Figure 5 as the structural model to be analyzed, the tip displacement can easily be calculated, with the following equations:

$$U = \frac{PL^3}{3EI} \tag{1}$$

for displacement due to the concentrated force, and

$$U = \frac{ML^3}{2EI} \tag{2}$$

for displacement due to the moment.

9

The values inputted in these equations, such as material properties and dimensions of the beam along with the results of Equations 1 and 2 are presented in Table 2:

Table 2: Displacement due to the load P and moment M acting on the rubber beam

	Description	Calculation	Value	Unit
P	Force on the plate	$0.25 \; x \; 92.41$	23.10	N
M	Moment caused by the plate	$23.10 \; x \; 0.25$	5.78	Nm
L	Length of the beam	$-$	1	m
I	Moment of inertia	$-$	$7.03 \; x \; 10^{-5}$	m^4
E	Young modulus	$-$	50	MPa
U	Total displacement	$Eq \; 1 + Eq \; 2$	3.013	mm

Hence the value found for tip displacement is U= 3.013 mm, which is an acceptable value considering the dimensions and materials properties of the beam.

With these results in mind, all the successive calculations, models and analysis in this work follow the simplified model in Figure 5.

10

3   Wind load study

3.1   Introduction on random vibrations

Structures can be subjected to loads that are treated as static or dynamic. They are called "static loads" if they exert a constant (generalized) force over time. Dynamic loads are loads in which the duration of application and the moment when they occur are relevant and affect the reaction of the structure, because they exert varying amounts of force upon the structure that is subject to them.

Dynamic loads can have determined characteristics, where the future inputs - and therefore future behavior and reaction of the structure - can be precisely predicted, such as harmonic, triangular shape or impulse loads. However, dynamic loads can also present themselves as having no pre-determined characteristics and yield motions which are non-deterministic. This last class of dynamic loads are described as random processes.

Random processes can be formally defined as a parameterized family of random variables, with the parameters belonging to an indexing set, or as an ensemble of functions that can be characterized statically. A random load, as all dynamic loads, can be described with graphs that show the relation between time and input force, as showed in Figure 6. The difference here from a simple dynamic load is in the case of random loads, Figure 6 would represent only one of the infinite possible samples. In Figure 6, the graph represents the variation of load with time for a specific sample. Equivalently, in Figure 7, the wind velocity is shown to variate for different random samples, for a given fixed time.

11
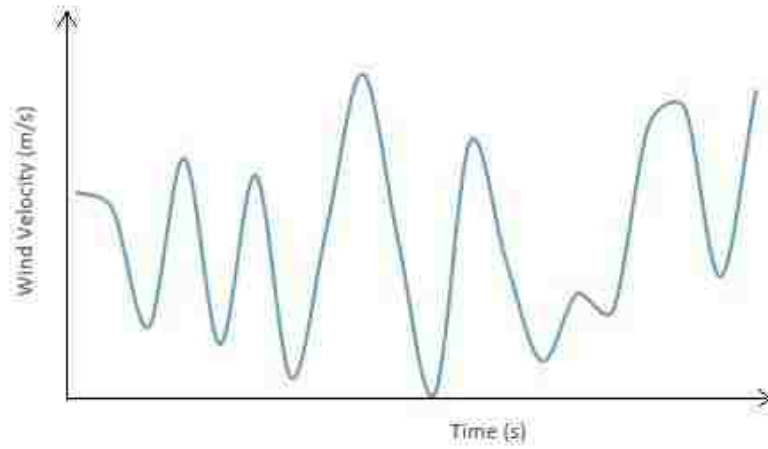
Figure 6: Representation of dynamic load variating with time – one of infinite random samples
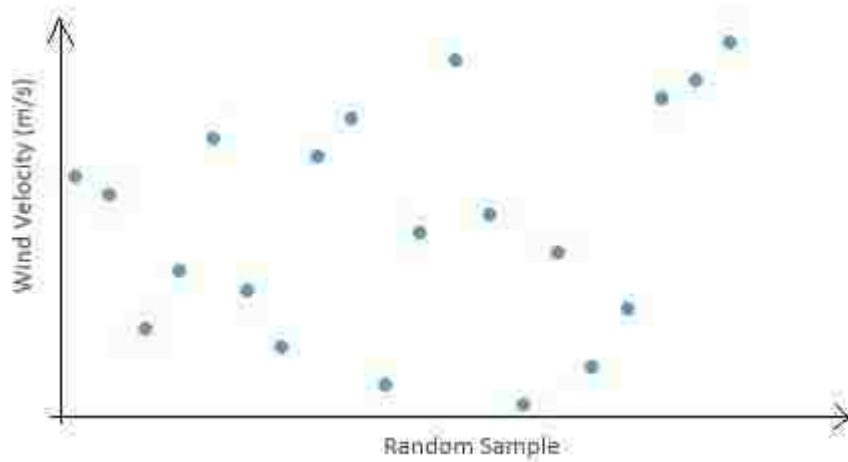
Figure 7: Representation of several samples of wind load – for one fixed time

As examples of random loads in the civil engineering field, there are earthquake loads and wind loads, among many others. In this work the focus is on wind loads, which is the most popular and studied example of a random vibration.

12

3.2 Introduction on wind loads

3.2.1 Spectral representation

There are several different spectra that can characterize different phenomena of random load, such as Idealized White Noise, Band-limited White Noise, Kanai-Tajimi Spectrum and Kaimal Spectrum. For different types of loads, each spectrum has been studied and proved to be a better or worse fit. The Kaimal Spectrum is a spectrum that fits well for wind loads and therefore is used in this project.

3.2.2 Kaimal Spectrum

The load to be worked with, as mentioned previously, is wind load and it is modeled by the Kaimal Spectrum, given by Equation 3:

$$S_{xx} = \frac{1}{2} * \left(\frac{200}{2\pi}\right) * (u_*)^2 * \frac{z1}{u(z)} * \frac{1}{[1+50*\left(\frac{|w|*z1}{2\pi*u(z)}\right)]^{5/3}} \qquad (3)$$

Where,

u_* = shear velocity of the flow, considered 1.76 m/s,

$z1$ = height from the ground, in m

w = frequency, in Hz

13

The logarithmic law of fluid dynamics is used in calculations to determine $u(z)$, which can be defined as the mean wind speed at height $z1$.

$$u(z) = \frac{1}{K} * ln\left(\frac{z1}{z_0}\right) \qquad\qquad (4)$$

In equation 4, K is Von Karman's constant equal to 0.4 and z_0 is the surface roughness assumed as 0.001266 m. In these calculations, the wind profile is defined at 35 m as $u(z) = 45\ m/s$.

The values used in equations 3 and 4 are calibrated as suggested in [11], pages 299-304.

Using Equation 3 and 4, with the values specified here, the Kaimal Spectrum is plotted, as shown in Figure 8.
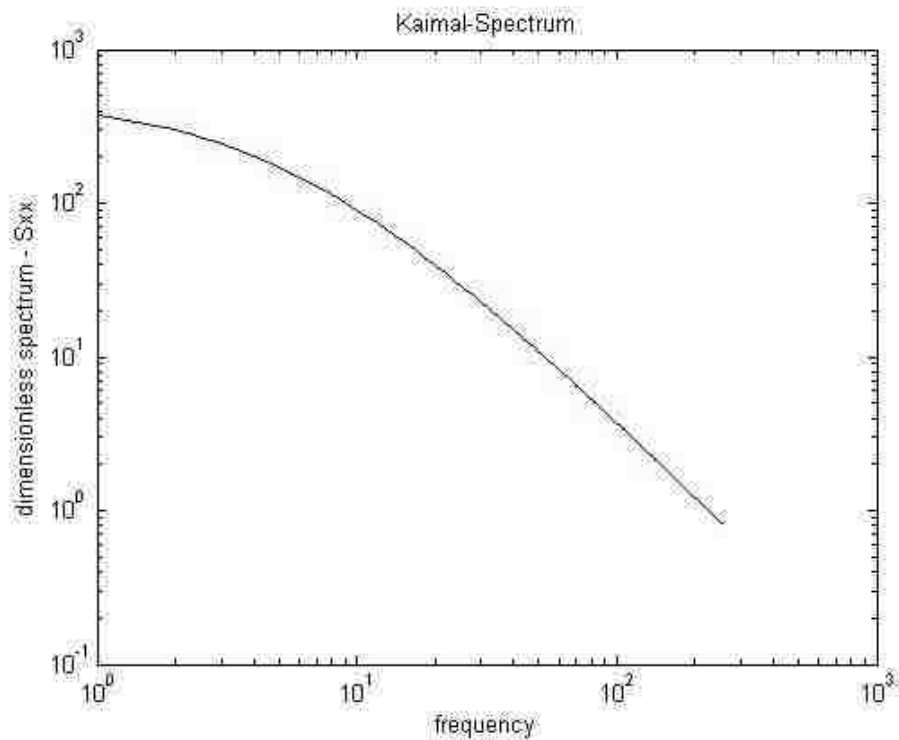
Figure 8: Kaimal-Spectrum wind representation (Sxx)

14

3.3 Monte-Carlo simulation

3.3.1 Concept

Considering that the wind load is modeled as a random process, then also the structural response is probabilistic. Different input samples following the specified probabilistic characteristics are obtained using simulations. The simulation technique used in this work is Monte Carlo Simulation (MCS).

MCS is an approach that aims at assessing the probability of a certain event through the repetition of a large number (in theory, it would be an infinite number) of deterministic experiments. Here, the structure has deterministic properties and the load has probabilistic properties.

The structural analysis happens in such a way that the deterministic structure is kept the same, and each time the different probabilistic wind load is applied and a different output is obtained. In this work, 590 samples of wind velocity are simulated, using MCS, each of them describing the wind at 513 time steps.

3.3.2 Simulation formula

The initial input S_{xx}, from Equation 3, is used in Equation 5 to generate simulations of random samples that represent the wind velocity obtained from the Kaimal Spectrum.

$$f_k(t) = \sqrt{2} * \sum_{j=0}^{N-1} \sqrt{2 * S_{xx}(w_j) * \Delta w} * cos(w_j * t + \varphi_{kj}) \qquad (5)$$

The parameters used in the simulation formula are detailed as follows:

15

$f_k(t)$ = each sample wind velocity, in m/s, in the matrix of simulated inputs

N = 256 = the number of points used for discretization of the frequency domain Spectral Density Function (SDF)

j = index for frequency variation, going from 0 to N-1

t = time instance, going from 0 to 256 seconds, with increments given by Δt.

$\Delta t = 0.5$ = time increment used in the equation

The time increment (Δt) is determined by Equation 6, which gives a maximum threshold for it to prevent aliasing.

$$\Delta t < \frac{2\pi}{2 * w_u} \qquad (6)$$

In Equation 6, $w_u = 6.28$ rad/s is the upper cutoff frequency chosen by engineering judgment where spectral density is assumed to be zero, which leads the time increment to be selected as 0.5 seconds.

$$\Delta t < \frac{2\pi}{2 * 6.28}$$

$$\Delta t < 0.5\,002389 \qquad (7)$$

k = index for time variation, going from 0 to 513 (256/0.5 =512)

φ_{kj} = independent random phase angles in [0, 2π]

To find the values for φ_{kj} , the Matlab function "rand" is adopted and random uniformly distributed numbers between 0 and 1 are generated, with a sample size chosen by the user. This

16

sample is multiplied by 2π and random numbers between $(0, 2\pi)$ are generated, which represent the distribution for phase angles φ in the simulation formula. A sample of 590 lines and 256 columns is generated for this input.

Δw = increment on the frequency values

$$\Delta w = \frac{w_u}{N} = 0.0244 \qquad (8)$$

w_j = wind frequency, which has its samples generated by $w_j = \Delta w * j$

$S_{xx}(w_j)$ = samples generated from Equation 3 using different values for w

With the use of Equation 5 by variating the parameters explained above, using MCS, a matrix F_k is obtained, containing the simulated wind time histories. Because of the nature of this type of approach, probabilistic with a very large number of simulations, the software Matlab is adopted.

In the following figure, Figure 9, the plot of 513 time-steps $f_k(t)$ values is shown as the load is considered to be applied at every increment of 0.5 seconds in the considered interval of 256 seconds for illustration. Therefore the dynamic wind load is considered to be applied on the beam for 4.27 minutes and the response is analyzed also for this duration. Five hundred ninety similar graphs to Figure 9 can be generated with the input values.

17
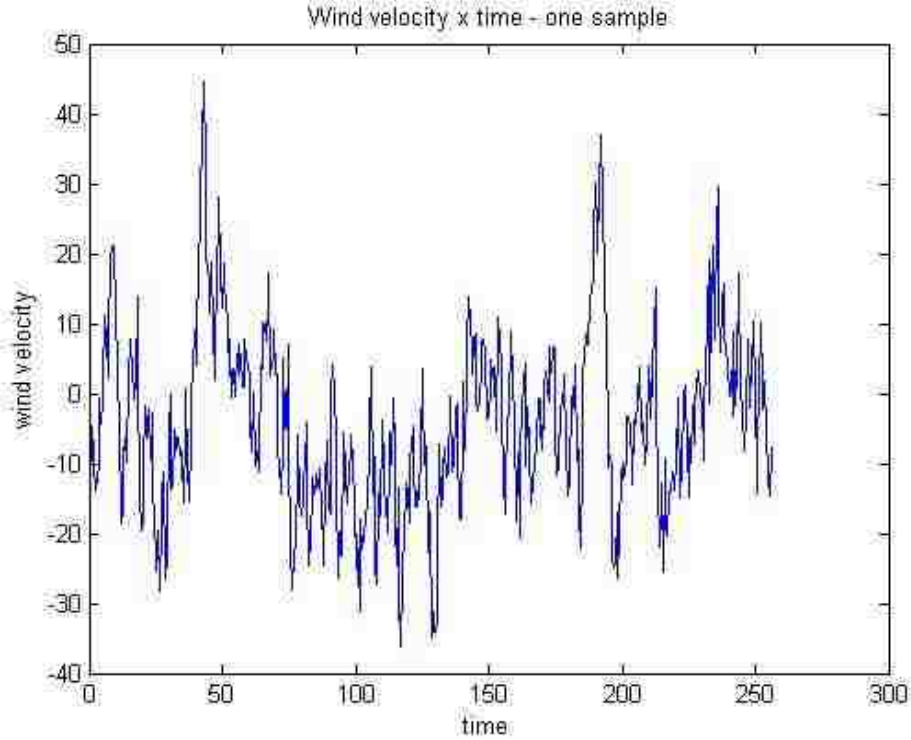
Figure 9: Example of wind velocity $f_k(t)$ fluctuation with time t, for 256 seconds, considering Kaimal Spectrum modeling

3.4   Wind load values

As previously mentioned, the values in matrix F_k using the Kaimal Spectrum refer to wind load velocities. The values obtained in $f_k(t)$ and in Figure 9 are values of wind velocity, in m/s. As this wind data is necessary for a structural analysis, the input given should be a load, not a velocity. Using Equation 9, from [20], this value can be determined:

$$Qs(t) = 0.613 * Kz * Kzt * Kd * f_k(t) * |f_k(t)| * I \qquad (9)$$

18

Where:

$Qs(t)$ = wind pressure load, in Pa (N/m^2),

$Kz = 0.85$ = velocity pressure coefficcient

$Kzt = 1$

$Kd = 1$ = directionality factor

$I = 1$ = importance factor

For each point value of $f_k(t)$ in Figure 9, a load value $Qs(t)$ is obtained. The following Figure 10 shows the values for load from the same sample used for Figure 9, being applied to Equation 9.
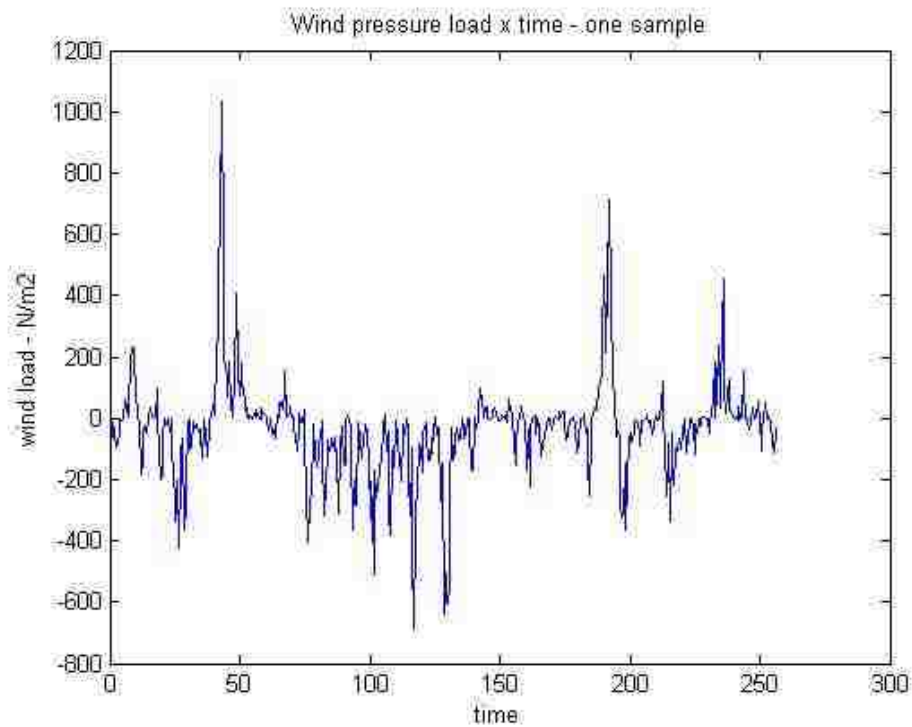
Figure 10: Example of pressure load ($Q_S(t)$) fluctuation with time t, for 256 seconds, considering Kaimal Spectrum

19

As a final step to obtain the wind load, the value obtained in Equation 9 is transformed into a concentrated load. As described in Chapter 2, this load is applied in a device of area $A = 0.25m^2$, and thus the concentrated load is used for the finite element analysis, using Equation 10.

$$f(t) = Q_s(t) * A \qquad (10)$$

The value $f(t)$ is obtained in Newtons (N) and is shown in Figure 11, considering Figure 10 as the input.
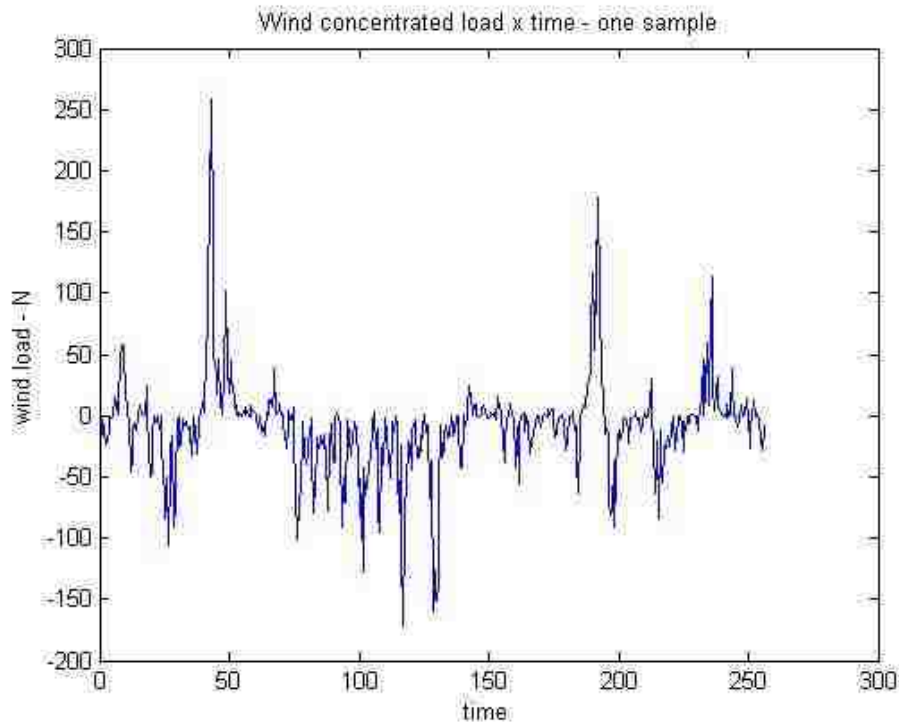
Figure 11: Example of concentrated load ($f(t)$) fluctuation with time t, for 256 seconds, considering Kaimal Spectrum

20

With this graph in mind, it is easier to comprehend in which direction the analysis is going. With the total of 590 wind loads, each of them will be inputted in Abaqus for analysis and the corresponding output values could be obtained and post-processed. This process clearly has to be automated, so the software package Matlab is adopted.

4 Piezoelectric devices

4.1 Piezoelectric theory

Transducers are devices that convert one form of energy to another. In this work, the transducers of interest are the ones which convert mechanical energy to electrical energy, by generating an electrical voltage. According to [1], the three basic vibration-to-energy conversion mechanisms are the electromagnetic, electrostatic and piezoelectric transducers. With a simple research and a comparison of publications about these three devices, it is clear that the piezoelectric transduction has received the greatest attention. The advantage is due to the power density versus voltage that is bigger in piezoelectric devices than in electromagnetic and electrostatic; the voltage obtained is usually in useable values and the devices can be fabricated both at a micro-scale and macro-scale due to the well-established thick-film and thin-film manufacturing techniques. However, piezoelectric elements are still elements which generate low voltage. The actual value will also depend on the design of the device. The optimization of such design is not covered in this thesis, but suggested as further work.

Piezoelectric elements are found in two formats: piezoceramic and single crystals. The piezoelectric energy harvester chosen to be examined throughout this thesis is of the piezoceramic type in the form of cantilevered beam with two piezoceramic layers – also addressed as bimorph, as shown in Figure 12.

22
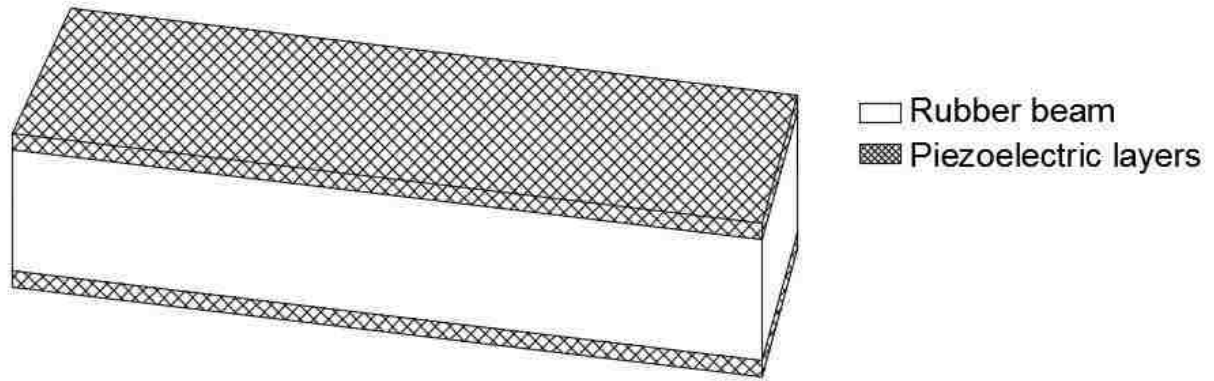
Figure 12: Sketch of the piezoelectric element

Piezoelectric elements are usually classified into two different types based on the energy conversion direction – actuator type and sensor type. Actuator type piezoelectric elements are responsible for the so called indirect piezoelectric effect, whereas the sensor type produces the direct piezoelectric effect. The indirect piezoelectric effect is when the piezoelectric element undergoes a change in size when an electric field is applied, i.e. the electric energy is converted into mechanical energy. In the second type, where the direct piezoelectric effect takes place, the electric charge is produced when a mechanical stress is applied. This thesis is focused only on the direct piezoelectric effect. These definitions are summarized in Table 3.

Table 3: Definitions for piezoelectric elements

Piezoelectric elements			
Type	Piezoelectric effect	Input	Output
Actuator	Indirect	Electrical energy	Mechanical Displacement
Sensor	Direct	Mechanical Displacement	Electrical energy

23

According to [3], subsequent to the classification based on the energy conversion direction, piezoelectric power generators are also identified by the directions between the mechanical stresses and electrical charge vectors, as shown in Figure 13. The directions that are determined here are usually called "31" or "33". The direction of polarization is conventionally denoted as direction "3". Therefore, for a device to be classified in "31" or "33", it depends on the relation between the direction of the mechanical stress and the direction of the electrical potential output. Device "33" implies that electrical charges are collected in the same direction as the mechanical forces are applied and device "31" shows that the electrical charges are collected in a perpendicular direction from where the mechanical forces are applied.
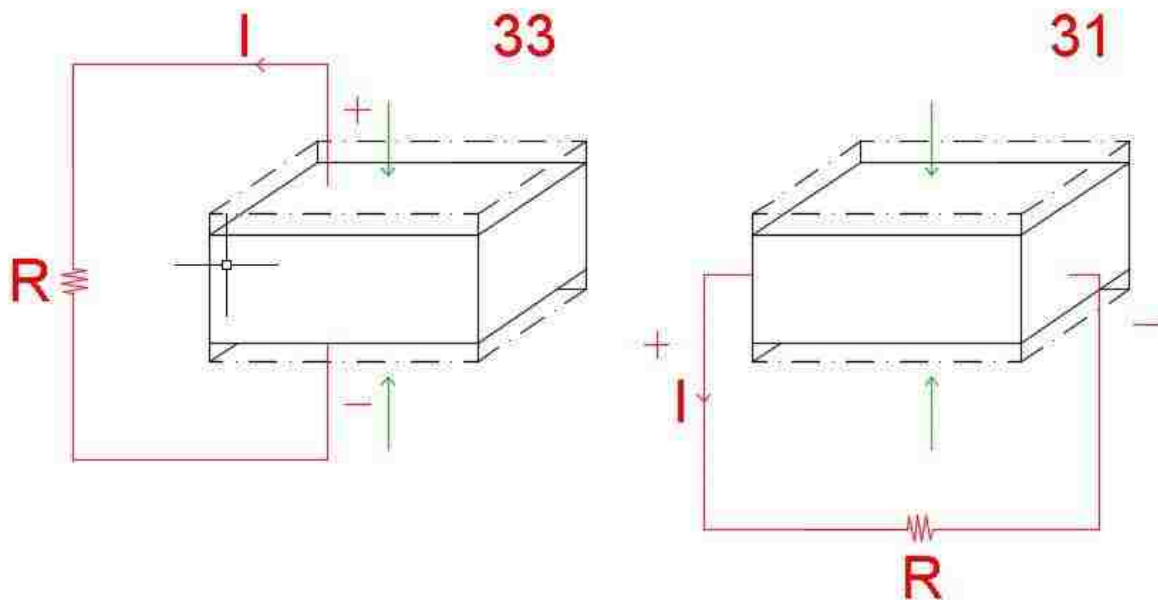
Figure 13: Sketch of piezoelectric elements with the two different coupling modes (Adapted from [3])

24

In this work, the direction used is "31", as illustrated in Figure 14:
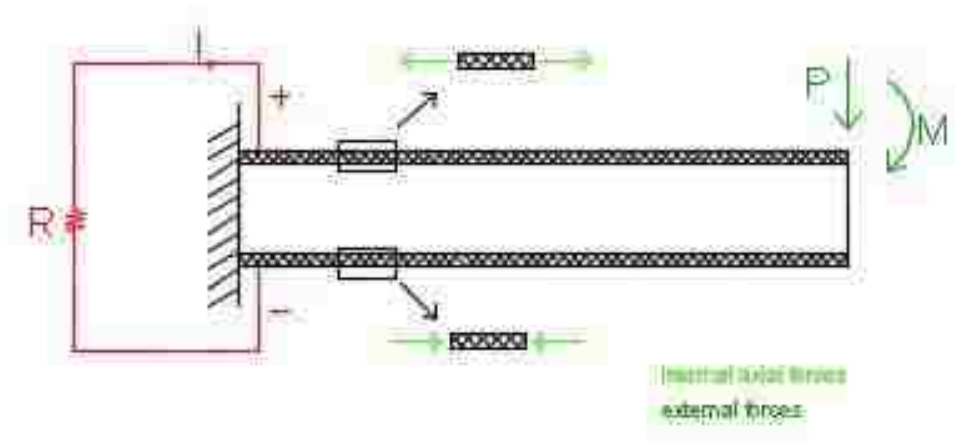
Figure 14: Illustration of direction on the piezoelectric generator

The energy flow of the piezoelectric generator consists of two energy transformation steps. Firstly, the environment (wind) energy is transformed to the mechanical vibration energy of the beam mass. In the second step, the mechanical vibration energy is transformed into electrical energy, in which the direct piezoelectric effect of the materials is used [3]. As in all energy transformation processes, these steps have built-in losses, shown by equations of efficiency:

$$\eta_{me} = \frac{E_e}{E_m} \qquad\qquad (11)$$

$$\eta_m = \frac{E_m}{E_s} \qquad\qquad (12)$$

25

Where,

η_m = total efficiency of the system, from wind energy to mechanical energy and to electrical energy

E_m= mechanical vibration energy stored in the mechanical system

E_s= energy from the load on the piezoelectric element

E_e = electrical energy generated

η_{me}= mechanical to electrical energy efficiency

For this step of this work and analysis, the efficiency is considered to be ideal η_m=1 and no loss is considered. This can be improved in further work, with performance analysis of all the transformations.

4.2   Piezoelectric properties

Piezoelectric devices can be characterized with some specific properties. In [1], PZT-5A and PZT-5H are presented as the most commonly used piezoceramic materials for Euler-Bernoulli and Rayleigh beam theories. As indicate in this source, typical properties of this materials can be found on the Web [12], and the ones which are useful for this analysis are reproduced in Table 4:

26

Table 4: Piezoelectric properties of piezoceramic materials

Material	Lead Zirconate Titanate (PZT-5A)	Lead Zirconate Titanate (PZT-5H)
Density (kg/m^3)	7750	7500
Piezoelectric Coupling d (C/N)	$\begin{bmatrix} 0 & 0 & 0 & 0 & 584 & 0 \\ 0 & 0 & 0 & 584 & 0 & 0 \\ -171 & -171 & 374 & 0 & 0 & 0 \end{bmatrix} * 10^{-12}$	$\begin{bmatrix} 0 & 0 & 0 & 0 & 741 & 0 \\ 0 & 0 & 0 & 741 & 0 & 0 \\ -274 & -274 & 593 & 0 & 0 & 0 \end{bmatrix}$ $* 10^{-12}$
Compliance s_E (m^2/N)	$\begin{bmatrix} 16.4 & -5.74 & -7.22 & 0 & 0 & 0 \\ -5.74 & 16.4 & -7.22 & 0 & 0 & 0 \\ -7.22 & -7.22 & 18.8 & 0 & 0 & 0 \\ 0 & 0 & 0 & 47.5 & 0 & 0 \\ 0 & 0 & 0 & 0 & 47.5 & 0 \\ 0 & 0 & 0 & 0 & 0 & 44.3 \end{bmatrix}$ $* 10^{-12}$	$\begin{bmatrix} 16.5 & -4.78 & -8.45 & 0 & 0 & 0 \\ -4.78 & 16.5 & -8.45 & 0 & 0 & 0 \\ -8.45 & -8.45 & 20.7 & 0 & 0 & 0 \\ 0 & 0 & 0 & 43.5 & 0 & 0 \\ 0 & 0 & 0 & 0 & 43.5 & 0 \\ 0 & 0 & 0 & 0 & 0 & 42.6 \end{bmatrix}$ $* 10^{-12}$

Hereafter, these properties will be approached with more detail.

5   Study on the use of piezoelectric elements in Abaqus

For comprehension and verification of Abaqus procedures and criteria from the use of piezoelectric elements, the simple cubic element in Figure 15 is created and analyzed in several steps. Outputs as stress, strain, electrical potential and displacement are analyzed from the structure.
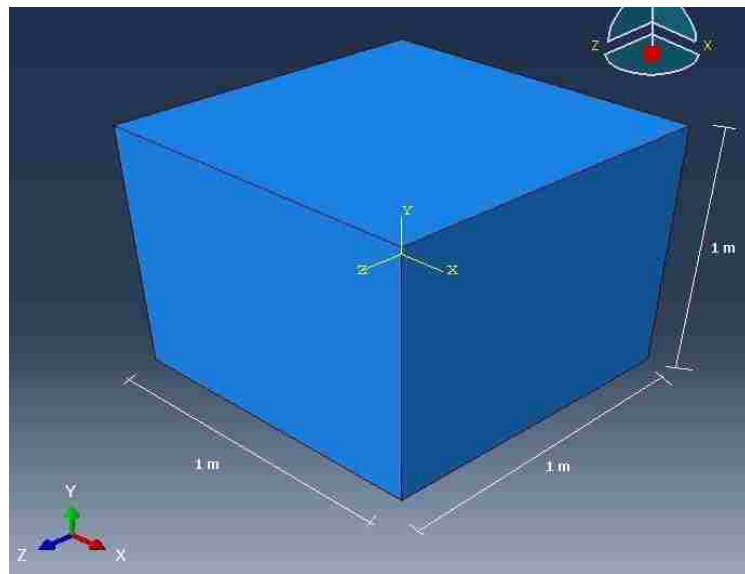
Figure 15: Cubic element created for verification of piezoelectric properties, with its dimensions

The analysis consists in two steps. At first, a comparison of hand calculations and Abaqus results for the consideration of only mechanical properties on the cube is performed. In a second step, piezoelectric properties are inserted and the comparison combines both mechanical and piezoelectric properties of the element, using Abaqus outputs and outputs from the equations showed hereafter.

28

5.1 Mechanical properties

The mechanical material properties of the cube are found in Table 5 and are used in the equations and in the Abaqus finite element model. It is important to notice that both cubes, with only mechanical properties and with piezoelectric properties, are considered to have mechanical homogenous and isotropic behavior.

Table 5: Mechanical properties for the cube

Component		Cube
Material		rubber
Elastic properties	**Young`s modulus (MPa)**	50
	Poisson`s ratio	0.41

5.1.1 Abaqus analysis

For the cube shown in Figure 15, a simple static load analysis is performed with Abaqus. A pressure load is applied on the top surface of the cube and some of the Degrees of Freedom (DOF`s) are restrained on the bottom surface to prevent vertical displacements and rigid body motions, as shown in Figure 16.

29
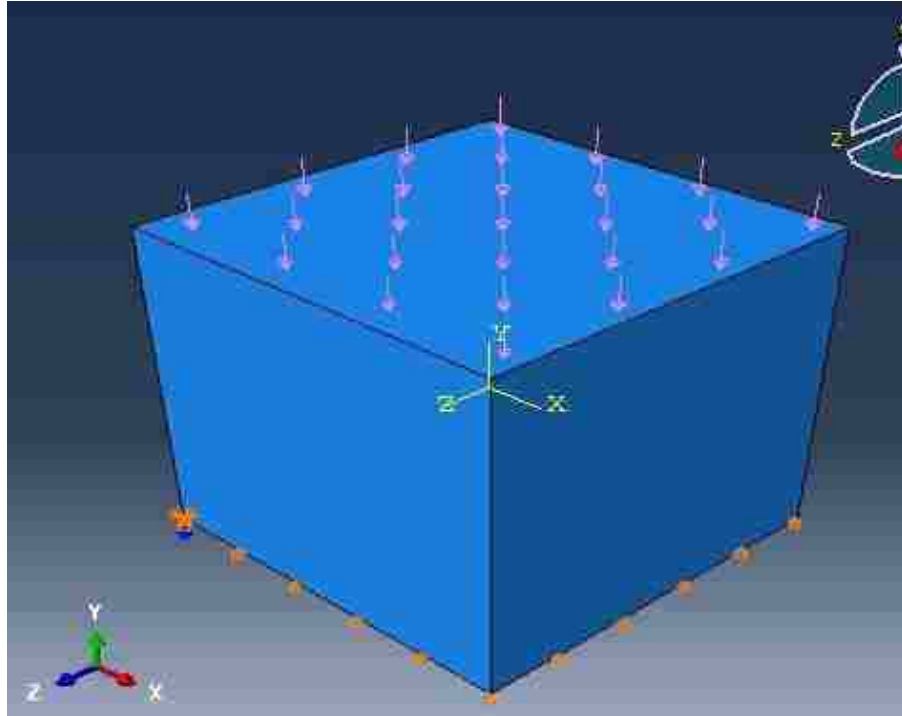
Figure 16: Load and Boundary Conditions applied to the cube in Abaqus

A static, linear perturbation analysis is performed and the displacements outputs are obtained. Also, as a result of a finite element structural analysis, outputs as strain and stresses on the component are obtained. These values are the ones used for the comparison with the hand calculations. Figure 17 shows the nodes that are selected to be analyzed from the mesh on the software and Table 6 and Table 7 show the stress and strain values obtained from the study using Abaqus, directly from its nodes output values.
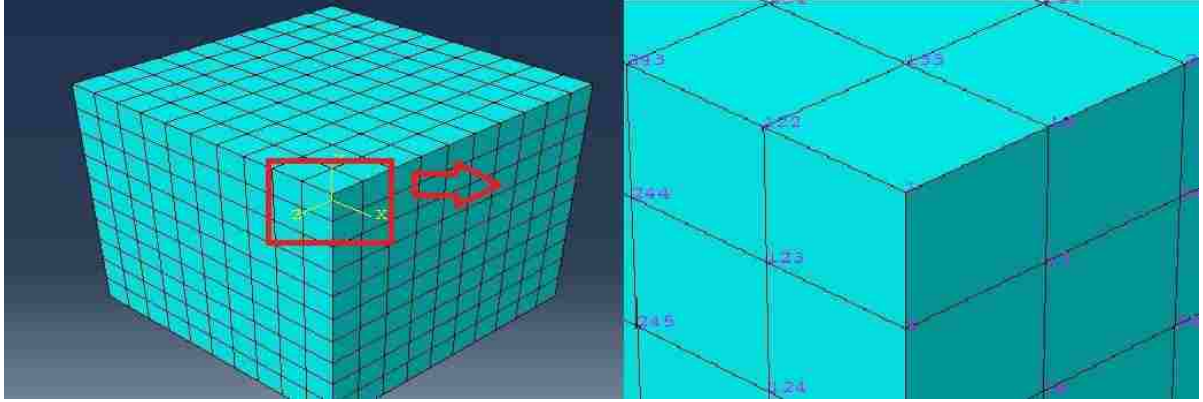
Figure 17: Identification of nodes on the FE mesh on the cube

Table 6: Stress values obtained from Abaqus analysis

node	stress (Mpa)		
	S11 (σ_x)	S22 (σ_y)	S33 (σ_z)
1	1.02318E-06	-1E+09	-8E-07
2	1.02318E-06	-1E+09	1.36E-06
12	2.44427E-06	-1E+09	8.53E-07
13	5.4001E-07	-1E+09	3.41E-07
122	-3.4106E-07	-1E+09	-1.5E-06
123	4.26326E-07	-1E+09	8.81E-07
133	2.30216E-06	-1E+09	7.96E-07

31

source	node	strain		
		E11 (εx)	E22 (εy)	E33 (εz)
Abaqus	1	8.20E-06	-2.00E-05	8.20E-06
	2	8.20E-06	-2.00E-05	8.20E-06
	12	8.20E-06	-2.00E-05	8.20E-06
	13	8.20E-06	-2.00E-05	8.20E-06
	122	8.20E-06	-2.00E-05	8.20E-06
	123	8.20E-06	-2.00E-05	8.20E-06
	133	8.20E-06	-2.00E-05	8.20E-06

In the next section, the analysis with the equations is clarified.

5.1.2 Equations analysis

A theoretical analysis on mechanics of materials follows. As described in [13], for a three-dimensional state of stress, each of the six stress components is expressed as a linear function of six components of strain within the linear elastic range and vice versa. Therefore, the generalized Hooke`s law to describe stress and strain relation for homogeneous elastic materials can be expressed in the following:

$$\begin{pmatrix} \sigma_x \\ \sigma_y \\ \sigma_z \\ \tau_{xy} \\ \tau_{yz} \\ \tau_{xz} \end{pmatrix} = \begin{pmatrix} c_{11} & c_{12} & c_{13} & c_{14} & c_{15} & c_{16} \\ c_{21} & c_{22} & c_{23} & c_{24} & c_{25} & c_{26} \\ c_{31} & c_{32} & c_{33} & c_{34} & c_{35} & c_{36} \\ c_{41} & c_{42} & c_{43} & c_{44} & c_{45} & c_{46} \\ c_{51} & c_{52} & c_{53} & c_{54} & c_{55} & c_{56} \\ c_{61} & c_{62} & c_{63} & c_{64} & c_{65} & c_{66} \end{pmatrix} \begin{pmatrix} \varepsilon_x \\ \varepsilon_y \\ \varepsilon_z \\ \gamma_{xy} \\ \gamma_{yz} \\ \gamma_{xz} \end{pmatrix} \qquad (13)$$

Where,

σ = axial stress on the material, on directions x, y or z; given in Pa

τ = shear stress on the material, on directions xy, yz or xz; in Pa

ε = strain on the material, on directions x, y or z; unitless

γ = shear on the material, on directions xy, yz or xz; unitless

c_{ij} = coefficients of material-dependent elastic constants

The matrixes in Equation 13 can be also commonly represented by the notation

$$\tau_{ij} = c_{ijmn}\varepsilon_{mn} \qquad (14)$$

Which is the notation adopted later in the Abaqus analysis equations for the piezoelectric properties, based on a variation of Einstain`s notation with implicit summations for repeated subscripts. To clarify the parallel between the notations, the matrixes on Equation 13 are rewritten on Equation 15 using the notation on Equation 14. It is important to notice that

33

in both Equations 13 and 15, the equivalent terms are being excluded for simplification, for example, τ_{zy} is omitted because it has the same value as τ_{yz}.

$$
\begin{pmatrix} \sigma_{11} \\ \sigma_{22} \\ \sigma_{33} \\ \tau_{12} \\ \tau_{23} \\ \tau_{13} \end{pmatrix} = \begin{pmatrix} c_{1111} & c_{1122} & c_{1133} & c_{1112} & c_{1123} & c_{1113} \\ c_{2211} & c_{2222} & c_{2233} & c_{2212} & c_{2223} & c_{2213} \\ c_{3311} & c_{3322} & c_{3333} & c_{3312} & c_{3323} & c_{3313} \\ c_{1211} & c_{1222} & c_{1233} & c_{1212} & c_{1223} & c_{1213} \\ c_{2311} & c_{2322} & c_{2333} & c_{2312} & c_{2323} & c_{2313} \\ c_{1311} & c_{1322} & c_{1333} & c_{1312} & c_{1323} & c_{1313} \end{pmatrix} \begin{pmatrix} \varepsilon_{11} \\ \varepsilon_{22} \\ \varepsilon_{33} \\ \gamma_{12} \\ \gamma_{23} \\ \gamma_{13} \end{pmatrix}
$$
(15)

For now the simplified version with the matrix in Equation 13 will be used.

As previously mentioned, the materials treated here, rubber and piezoelectric layers, are considered to have isotropic mechanical behavior. Using mechanical properties and equations found in most mechanics of materials book and thus not detailed here, it can be said that, for isotropic materials, the matrix in Equation 13 becomes the following:

$$
\begin{pmatrix} c_{11} & c_{12} & c_{13} & 0 & 0 & 0 \\ c_{21} & c_{22} & c_{23} & 0 & 0 & 0 \\ c_{31} & c_{32} & c_{33} & 0 & 0 & 0 \\ 0 & 0 & 0 & c_{44} & 0 & 0 \\ 0 & 0 & 0 & 0 & c_{55} & 0 \\ 0 & 0 & 0 & 0 & 0 & c_{66} \end{pmatrix}
$$
(16)

Which leads to the equations for stress-strain generic representation as:

34

$$\sigma_x = c_{11}\varepsilon_x + c_{12}\varepsilon_y + c_{13}\varepsilon_z$$

$$\sigma_y = c_{12}\varepsilon_x + c_{22}\varepsilon_y + c_{23}\varepsilon_z$$

$$\sigma_z = c_{13}\varepsilon_x + c_{23}\varepsilon_y + c_{33}\varepsilon_z$$

$$\tau_{xy} = c_{44}\gamma_{xy} \quad\quad\quad (17)$$

$$\tau_{yz} = c_{55}\gamma_{yz}$$

$$\tau_{xz} = c_{66}\gamma_{xz}$$

The inverse form of Equation 17 may be expressed as follows:

$$\varepsilon_x = \frac{1}{E}[\sigma_x - \nu(\sigma_y + \sigma_z)]$$

$$\varepsilon_y = \frac{1}{E}[\sigma_y - \nu(\sigma_x + \sigma_z)]$$

$$\varepsilon_z = \frac{1}{E}[\sigma_z - \nu(\sigma_x + \sigma_y)]$$

$$\gamma_{xy} = \frac{\tau_{xy}}{G} \quad\quad\quad (18)$$

$$\gamma_{yz} = \frac{\tau_{yz}}{G}$$

$$\gamma_{xz} = \frac{\tau_{xz}}{G}$$

Where,

$E =$ Young's modulus/elasticity

$\nu =$ Poisson`s ratio

$G =$ shear modulus of elasticity

35

Using Equation 18, the value of stress applied in several nodes in one element of a structure in Abaqus is computed, as shown in Table 6 and used as input for the strain hand calculations. The results obtained from the use of the equations is shown in Table 8.

Table 8: Strain values obtained from the analytical approach

source	strain		
	E11 (εx)	E22 (εy)	E33 (εz)
Hand calc	8.20E-06	-2.00E-05	8.20E-06

5.1.3 Comparison of FEM and analytical method

Adding together the work done in the last two sections, Table 9 shows the comparison on the values obtained for strain.

36

Table 9: Comparison of strain values obtained with Abaqus x analytical method

source	node	strain		
		E11 (εx)	E22 (εy)	E33 (εz)
Abaqus	1	8.20E-06	-2.00E-05	8.20E-06
	2	8.20E-06	-2.00E-05	8.20E-06
	12	8.20E-06	-2.00E-05	8.20E-06
	13	8.20E-06	-2.00E-05	8.20E-06
	122	8.20E-06	-2.00E-05	8.20E-06
	123	8.20E-06	-2.00E-05	8.20E-06
	133	8.20E-06	-2.00E-05	8.20E-06
Hand calc	-	8.20E-06	-2.00E-05	8.20E-06

In Table 9, it can be observed that the values obtained are exactly the same, showing that Abaqus uses the same theories and equations for analysis as described above. Having these results validated, now the approach continues with the addition of piezoelectric properties of the material.

5.2 Piezoelectric properties

Having the finite element analysis from Abaqus and analytical methods compared and validated, the piezoelectric properties are added to the structure. The presence of electrical

37

potential, together with the other electrical properties of this type of material, affects the general behavior of the structure, therefore its strain and stresses values are also affected. Hence, equations 13-18 shown above cannot be used anymore.

In Abaqus documentation, one can find the theoretical information and users guide for the equations that constitute the analysis outputs, as stress, electrical output, etc. There are several variables involved, some being more familiar for mechanical analysis, from a civil engineer point of view. Nonetheless, in this analysis there are also several variables regarding electrical properties, which could be more familiar for electrical engineers. The physics laws used for understanding these materials are equivalent, therefore in engineering is common to make analogies of behavior on physical forces with fluids behavior or electrical behavior. To simplify the comprehension for structural engineers, Table 10 defines a parallel of behavior and definitions of the variables used in Abaqus to describe mechanical properties and electrical properties.

Table 10: Parallel on mechanical and electrical constants used in Abaqus

Mechanical constant	Definition	Units	Electrical constant	Definition	Units
σ_{ij}	Mechanical stress tensor	Pa	q_i	Electric "displacement" vector (electric flux)	Vm
u	Displacement	m	φ	Electrical potential	V
ε_{ij}	Strain tensor $-\dfrac{\partial \delta u}{\partial x}$	-	E_m	Electrical potential gradient vector $-\dfrac{\partial \varphi}{\partial x_i}$	-

D_{ijkl}^{E}	Elastic stiffness matrix	MPa	e_{mij}^{φ}	Piezoelectric stress coefficient matrix	C/m^2
D_{ijkl}^{E}	Elastic stiffness matrix	MPa	D_{ij}^{φ}	Dielectric property matrix	F/m

Having these variables in mind, it is given that the constitutive equations used in Abaqus for the analysis of piezoelectric elements are:

$$\sigma_{ij} = D_{ijkl}^{E}\varepsilon_{kl} - e_{mij}^{\varphi}E_m \qquad (19)$$

$$q_i = e_{ijk}^{\varphi}\varepsilon_{jk} + D_{ij}^{\varphi(\varepsilon)}E_j \qquad (20)$$

Considering Equations 19 and 20, it can be noticed that the same comparison on stress and strain results accomplished in the previous step can now be performed using Abaqus outputs and these theoretical formulas, only now with more variables and equations involved.

These equations, for stress and the electrical flux calculation, determine each stress and the electrical flux in each direction for each node of the Abaqus model. Therefore, all the calculations shown here refer to one node only and this will be enough for verification and comprehension of Abaqus analysis methods. The following sections explain each component of these equations, with complete analysis and calculations presented later on. In this section, different than the previous one, the equations are exposed first and then the Abaqus analysis is shown, for better clarification of the variables.

39

5.2.1 Equations analysis

5.2.1.1 Stress equation

This analysis is for the equation that calculates stress (Eq. 19). Equation 20 will not be worked with detail in this thesis. For each node, as shown previously, the equation inputs and outputs are displayed with the use of the indexes in Abaqus. Nonetheless, another way of displaying the same information from this equation for that same data is to store it in the form of matrixes. Therefore, Eq 19 is analyzed as composed by matrixes in the subsequent format:

$$
\begin{pmatrix} \sigma_{11} \\ \tau_{12} \\ \tau_{13} \\ \tau_{21} \\ \sigma_{22} \\ \tau_{23} \\ \tau_{31} \\ \tau_{32} \\ \sigma_{33} \end{pmatrix} =
\begin{pmatrix}
c_{1111} & c_{1112} & c_{1113} & c_{1121} & c_{1122} & c_{1123} & c_{1131} & c_{1132} & c_{1133} \\
c_{1211} & c_{1212} & c_{1213} & c_{1221} & c_{1222} & c_{1223} & c_{1231} & c_{1232} & c_{1233} \\
c_{1311} & c_{1312} & c_{1313} & c_{1321} & c_{1322} & c_{1323} & c_{1331} & c_{1332} & c_{1333} \\
c_{2111} & c_{2112} & c_{2113} & c_{2121} & c_{2122} & c_{2123} & c_{2131} & c_{2132} & c_{2133} \\
c_{2211} & c_{2212} & c_{2213} & c_{2221} & c_{2222} & c_{2223} & c_{2231} & c_{2232} & c_{2233} \\
c_{2311} & c_{2312} & c_{2313} & c_{2321} & c_{2322} & c_{2323} & c_{2331} & c_{2332} & c_{2333} \\
c_{3111} & c_{3112} & c_{3113} & c_{3121} & c_{3122} & c_{3123} & c_{3131} & c_{3132} & c_{3133} \\
c_{3211} & c_{3212} & c_{3213} & c_{3221} & c_{3222} & c_{3223} & c_{3231} & c_{3232} & c_{3233} \\
c_{3311} & c_{3312} & c_{3313} & c_{3321} & c_{3322} & c_{3323} & c_{3331} & c_{3332} & c_{3333}
\end{pmatrix}
\begin{pmatrix} \varepsilon_{11} \\ \gamma_{12} \\ \gamma_{13} \\ \gamma_{21} \\ \varepsilon_{22} \\ \gamma_{23} \\ \gamma_{31} \\ \gamma_{32} \\ \varepsilon_{33} \end{pmatrix}
-
\begin{pmatrix}
e_{111} & e_{211} & e_{311} \\
e_{112} & e_{212} & e_{312} \\
e_{113} & e_{213} & e_{313} \\
e_{121} & e_{221} & e_{321} \\
e_{122} & e_{222} & e_{322} \\
e_{123} & e_{223} & e_{323} \\
e_{131} & e_{231} & e_{331} \\
e_{132} & e_{232} & e_{332} \\
e_{133} & e_{233} & e_{333}
\end{pmatrix}
\begin{pmatrix} EPG_1 \\ EPG_2 \\ EPG_3 \end{pmatrix}
$$

(21)

Equation 21 summarizes clearly what is the data necessary to perform the calculation. Each variable on it is worked and explained in more detail as follows:

$\boldsymbol{\sigma_{ij}}$

40

It represents the stresses present on the node in all three axial directions and all three shear directions. It is expressed by the matrix:

$$\sigma = [\sigma_{11}\ \tau_{12}\ \tau_{13}\ \tau_{21}\ \sigma_{22}\ \tau_{23}\ \tau_{31}\ \tau_{32}\ \sigma_{33}]^T \qquad (22)$$

As mentioned before, the notation used in Equation 13 from mechanics of materials books and Abaqus notations are slightly different. For better understanding, Table 11 shows the equivalence between them.

Table 11: Comparison of notation used in the literature and in Abaqus for clarification

Abaqus	σ_{11}	τ_{12}	τ_{13}	τ_{21}	σ_{22}	τ_{23}	τ_{31}	τ_{32}	τ_{33}
Literature	σ_x	τ_{xy}	τ_{xz}	τ_{yx}	σ_y	τ_{yz}	τ_{zx}	τ_{zy}	σ_{zz}

Subsequently, as it applies for most of the variables here, matrixes in Equation 13 show only six of the nine variables here involved. As explained before, this is a simplification commonly adopted due to the consideration of $\tau_{ij} = \tau_{ji}$. Here this is still valid, but both values are specified in the matrix to make the math clear for the reader.

ε_{kl}

It represents the strain tensor on the node, with the same directions as in the stress values, and it is expressed by the matrix:

$$\varepsilon = [\varepsilon_{11}\ \gamma_{12}\ \gamma_{13}\ \gamma_{21}\ \varepsilon_{22}\ \gamma_{23}\ \gamma_{31}\ \gamma_{32}\ \varepsilon_{33}]^T \qquad (23)$$

41

The comparison of notations used in Abaqus and in literature is equivalent to the one found in Table 11, which is also shown in Table 12 for clarification.

Table 12: Comparison of notation used in the literature and in Abaqus for clarification

Abaqus	ε_{11}	γ_{12}	γ_{13}	γ_{21}	ε_{22}	γ_{23}	γ_{31}	γ_{32}	ε_{33}
Literature	ε_x	γ_{xy}	γ_{xz}	γ_{yx}	ε_y	γ_{yz}	γ_{zx}	γ_{zy}	ε_z

In a similar situation as with the values of stress σ, the vector of ε in Equation 12 shows only six of the nine variables involved. As explained before, this is a simplification commonly adopted due to the consideration of $\varepsilon_{ij} = \varepsilon_{ji}$. . Here this is still valid, but both values are specified in the matrix to make the math clear for the reader.

D_{ijkl}^E

It represents the material`s static stiffness properties. It is defined at zero electrical potential gradient and it is expressed by the symbolic matrix that shows the connection between strains and stresses variables, considering its directions. Matrix D is composed as shown in Equation 21 and reproduced here. The notation c_{ijmn} is equivalent to D_{ijkl}^E and it is kept like this for easy analogy to Equation 13.

42

$$D_{ijkl}^{E} = \begin{pmatrix} c_{1111}^{E} & c_{1112}^{E} & c_{1113}^{E} & c_{1121}^{E} & c_{1122}^{E} & c_{1123}^{E} & c_{1131}^{E} & c_{1132}^{E} & c_{1133}^{E} \\ c_{1211}^{E} & c_{1212}^{E} & c_{1213}^{E} & c_{1221}^{E} & c_{1222}^{E} & c_{1223}^{E} & c_{1231}^{E} & c_{1232}^{E} & c_{1233}^{E} \\ c_{1311}^{E} & c_{1312}^{E} & c_{1313}^{E} & c_{1321}^{E} & c_{1322}^{E} & c_{1323}^{E} & c_{1331}^{E} & c_{1332}^{E} & c_{1333}^{E} \\ c_{2111}^{E} & c_{2112}^{E} & c_{2113}^{E} & c_{2121}^{E} & c_{2122}^{E} & c_{2123}^{E} & c_{2131}^{E} & c_{2132}^{E} & c_{2133}^{E} \\ c_{2211}^{E} & c_{2212}^{E} & c_{2213}^{E} & c_{2221}^{E} & c_{2222}^{E} & c_{2223}^{E} & c_{2231}^{E} & c_{2232}^{E} & c_{2233}^{E} \\ c_{2311}^{E} & c_{2312}^{E} & c_{2313}^{E} & c_{2321}^{E} & c_{2322}^{E} & c_{2323}^{E} & c_{2331}^{E} & c_{2332}^{E} & c_{2333}^{E} \\ c_{3111}^{E} & c_{3112}^{E} & c_{3113}^{E} & c_{3121}^{E} & c_{3122}^{E} & c_{3123}^{E} & c_{3131}^{E} & c_{3132}^{E} & c_{3133}^{E} \\ c_{3211}^{E} & c_{3212}^{E} & c_{3213}^{E} & c_{3221}^{E} & c_{3222}^{E} & c_{3223}^{E} & c_{3231}^{E} & c_{3232}^{E} & c_{3233}^{E} \\ c_{3311}^{E} & c_{3312}^{E} & c_{3313}^{E} & c_{3321}^{E} & c_{3322}^{E} & c_{3323}^{E} & c_{3331}^{E} & c_{3332}^{E} & c_{3333}^{E} \end{pmatrix} \qquad (24)$$

As an example to understand matrix D^E, the element D_{3122}^E connects σ_{31} to ε_{22}. To represent σ_{31}:

$$\sigma_{31} = D_{3111}^E \varepsilon_{11} + D_{3112}^E \gamma_{12} + D_{3113}^E \gamma_{13} + D_{3121}^E \gamma_{21} + D_{3122}^E \varepsilon_{22} + D_{3123}^E \gamma_{23} + D_{3113}^E \gamma_{13} + D_{3123}^E \gamma_{23} \qquad (25)$$

And when this is executed for the whole matrix and both vectors, the result is

$$\sigma_{ij} = D_{ijkl}^E \varepsilon_{kl} \qquad (26)$$

Now the analysis focuses on the second part of the stress equation, regarding the electrical and piezoelectric properties of element

43

E_m

It represents the electrical potential gradient vector, where for one node, there is gradient of electrical potential in all three directions, as shown in Figure 18. In Abaqus graphical interface, the individual components of E_m are called EPG_1, EPG_2 and EPG_3
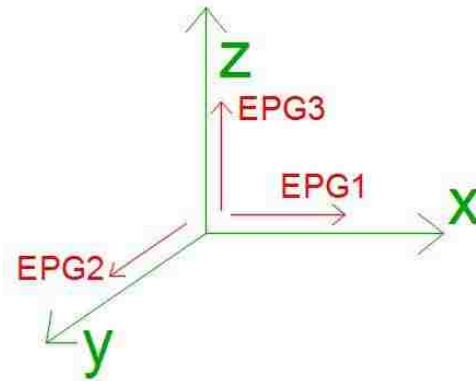
Figure 18: Representation of gradient vector of electrical potential in three directions

Thus, vector E_m is represented by:

$$E_m = [EPG_1 \ EPG_2 \ EPG_3 \ ]^T \qquad (27)$$

e_{mij}^{φ}

It is the material`s piezoelectric stress coefficient matrix, which represents the coupling between the mechanical properties of the component and its electrical properties, defining the stress σ_{ij} caused by the electrical potential gradient E_m. This property is not isotropic, since the electrical potential and stress of the material are related with specifics directions.

44

The piezoelectric constants are stored in this matrix, which relates the stress directions and the electrical output directions, according to a local coordinate system defined to each piezoelectric layer in Abaqus. The first index m in these coefficients refers to the component of electric displacement q_i (electric flux), while the last pair ij indicates the component of mechanical stress, equivalent to σ_{ij}.

In Abaqus graphical interface, the representation of the input values to be added for this matrix are in the following format:

$$e^{\varphi}_{mij} = \begin{pmatrix} e_{111} & e_{122} & e_{133} & e_{112} & e_{113} & e_{123} \\ e_{211} & e_{222} & e_{233} & e_{212} & e_{213} & e_{223} \\ e_{311} & e_{322} & e_{333} & e_{312} & e_{313} & e_{323} \end{pmatrix} \qquad (28)$$

For calculation purposes, Abaqus transforms this input given by the user in the following matrix shown in Eq. 28, obtained from Equation 21, considering that $e^{\varphi}_{mij} = e^{\varphi}_{mji}$.

45

$$e_{mij}^{\varphi} = \begin{pmatrix} e_{111} & e_{211} & e_{311} \\ e_{112} & e_{212} & e_{312} \\ e_{113} & e_{213} & e_{313} \\ e_{121} & e_{221} & e_{321} \\ e_{122} & e_{222} & e_{322} \\ e_{123} & e_{223} & e_{323} \\ e_{131} & e_{231} & e_{331} \\ e_{132} & e_{232} & e_{332} \\ e_{133} & e_{233} & e_{333} \end{pmatrix} \qquad (29)$$

The values of piezoelectric constants in the matrix of Equation 29 are given in $C/_{m^2}$. This matrix is put together with the E_m vector, which will generate the second part of the equation 19, shown in Equation 30.

$$\sigma_{ij} = -e_{mij}^{\varphi} E_m \qquad (30)$$

Having a clear understanding of the meaning of each of the values involved in Equation 19, the equations can be solved and compared to the results obtained in Abaqus.

5.2.2   Abaqus analysis

For the same cube shown in Figure 13, the same loads, boundary conditions and type of analysis are performed. However, the mechanical properties are modified and also added with values corresponded to piezoelectric materials, which are displayed next. Table 13 shows the

46

mechanical properties of the cube and Table 14 shows the values adopted as piezoelectric properties for it. In the next chapter, each of this properties explained.

Table 13: Material mechanical properties for the cube

Component		Cube
Material		rubber
Elastic properties	Young`s modulus (MPa)	62
	Poisson`s ratio	0.34

Table 14: Piezoelectric properties inserted in Abaqus

Property	Value	Unit
Piezoelectric stress coefficient matrix (e^{φ}_{mij})	$\begin{pmatrix} -5.3512 & -5.3512 & 15.7835 & 0 & 0 & 0 \\ 0 & 0 & 0 & 12.2947 & 0 & 0 \\ 0 & 0 & 0 & 0 & 12.2947 & 0 \end{pmatrix}$	C/m^2
Dielectric constant $(\varepsilon^T_{33}/\varepsilon_0)$	1700	F/m

Using these inputs, Abaqus will give the following outputs for the selected node, among others, found in Table 15, 16, 17.

47

Table 15: Stress values obtained from Abaqus analysis

	S11 (σ_{11})	S12 (τ_{12})	S13 (τ_{13})	S22 (σ_y)	S23 (τ_{23})	S33 (σ_z)
Stress (Mpa)	1.88E-11	6.85E-12	8.17E-12	-999.997	-2.67E-12	-1.57E-11

Table 16: Strain values obtained from Abaqus analysis

	E11 (ε_{11})	E12 (γ_{12})	E13 (γ_{13})	E22 (ε_{22})	E23 (γ_{23})	E33 (γ_{33})
Strain	5.48E-06	2.96E-19	3.53E-19	-1.61E-05	-1.16E-19	5.48E-06

Table 17: Electrical potential gradient vector values obtained from Abaqus analysis

	EPG1 (ε_{11})	EPG2 (γ_{12})	EPG3 (γ_{13})
Electrical potential gradient vector	-8.44E-08	-3.25E-21	1.86E-21

5.2.3. Comparison of FEM and analytical method

Subsequently to the illustration and identification of all the terms on Equation 19 and display of the results obtained with Abaqus graphical analysis, the values used for the analytical method are described and compared with the previously obtained results. Each of the variables are defined with the final goal of finding and comparing σ_{ij}.

ε_{kl}

48

It is taken directly from Abaqus output result.

$$\varepsilon = \begin{pmatrix} 5.48 \cdot 10^{-6} \\ 2.96 \cdot 10^{-19} \\ 3.53 \cdot 10^{-19} \\ 2.96 \cdot 10^{-19} \\ -1.61 \cdot 10^{-5} \\ -1.16 \cdot 10^{-19} \\ 3.53 \cdot 10^{-19} \\ -1.16 \cdot 10^{-19} \\ 5.48 \cdot 10^{-6} \end{pmatrix} \tag{31}$$

D_{ijkl}^E

In Abaqus, the input properties are Young`s modulus ($E$) and Poisson`s ratio (υ), as shown in Table 13. With this data, the shear modulus (G) and the quantity λ are estimated. They are called Lamé constants. The following equations show how they are computed:

$$G = \frac{E}{2(1+v)} \tag{32}$$

$$\lambda = \frac{v*E}{(1+v)*(1-2*v)} \tag{33}$$

Considering Abaqus inputs, the value obtained for Equations 31 and 32 are $G = 1.7730 * 10^{+7}$ Pa and $\lambda = 8.0772 * 10^{+7}$. With this values, using equations 13 to 18, from [13], the stress-strain relationships are obtained:

49

$$\sigma_x = 2G\varepsilon_x + \lambda e$$

$$\tau_{xy} = G\gamma_{xy}$$

$$\sigma_y = 2G\varepsilon_y + \lambda e \qquad (34)$$

$$\tau_{yz} = G\gamma_{yz}$$

$$\sigma_z = 2G\varepsilon_z + \lambda e$$

$$\tau_{xz} = G\gamma_{xz}$$

Where,

$$e = \varepsilon_x + \varepsilon_y + \varepsilon_z \qquad (35)$$

From these equations, the matrix D^E_{ijkl} is then built:

$$D^E = \begin{pmatrix} 2G+\lambda & 0 & 0 & 0 & \lambda & 0 & 0 & 0 & \lambda \\ 0 & G & 0 & 0 & 0 & 0 & 0 & 0 & 0 \\ 0 & 0 & G & 0 & 0 & 0 & 0 & 0 & 0 \\ 0 & 0 & 0 & G & 0 & 0 & 0 & 0 & 0 \\ \lambda & 0 & 0 & 0 & 2G+\lambda & 0 & 0 & 0 & \lambda \\ 0 & 0 & 0 & 0 & 0 & G & 0 & 0 & 0 \\ 0 & 0 & 0 & 0 & 0 & 0 & G & 0 & 0 \\ 0 & 0 & 0 & 0 & 0 & 0 & 0 & G & 0 \\ \lambda & 0 & 0 & 0 & \lambda & 0 & 0 & 0 & 2G+\lambda \end{pmatrix} \qquad (36)$$

With its values:

50

$$D^E = \begin{pmatrix} 9.5429 \cdot 10^7 & 0 & 0 & 0 & 4.9160 \cdot 10^7 & 0 & 0 & 0 & 4.9160 \cdot 10^7 \\ 0 & 2.3134 \cdot 10^7 & 0 & 0 & 0 & 0 & 0 & 0 & 0 \\ 0 & 0 & 2.3134 \cdot 10^7 & 0 & 0 & 0 & 0 & 0 & 0 \\ 0 & 0 & 0 & 2.3134 \cdot 10^7 & 0 & 0 & 0 & 0 & 0 \\ 4.9160 \cdot 10^7 & 0 & 0 & 0 & 9.5429 \cdot 10^7 & 0 & 0 & 0 & 4.9160 \cdot 10^7 \\ 0 & 0 & 0 & 0 & 0 & 2.3134 \cdot 10^7 & 0 & 0 & 0 \\ 0 & 0 & 0 & 0 & 0 & 0 & 2.3134 \cdot 10^7 & 0 & 0 \\ 0 & 0 & 0 & 0 & 0 & 0 & 0 & 2.3134 \cdot 10^7 & 0 \\ 4.9160 \cdot 10^7 & 0 & 0 & 0 & 4.9160 \cdot 10^7 & 0 & 0 & 0 & 9.5429 \cdot 10^7 \end{pmatrix} \qquad (37)$$

E_m

It is taken directly from Abaqus output result.

$$E_m = \begin{pmatrix} -8.44 \cdot 10^{-8} & -3.25 \cdot 10^{-21} & -1.86 \cdot 10^{-21} \end{pmatrix}^T \qquad (38)$$

e^{φ}_{mij}

Is it inputted in Abaqus in the format of a matrix, as follows:

$$e^{\varphi} = \begin{pmatrix} -5.3512 & -5.3512 & 15.7835 & 0 & 0 & 0 \\ 0 & 0 & 0 & 12.2947 & 0 & 0 \\ 0 & 0 & 0 & 0 & 12.2947 & 0 \end{pmatrix}$$

(39)

As mentioned before, Abaqus reorganizes this data in another matrix form, as shown:

51

$$
e^\varphi = \begin{pmatrix} -5.3512 & 0 & 0 \\ 0 & 12.2947 & 0 \\ 0 & 0 & 12.2947 \\ 0 & 0 & 0 \\ -5.3512 & 0 & 0 \\ 0 & 0 & 0 \\ 0 & 0 & 0 \\ 0 & 0 & 0 \\ 13.7835 & 0 & 0 \end{pmatrix}
$$

(40)

Finally, these variables are put together in the format of Equation 21, to find the resultant stress in the analyzed node. The results and comparison of equation and Abaqus output are shown in Table 18.

Table 18:Results from Abaqus x Equation

Stress direction	Equation results (MPa)	Abaqus results (MPa)
S11 (σ_{11})	-0.00145	-1.88E-11
S12 (τ_{12})	6.85E-12	6.85E-12
S13 (τ_{13})	8.17E-12	8.17E-12
S21 (τ_{21})	6.85E-12	6.85E-12
S22 (σ_y)	-999.999	-999.997
S23 (τ_{23})	-2.68E-12	-2.67E-12
S31 (τ_{31})	8.17E-12	8.17E-12
S32 (τ_{32})	-2.68E-12	-2.67E-12
S33 (σ_z)	-0.00144	-1.57E-11

52

Analyzing Table 18, it can be seen that the results are the same from both sources, as expected, which clarifies that this is the way Abaqus works through the calculation and it helps with the definition of the structure properties, mainly with the definition of piezoelectric parameters. The differences seen on the table values are acceptable, because all these values have order of magnitude very different from the one of the main result **S22 (σ_y)**.

6 Application of Finite Element Models on the harvester device

6.1 Static Load Model

In the same way as the analysis was completed for the cube, the harvester device is analyzed in this thesis with the use of the FEM software Abaqus. The following sections describe the parameters and properties used for the model.

6.1.1 Dimensions

The mechanical model chosen to represent this structure is shown in Figure 19, where it can be seen that there is a structural element - represented in blue color – which is the actual load resistant element. The two layers set on the bottom and top of it – represented in green color - are piezoelectric elements. Additionally, in Figure 19 the directions of the global coordinate system can be found in the left bottom corner. The dimensions of the beam component can be seen in Figures 20 and 21.
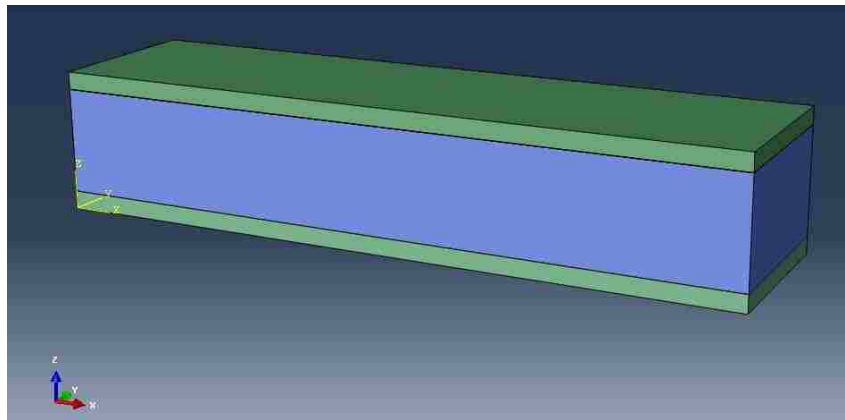

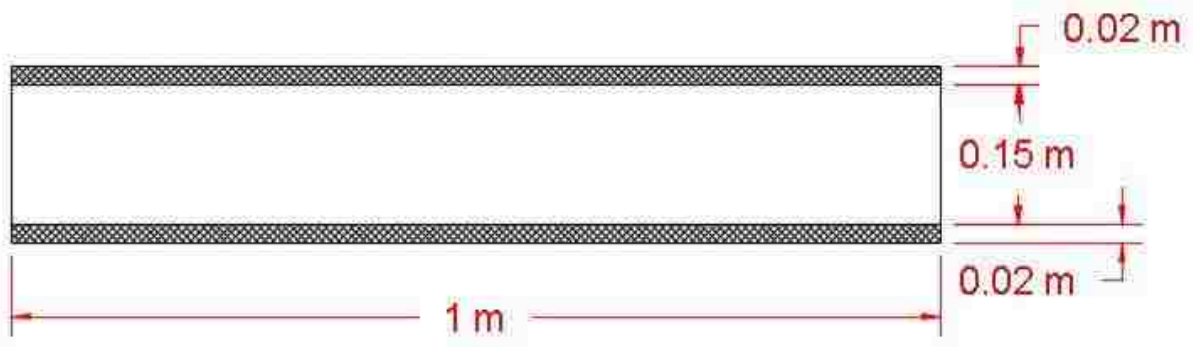*Figure 19: Representation of structural element and piezoelectric layer in Abaqus*

54

Figure 20: Dimensions of beam on XZ plane
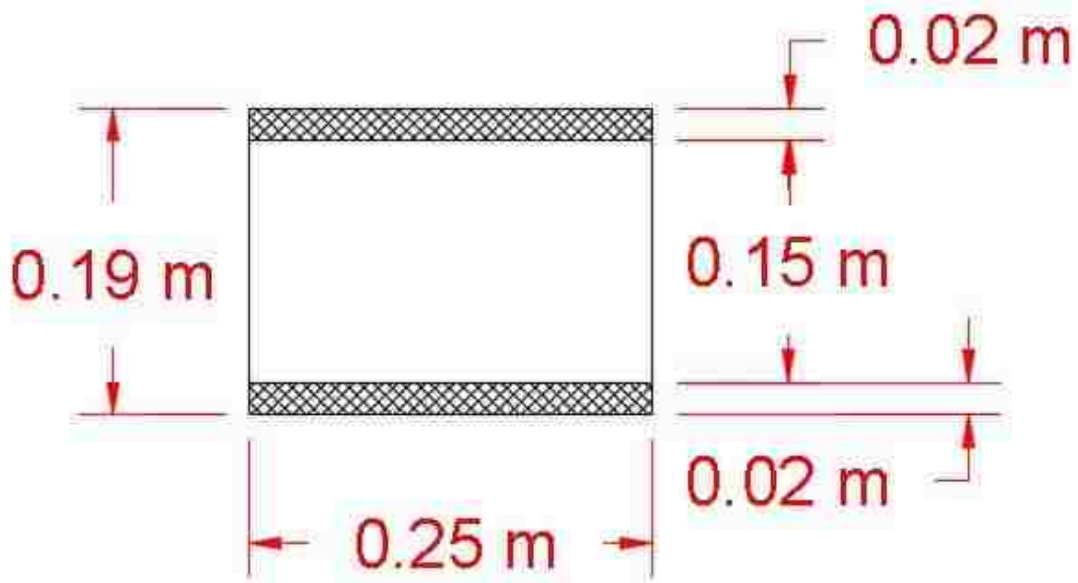
Figure 21: Dimensions of beam on YZ plane

55

As mentioned in Chapter 2, the beam is considered to have a device connected to it, which receives the load. This device is not modeled on the FE model, but chosen to be represented by a concentrated load and moment applied at the free-end of the cantilever beam, as shown in the sketch in Figure 4, reproduced in Figure 22.

Figure 22: Reproduction of figure 4, Sketch representing the analyzed beam

6.1.2   Material properties

The adopted materials are rubber, for the structural beam, and PZT-5A for the piezoelectric layers (for reasons exposed later) and their relevant elastic properties are listed in Table 19.

56

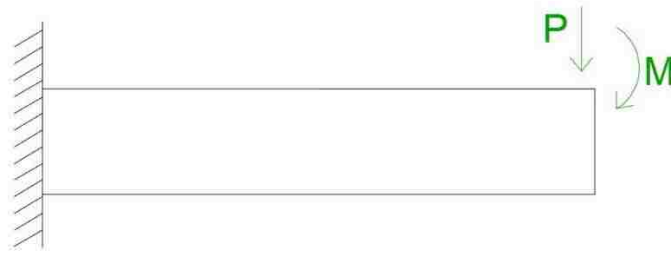| Component		Structural beam	Piezoelectric layers
Material		rubber	PZT- 5A
Elastic properties	Young`s modulus (MPa)	50	62
	Poisson`s ratio	0.47	0.34

The piezoelectric layers have also electrical properties, which are discussed in the next section.

6.1.3 Piezoelectric properties

In this section, it is clarified how to determine the piezoelectric properties of the material modeled in this analysis. Several different sources from the literature are considered, for materials with different properties and for each of them, a static analysis in Abaqus is performed, for a better comprehension of the considerations on inputs and outputs for this kind of material, so that an appropriate decision is made in the finite element modeling of this property.

As shown in Chapter 4, Table 20 shows the properties of the piezoelectric materials considered for the analysis.

57

Table 20: Pieozelectric properties of piezoceramic materials

Material	Lead Zirconate Titanate (PZT-5A)						Lead Zirconate Titanate (PZT-5H)					
Density (kg/m^3)	7750						7500					
Piezoelectric Coupling d (C/N)	$\begin{bmatrix} 0 & 0 & 0 & 0 & 584 & 0 \\ 0 & 0 & 0 & 584 & 0 & 0 \\ -171 & -171 & 374 & 0 & 0 & 0 \end{bmatrix}$ $* 10^{-12}$						$\begin{bmatrix} 0 & 0 & 0 & 0 & 741 & 0 \\ 0 & 0 & 0 & 741 & 0 & 0 \\ -274 & -274 & 593 & 0 & 0 & 0 \end{bmatrix}$ $* 10^{-12}$					
Compliance s_E (m^2/N)	$\begin{bmatrix} 16.4 & -5.74 & -7.22 & 0 & 0 & 0 \\ -5.74 & 16.4 & -7.22 & 0 & 0 & 0 \\ -7.22 & -7.22 & 18.8 & 0 & 0 & 0 \\ 0 & 0 & 0 & 47.5 & 0 & 0 \\ 0 & 0 & 0 & 0 & 47.5 & 0 \\ 0 & 0 & 0 & 0 & 0 & 44.3 \end{bmatrix}$ $* 10^{-12}$						$\begin{bmatrix} 16.5 & -4.78 & -8.45 & 0 & 0 & 0 \\ -4.78 & 16.5 & -8.45 & 0 & 0 & 0 \\ -8.45 & -8.45 & 20.7 & 0 & 0 & 0 \\ 0 & 0 & 0 & 43.5 & 0 & 0 \\ 0 & 0 & 0 & 0 & 43.5 & 0 \\ 0 & 0 & 0 & 0 & 0 & 42.6 \end{bmatrix}$ $* 10^{-12}$					

As seen in Chapter 5, Abaqus requires piezoelectric data to be entered with the piezoelectric stress coefficient matrix, in units of C/m^2. It is clear that the data from Table 20 is in a different format. This difference of information on piezoelectric properties is very common in different sources, noticing that certain finite element codes require piezo data entered as e, whereas vendors typically publish material data for d and g. Because of this, there are tables and transformation equations to relate each property and its units to the others and facilitate the use in different ways of analysis website [12, 14-15].

Among many others, the transformation equation used in this work is:

58

$$e = d * S_E^{-1} \tag{41}$$

Using Equation 40 and matrixes in Table 20, Table 21 is created, with the matrixes containing the properties of both piezoceramic materials regarding piezoelectric coupling coefficients for stress-charge form.

Table 21: Piezoelectric coupling coefficients for stress-charge matrixes, for piezoceramic materials

Material	Piezoelectric Stress coefficient e (C/m^2)					
PZT-5A	$\begin{bmatrix} 0 & 0 & 0 & 0 & 12.2947 & 0 \\ 0 & 0 & 0 & 12.2947 & 0 & 0 \\ -5.3512 & -5.3512 & 15.7835 & 0 & 0 & 0 \end{bmatrix}$					
PZT-5H	$\begin{bmatrix} 0 & 0 & 0 & 0 & 17.0345 & 0 \\ 0 & 0 & 0 & 17.0345 & 0 & 0 \\ -6.6228 & -6.6228 & 23.2403 & 0 & 0 & 0 \end{bmatrix}$					

Having properties values defined and clarified, they have to be placed in the correct entries of the corresponding matrixes, as explained in the following. For different models, the direction between tension and electric flux is different, as explained in Chapter 5. For this beam, the displacement u happens mainly along direction 3, and so does the electrical potential φ (EPOT). From structural analysis, it is know that for the beam of Figure 19, the axial tensions on the materials acts on direction 1.

Using Table 10, it can be seen that tension, or mechanical stress tensor σ_{ij} have a parallel relation with the electric flux q_i. Therefore, it can be inferred that, if both

59

displacement u and electrical potential φ are in direction 3, then both mechanical stress tensor σ_{ij} and electric flux q_i are in direction 1.

This conclusion is important to determine the positioning of the elements in the matrixes of Table 21, because, as mentioned before regarding the indexes of the matrixes: the first index m refers to the component of electric displacement (electric flux), while the last pair ij indicates the component of mechanical stress, equivalent to σ_{ij}.

Having that cleared, the matrixes used as data input for Abaqus static load analysis with the beam model are specified in Table 22:

Table 22: Piezoelectric coupling coefficients for stress-charge matrixes, for piezoceramic materials, in Abaqus input format

Material	Piezoelectric Stress coefficient e (C/m^2)					
PZT-5A	$\begin{bmatrix} -5.3512 & -5.3512 & 15.7835 & 0 & 0 & 0 \\ 0 & 0 & 0 & 12.2947 & 0 & 0 \\ 0 & 0 & 0 & 0 & 12.2947 & 0 \end{bmatrix}$					
PZT-5H	$\begin{bmatrix} -6.6228 & -6.6228 & 23.240 & 0 & 0 & 0 \\ 0 & 0 & 0 & 17.0345 & 0 & 0 \\ 0 & 0 & 0 & 0 & 17.0345 & 0 \end{bmatrix}$					

6.1.4 Dielectric properties

Various materials differ in their ability to support electric flux. Dielectric materials are rated depending on their ability to support electric flux in terms of a figure called dielectric constant [16]. The dielectric property of the piezoelectric element is also called electrical permittivity. Free space is the standard dielectric for purposes of permittivity, which, according

60

to [1] and [12], has the value of ε_0 = 8.854 pF/m. Therefore, the values for dielectric constants are given in reference to ε_0. Table 23, adapted from [1], page 302, displays values for the piezoceramic materials considered.

Table 23: Dielectric constant values for piezoceramic materials

Material	PZT-5A	PZT-5H
Dielectric constant ($\varepsilon_{33}^T / \varepsilon_0$)	1700	3400

The dielectric constants are the values inputted for the Abaqus analysis when considering the dielectric properties of a material. The materials here are considered isotropic with respect to this property.

6.1.5   Finite Elements properties

6.1.5.1   Rubber element

The rubber element is modeled using rectangular solid finite elements (bricks) with 3D stress properties. The type of element selected has eight nodes with three translational degrees of freedom (DOFs) each, for a total of 24 DOFs per element, as is clarified in Figure 23, where also the dimensions of the element used are shown. In Abaqus, this element is called C3D8, which is an element formulated with linear shape functions. It is an element appropriate for materials with only mechanical properties and with characterization simple enough, considering that it is not required for this work the detailed study of the interior behavior on this material,

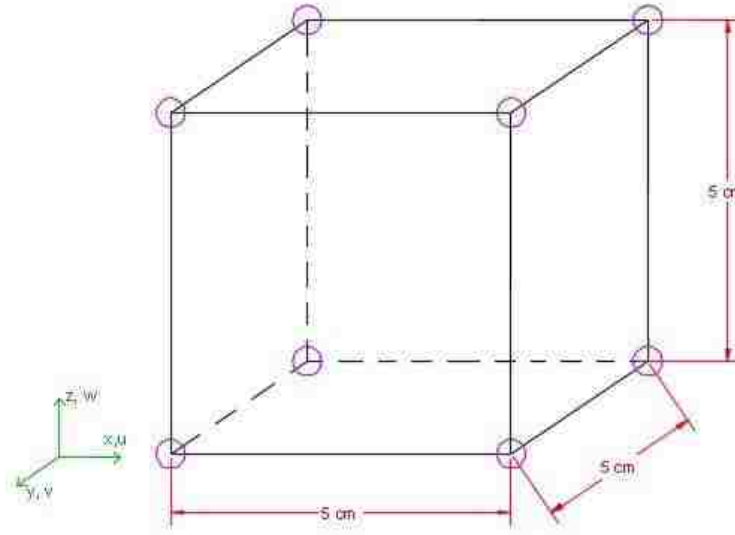as nothing more than a simple displacement and tension response is required in the rubber components.

Figure 23: Representation of the Finite Element used, its dimensions, its nodes and the DOF`s for each node - rubber component

In this model, as it can be seen in Figure 24, this component has 300 elements and 504 nodes, therefore 1512 DOFs are analyzed.
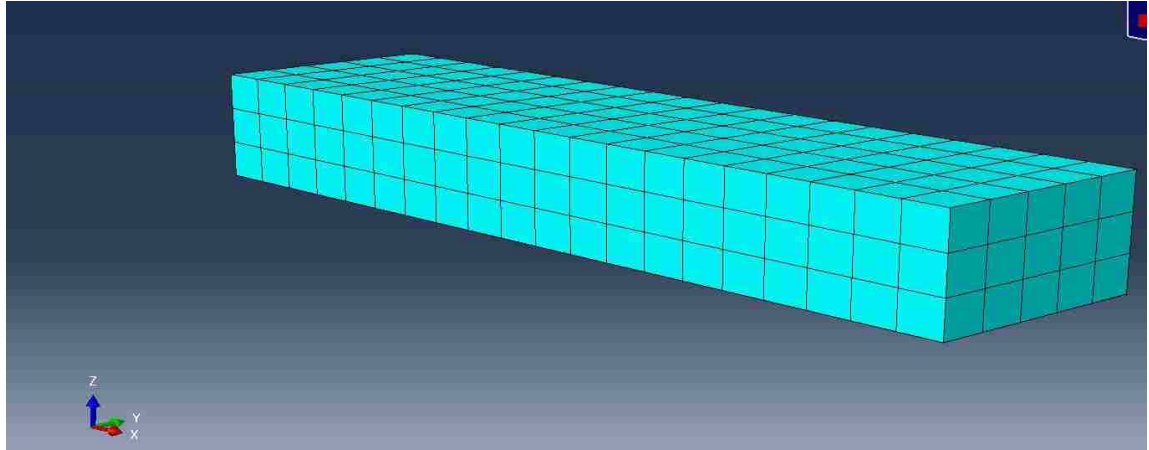
62

Figure 24: Mesh of brick type finite elements of the rubber component of Abaqus

As default, Abaqus performs the FE analysis using the reduced integration technique to prevent shear-locking, but it is important to notice that in some types of elements this can lead to larger displacements than in reality. The investigations with static analyses showed a difference of 6% between the analysis with reduced integration and without this technique. Therefore the modeler decided not to use reduced integration for a more conservative approach making sure that the structure is not responding with excessive flexibility.

6.1.5.2   Piezoelectric layers

The piezoelectric layers are modeled using rectangular solid finite elements (bricks) with mechanical and piezoelectric properties. In contrast with the elements used for the rubber, this brick element has 20 nodes. It has the same configuration as the brick in Figure 23, but with more nodes. Because the grid of node is not complete, this is called the "serendipity" version of the brick element. Each node has the same three translational DOFs and one

63

additional DOF for the electrical potential (EPOT), which is the required output, resulting in an 80 DOFs element. Therefore, the model includes significantly more DOFs in the piezoelectric layers than in the rubber component due to the fact that the output and analysis of interest foucs on the piezoelectric layers. Figure 25 shows the element properties for the piezoelectric layers. In Abaqus, this element is called C3D20E, which is an element formulated using quadratic shape functions.
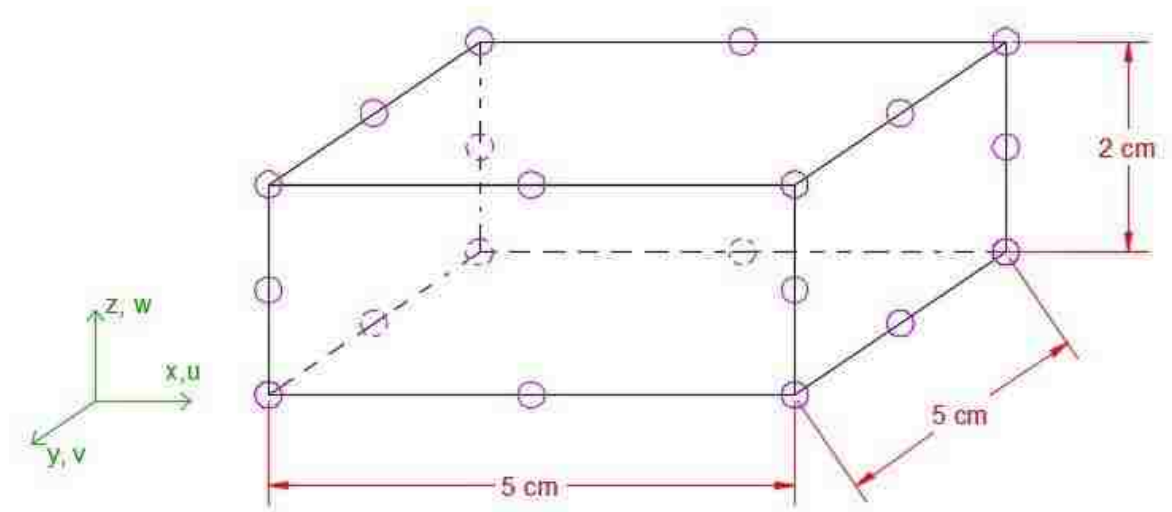

Figure 25: Representation of the Finite Element used, its dimensions, its nodes and the DOF`s for each node - piezoelectric layers

In this model, as it can be seen in Figure 26, each piezoelectric layer has 100 elements, in a total of 200 elements and 2056 nodes, therefore 8224 DOFs are analyzed.
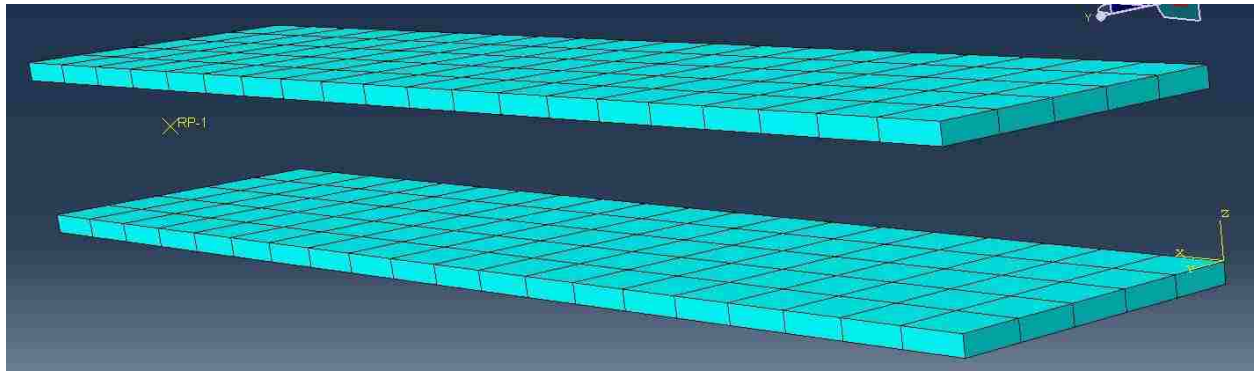
64

Figure 26: Mesh of brick type finite elements of the piezoelectri layers of Abaqus

As for the rubber beam component, the reduced integration technique is not used here in these elements modeling.

6.1.6   Boundary conditions

6.1.6.1   Mechanical boundary conditions

The mechanical boundary condition for this beam is of the type "encastre" (fixed end), where all displacements for the nodes are restrained, as it can be visualized in Figure 27:
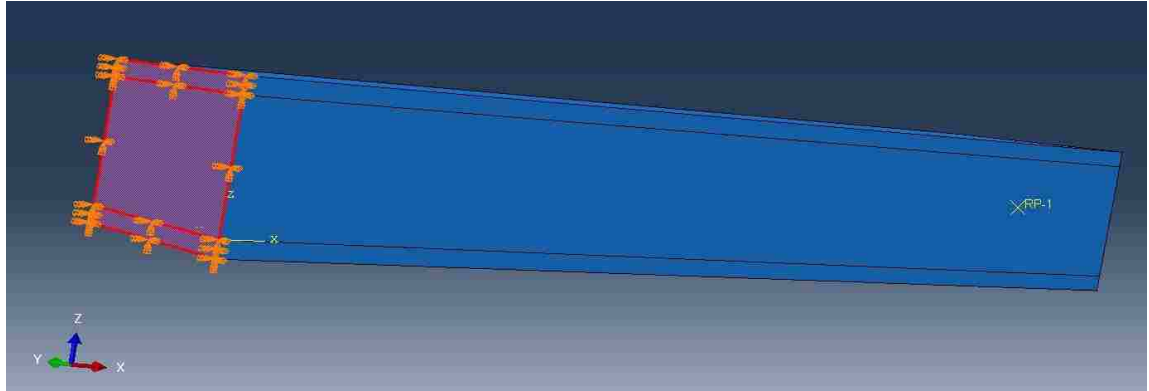
65

Figure 27: Mechanical boundary condition - fixed end cantilever beam. The constraints are applied to all the nodes on the red surfaces.

6.1.6.2 Electrical boundaries condition

For this type of analysis, due to the presence of electrical properties and behaviors, it is necessary to input a boundary condition (BC) for the electric potential. This has to be applied on a node of the surface of contact between the piezoelectric layer and the rubber beam, which represents where the electrical potential is zero. This BC is shown in Figure 28:
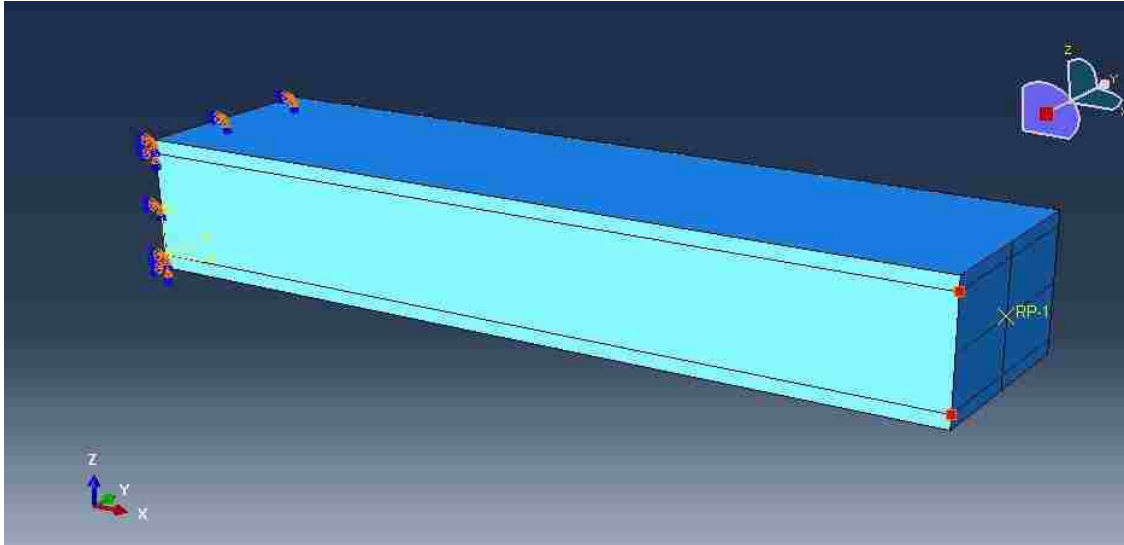
66

Figure 28: Electrical boundary conditions – one red node for each piezoelectric layer where is imposed EPOT=0

6.1.7   Loads

The loads applied to the FE model are applied in the way shown in Figure 4, in Chapter 2, one concentrated load and one moment load. They are shown again in Figure 29, now in the FE graphical interface, interacting with the model beam.
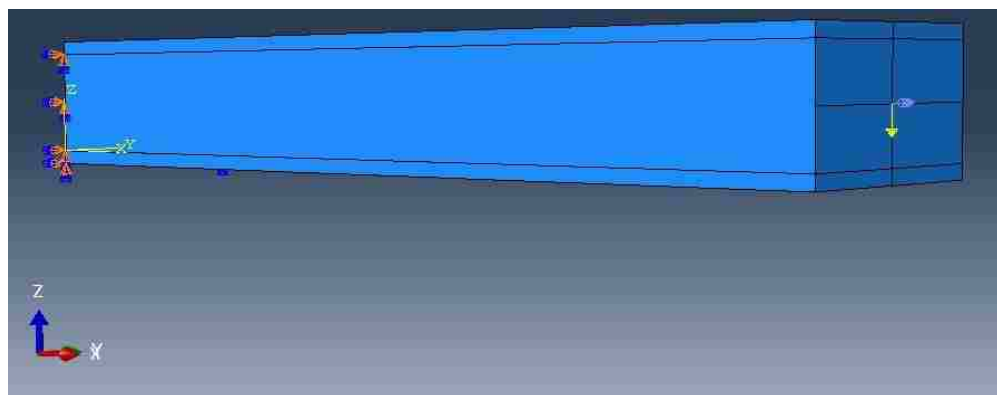

Figure 29: Loads in the Abaqus model - yellow arrow represents concentrated load, purple arrow represents moment load

At the free end of the beam, a shell element is added to the surface, so the loads cause displacements and rotations of the whole surface, not only at one point of application, as shown in Figure 30. This element is determined as a rigid body in Abaqus, therefore no internal stresses and displacements are considered and all the forces acting on it also act on the rubber beam and piezoelectric layers.
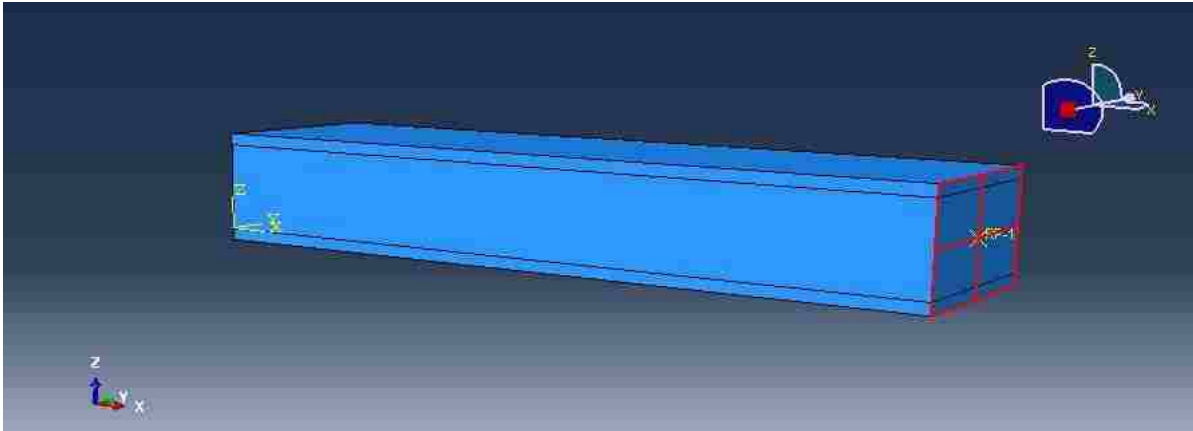

Figure 30: Surface marked in red showing the shell element added to the beam

To ensure that the different components of the structure – rubber beam and piezoelectric layers – have compatible and consistent response to the loads, they are constraint together with the use of "ties" in Abaqus. The different ties used are shown in Figure 31.
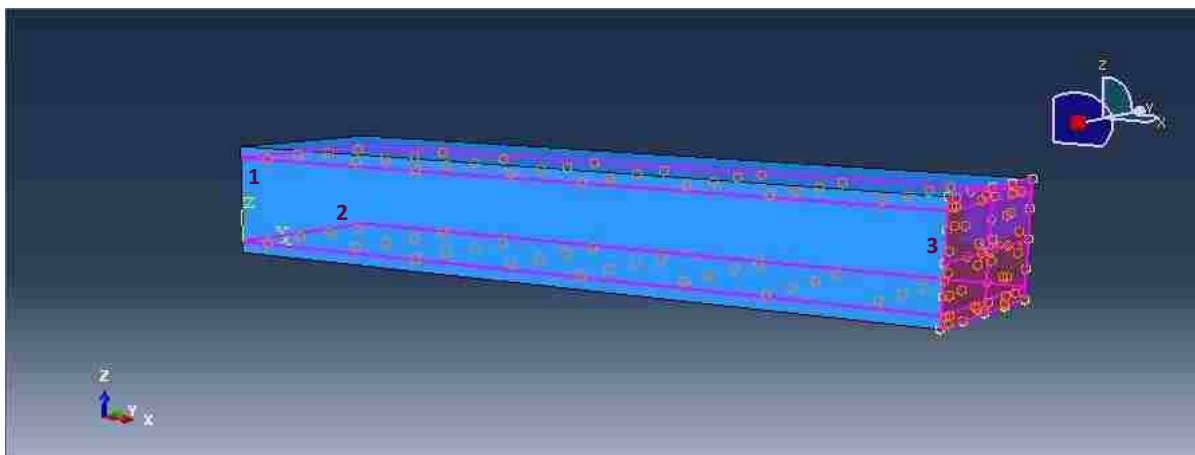

Figure 31: Ties constraints on FE model. 1- tie between rubber beam and top piezoelectric layer 2- tie between rubber beam and bottom piezoelectric layer 3- tie between rigid body (shell element) and rubber beam

68

The loads shown in Figure 29 are used for both static load application and later for dynamic load application as well, as explained in following sections.

6.1.8   Model validation

It is important for every scientific work to have a valid model for the analysis, especially for numerical models. Having this is mind, it is proposed a fast verification of the model made in Abaqus through the comparison with a known theoretical formula. Therefore, it is proposed the comparison of the displacement at the free end of the beam, only considering – at first – the mechanical model with the rubber beam structure. Figure 4, presented previously, indicates the closed form configuration considered for the beam.

The formulas used for the hand calculation analysis are:

$$U = \frac{PL^3}{3EI} \qquad\qquad (42)$$

For displacement due to the concentrated force and

$$U = \frac{ML^3}{2EI} \qquad\qquad (43)$$

For displacement due to moment

The values used for these formulas are determined in Table 24:

69

Table 24: Values used on Equations 44 and 45

	Value	Unit
L	1	m
E	50	MPa
P	100	N
I	$1.43 \, x \, 10^{-4}$	m^4
M	20	Nm

Table 25 shows the comparison results of the two obtained values:

Table 25: Comparison of displacement values obtained with Abaqus and Theoretical equations

	Abaqus	Theoretical equations
Displacement U (mm)	5.930	6.065

The difference between the two values is 2.23%, which is an acceptable difference and the model can be considered validated. This type of verification is also performed in a fast manner throughout the different iterations of the model design, with different loads, dimensions and properties of the beam, in order to make sure that the mechanical model is working perfectly before inserting the piezoelectric properties into the analysis.

70

6.1.9 Static load analysis results

The final goal of this work is to perform a dynamic analysis with the wind loads. However, to further validate the model, a preliminary static analysis is performed, adjusted and calibrated so that the model response is manifesting the expected behavior.

The static load is applied as explained in Chapter 2.

The following figures show the final Abaqus results for the static analysis, considering the properties and parameters described beforehand.
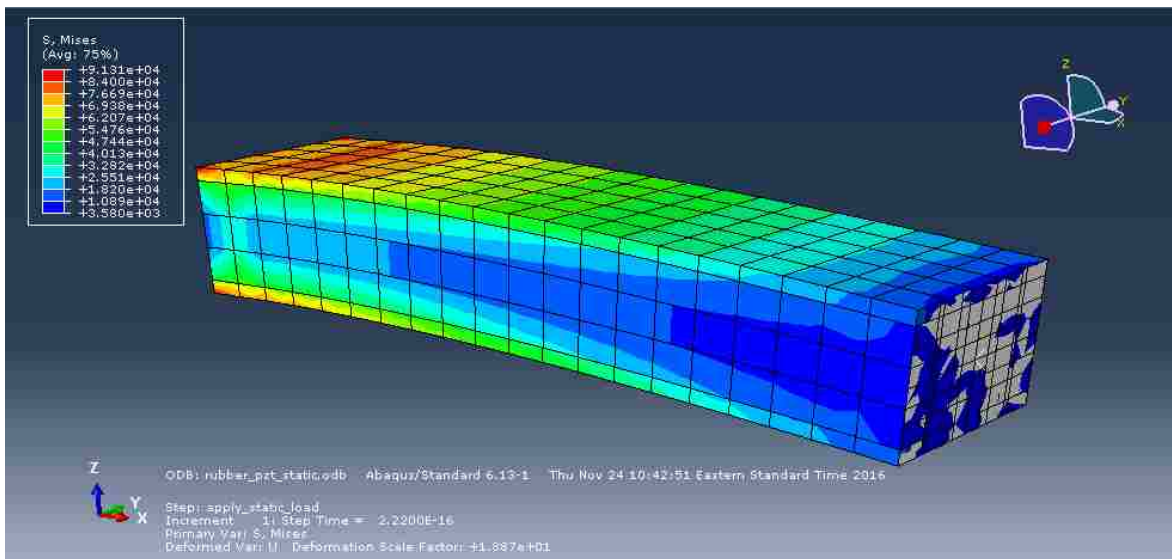

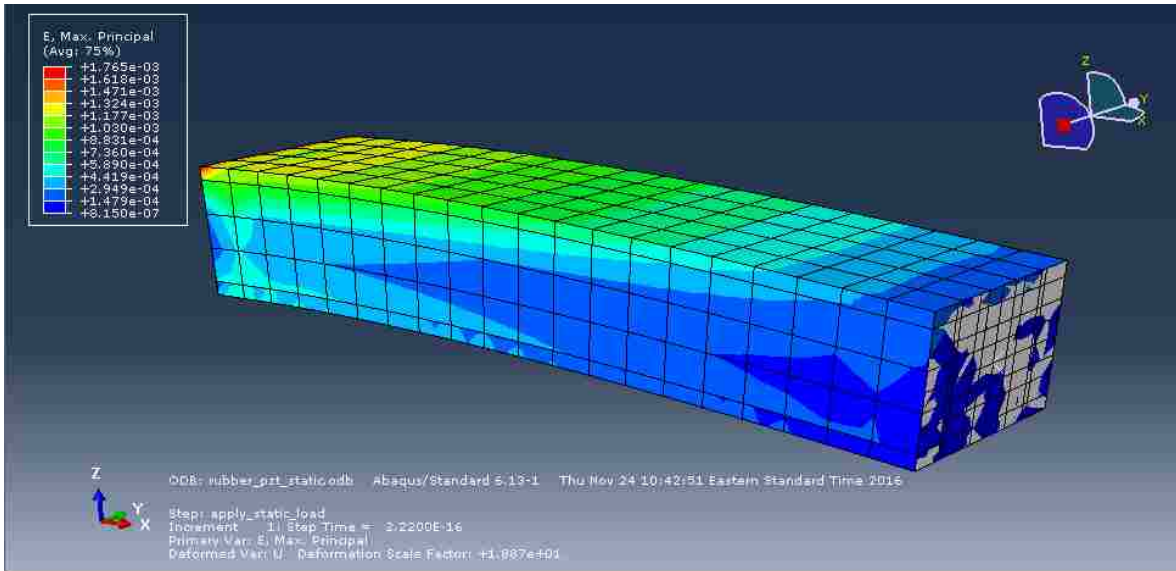*Figure 32: Stress S for the static load beam model*

71

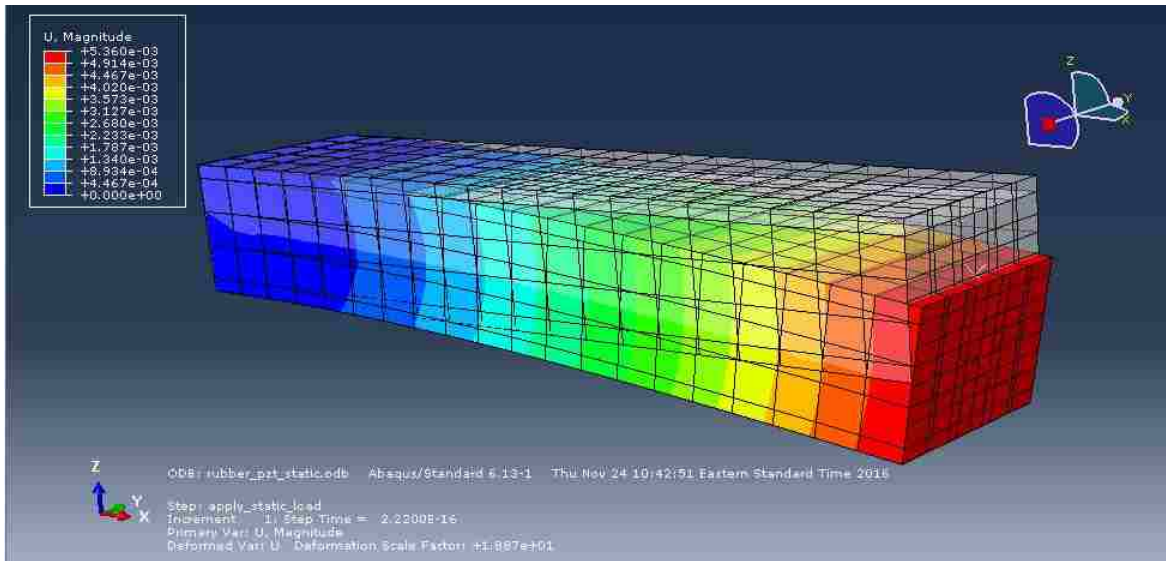*Figure 33: Strain E for the static load beam model*

Figure 34: Displacement U3 for the static load beam model – showing the non-deformed shape as well
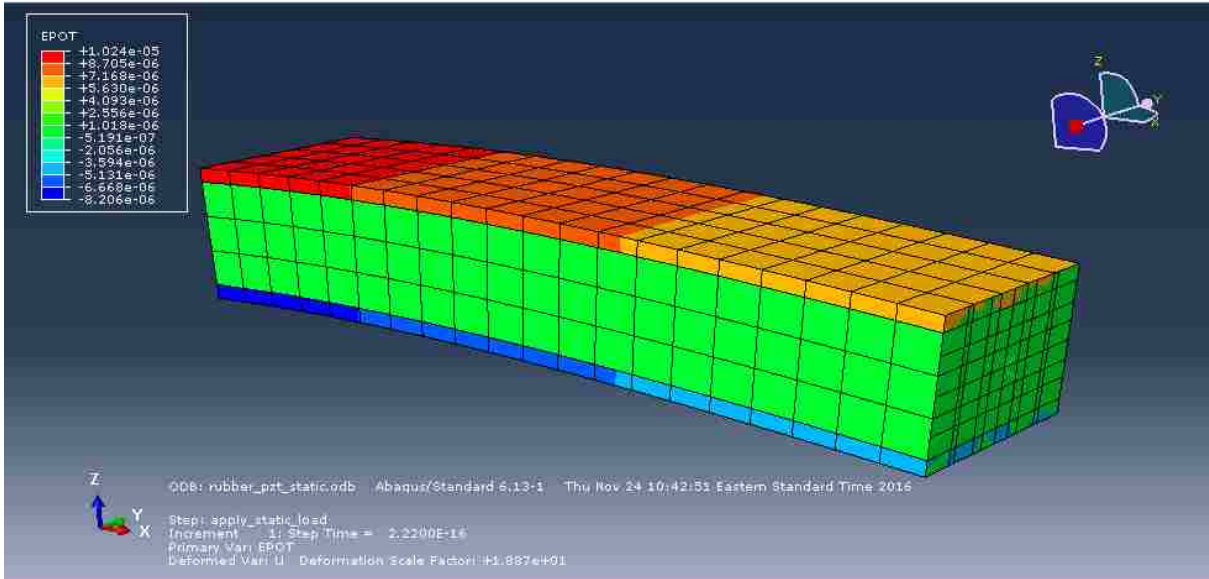
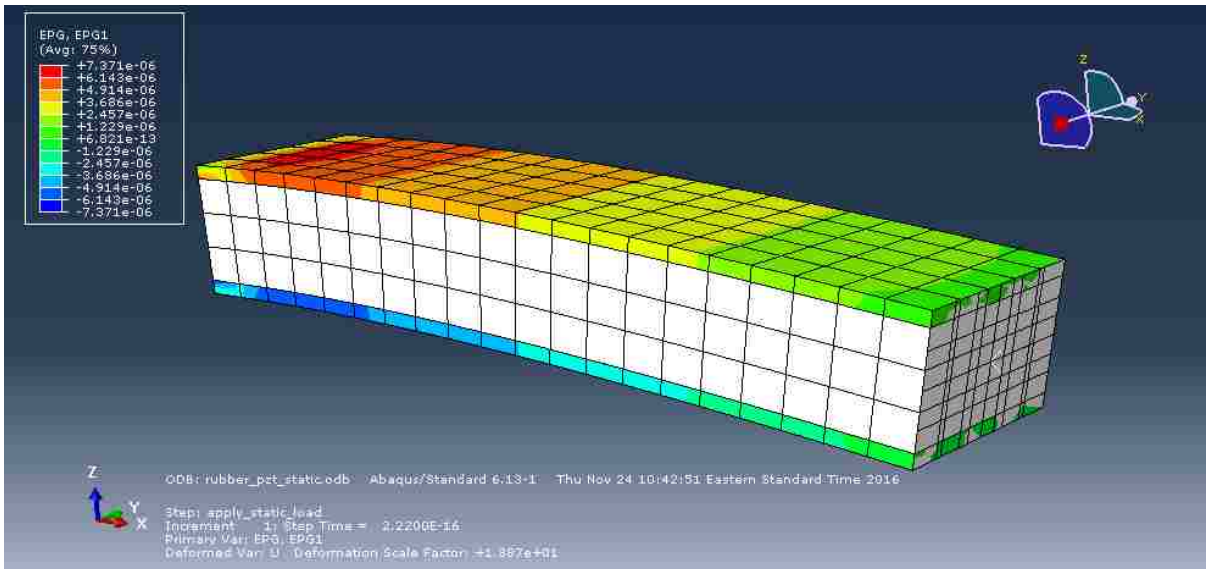*Figure 35: Electrical Potential EPOT for the static load beam model*

Figure 36: Electrical Flux on direction X EPG1 for the static load beam model

With the analysis of Figures 32 to 36, it can be seen that these results are consistent

with the expected results from engineering analysis. It is important to mention the specific

analysis of the EPOT value in Figure 35, with the essential points described below:

73

- EPOT varies linearly with the tension. It is larger in proximity of the supports, where the axial tension is also larger and having its peak value very close to the support.

- For this static load, which acts from top to bottom along axis Z, the EPOT on all the finite elements on the top piezoelectric layer has positive values and all value at the bottom layer has negative values.

- The order of magnitude of this output is consistent with what is found in the references used for this work, including [3].

Additionally, Figure 36 shows that EPG1 is consistent with those of EPOT, varying linearly from the tip to the fixed end of the beam. However, the electrical flux EPG1 is acting in direction X, which causes the EPOT to exist in the direction Z. In the analogy of Table 10, it can be observed that this directions relate to each other in the same way that the displacement U3 is related to the axial tension σ on the beam as mentioned in section 6.1.3.

6.2   Dynamic load model

Considering the static load analysis complete and accurate in its results, as showed in the previous section, the next step is the input of dynamic loads, to perform a dynamic analysis of the structure.

74

6.2.1 Model properties

The dimensions, material properties, BC, finite element properties and load application points are kept the same as in the static load model, with some extra input added, as shown in Table 26:

Table 26: Density for rubber and piezoelectric materials

Component	Structural beam	Piezoelectric layers
Material	rubber	PZT- 5A
Density (kg/m^3)	2900	7750

6.2.2 Loads

For this step, the dynamic load is inputted in Abaqus, with the input being the values shown for $f(t)$ in Figure 10 for the concentrated force. Together with this value, the moment caused by the application of the force in the device is inputted, with the value of d * $f(t)$, where "d" is the lever arm, as described in Chapter 2. Therefore, Abaqus works here with 513 x 1 different values over time for the force and 513 x 1 different values for the moment.

6.2.3 Dynamic load analysis results

The type of analysis for this step is "dynamic,implicit", where a time-history analysis is performed. The Abaqus procedure for the dynamic analysis works as follows: all the 513 values for each concentrated load and moment are inserted as input and Abaqus performs a time-step analysis using HHT integration over time and stores the output. For every step, one frame as the ones shown in Figures 30-36 is obtained. For illustration of the dynamic results, one node is selected, displayed in Figure 37, and the graphs relative to Electrical Potential (EPOT), Displacement in direction Z (U3), Stress (S) and Strain (E) are printed in Figures 38-41:
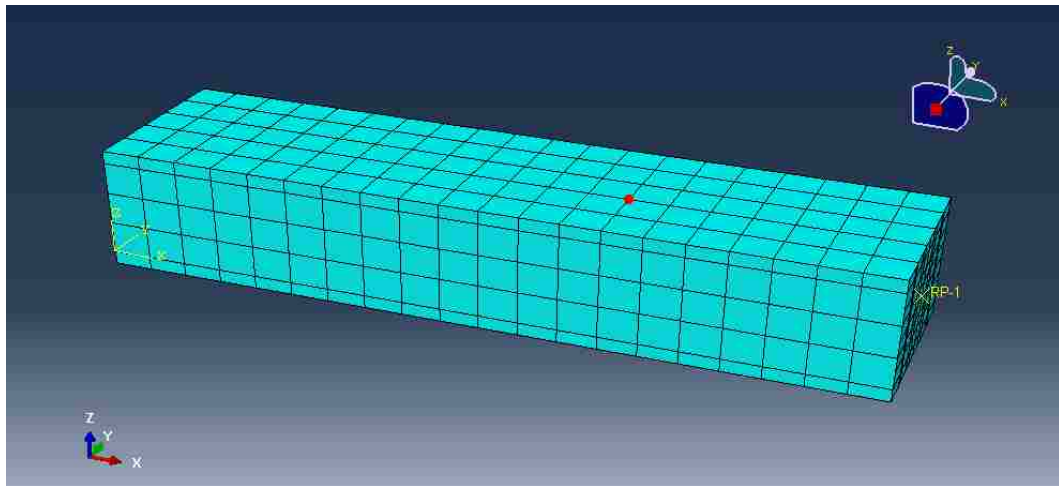

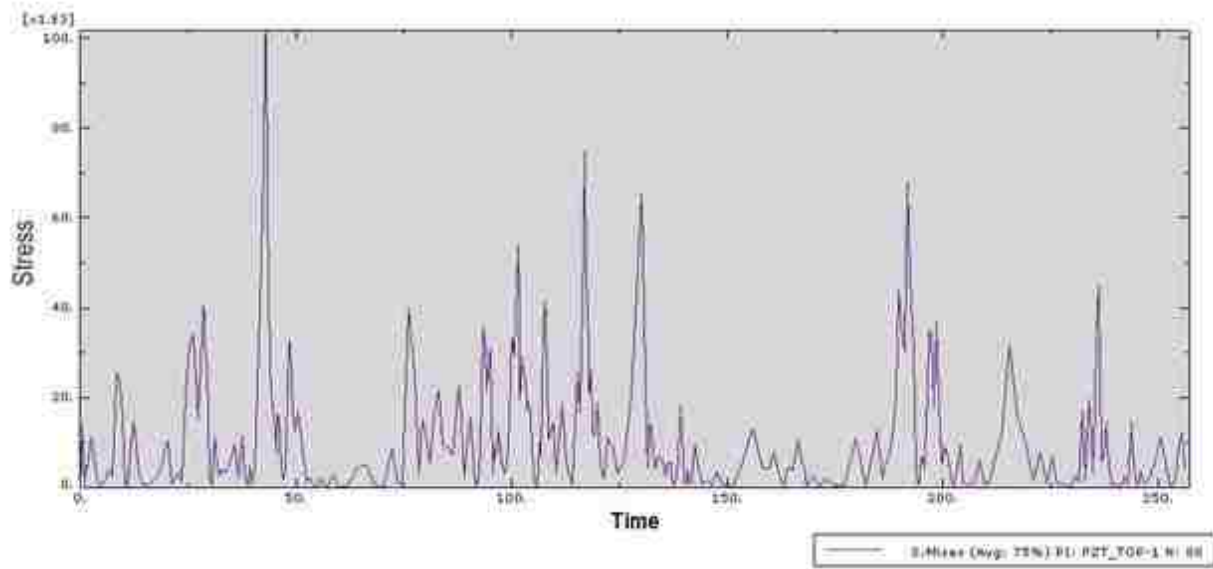*Figure 37: Node selected for the output display for the dynamic load model*

Figure 38: Time-history of Von Mises Stress S for the dynamic load beam model
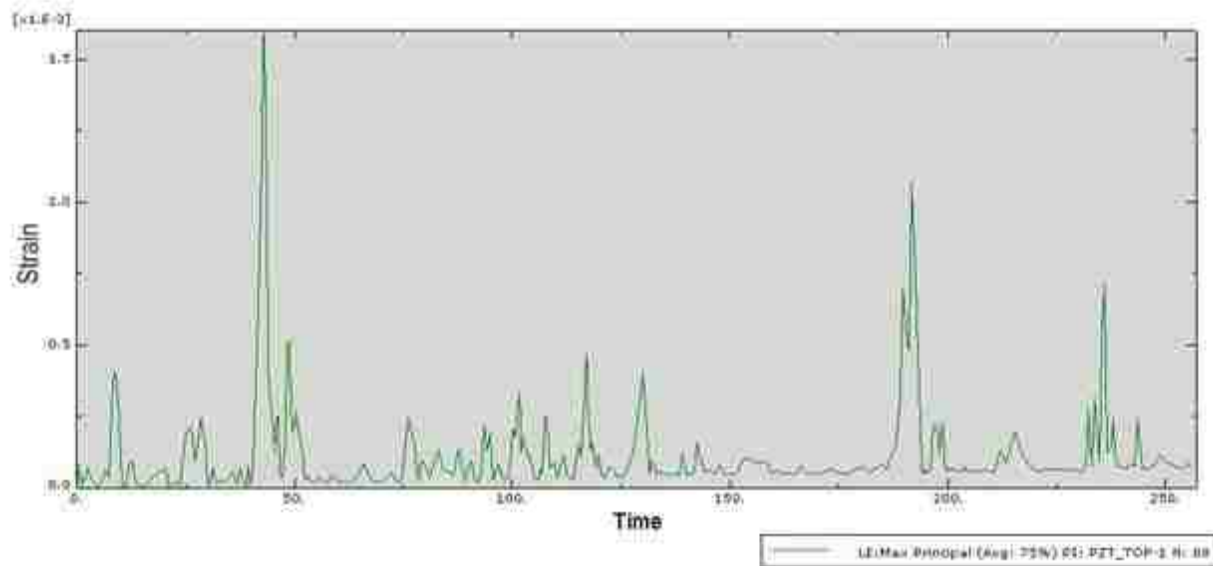

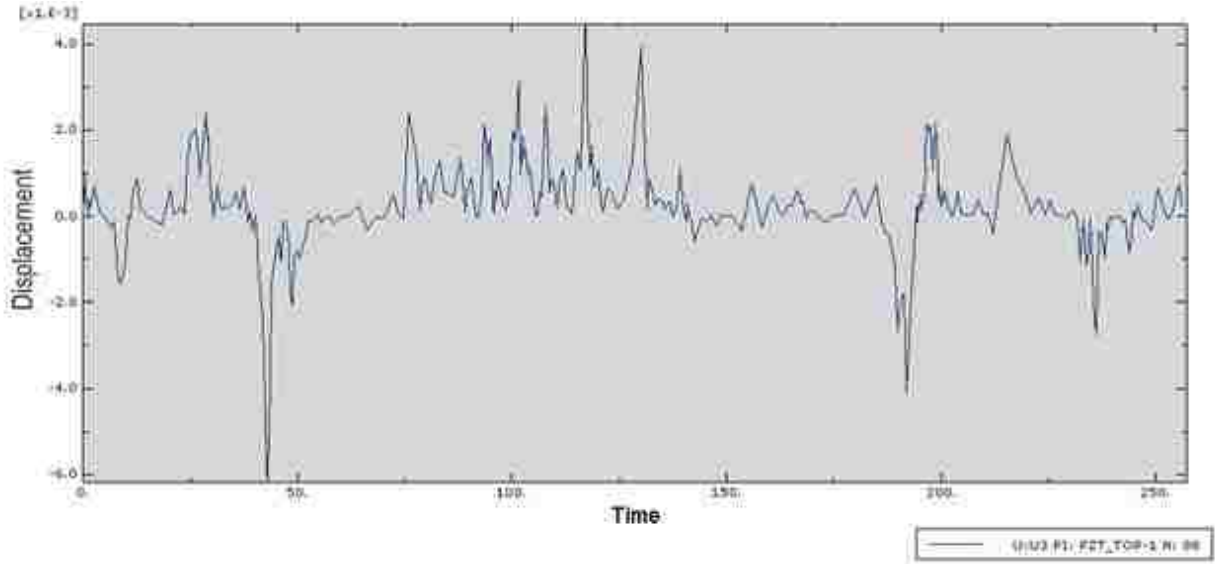*Figure 39: Time-history of the absolute Strain E for the dynamic load beam model*

77

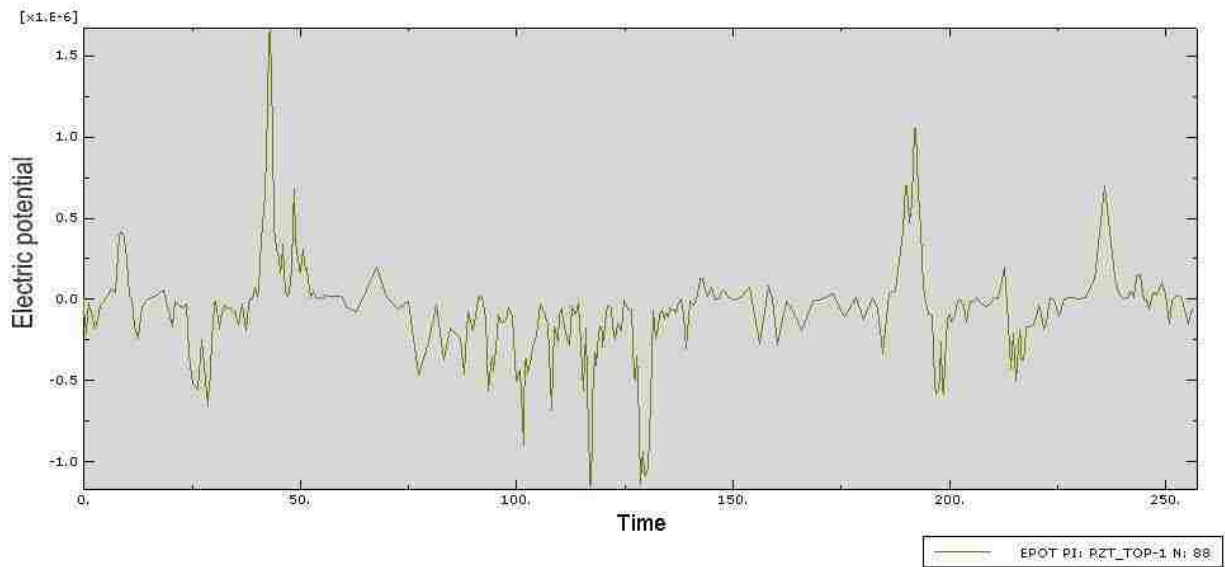*Figure 40: Time-history of Displacement U3 for the dynamic load beam model*

Figure 41: Time-history of Electrical Potential EPOT for the dynamic load beam model

78

6.2.3.1 Comparison of PZT-5A and PZT-5H

Figures 42 shows the electrical potential obtained for the same structure, for one wind load sample, with different coupling piezoelectric properties. Figure 42 a) shows the values obtained with PZT-5A and Figure 42 b) shows the values obtained with PZT-5H.
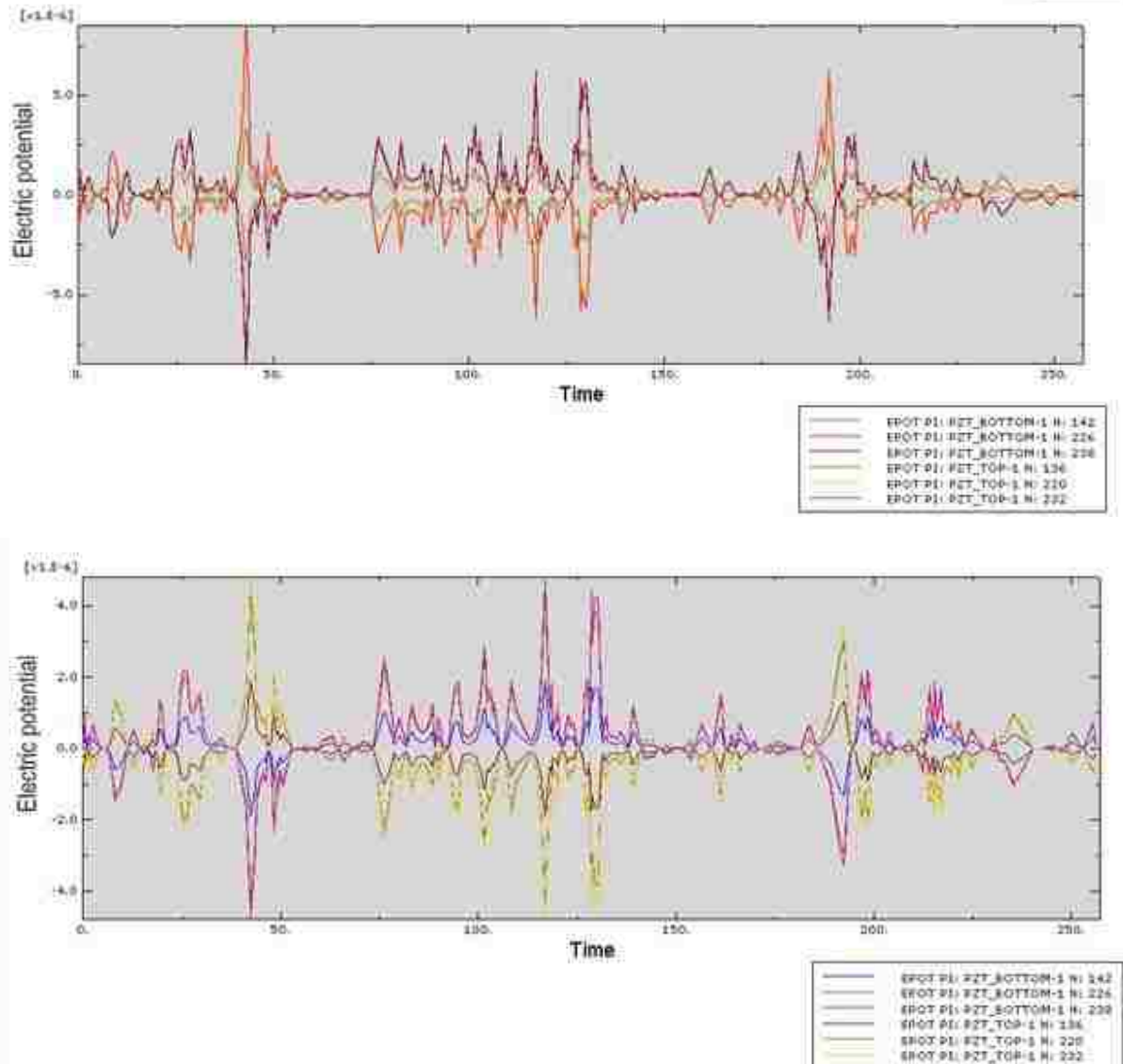

Figure 42: EPOT values obtained for one sample with a) PZT-5A b)PZT-5H

79

With a fast visual analysis, it can be seen that PZT-5A generates more electrical potential than PZT-5H, therefore PZT-5A is chosen as the studied material.

6.2.4 Output selection

As in all complex Finite Element Analyses, due to the ramification of Matlab/Abaqus, to the time, to the quantity of nodes of the structure and to the points of interest, considering the dynamic load and several samples, not all results given by Abaqus can be stored. Considering that, the following shows the nodes and outputs of interest from the FEM of the rubber and piezoelectric beam with wind loads.

The outputs stored from this analysis are the displacement and electrical potential. An initial attempt was performed to store also strain, stresses and electrical fluxes from each analysis. However, it was affecting negatively the processing time of the simulation and not adding value to the analysis, as these values were before analyzed and compared on the cube analysis, in the static load analysis and in the simple dynamic analysis of the beam and hence, they were removed.

6.2.4.1 Electrical Potential and Displacement

The outputs of interest are the vertical displacement of the beam (direction z), referred as U3, and, the main goal of this work, and the Electrical Potential, referred to as EPOT in Abaqus. These quantities are called nodal quantities, e.g., they take values at the nodes of the finite

elements of the analysis. The nodes used for reference, for both beam and piezoelectric layer parts, are presented in Figure 43 and 44.
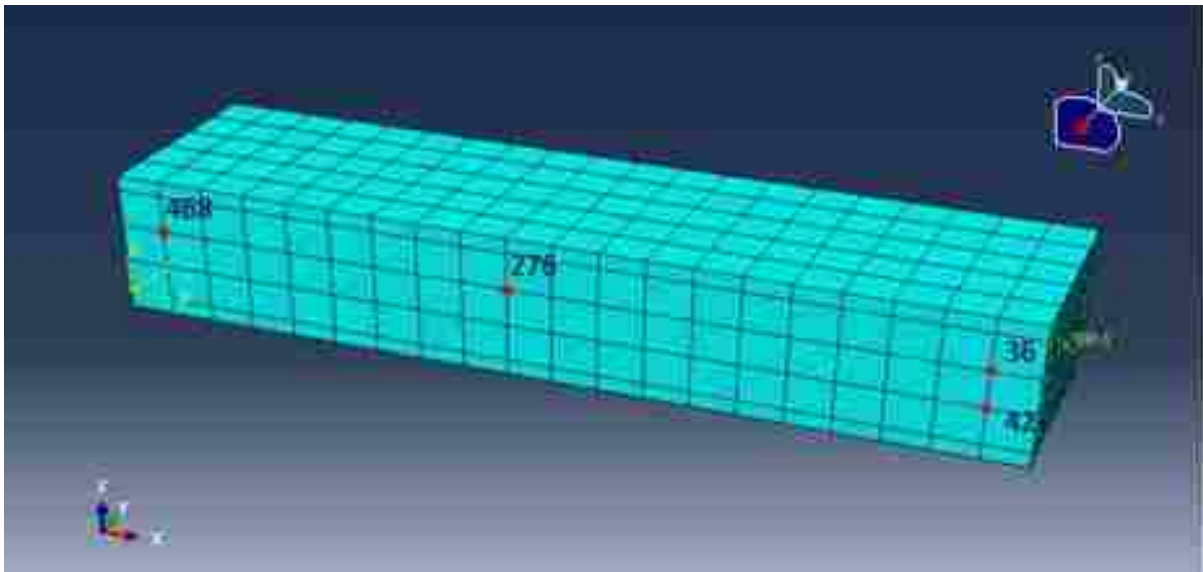

Figure 43: Identification of nodes used for output recording - rubber beam part

From Figure 43 it can be seen that four nodes were chosen to have their outputs registered from the rubber beam, for comparison and analysis of the displacements of the beam. The nodes chosen seen in the figure are nodes 36, 42, 276 and 468.
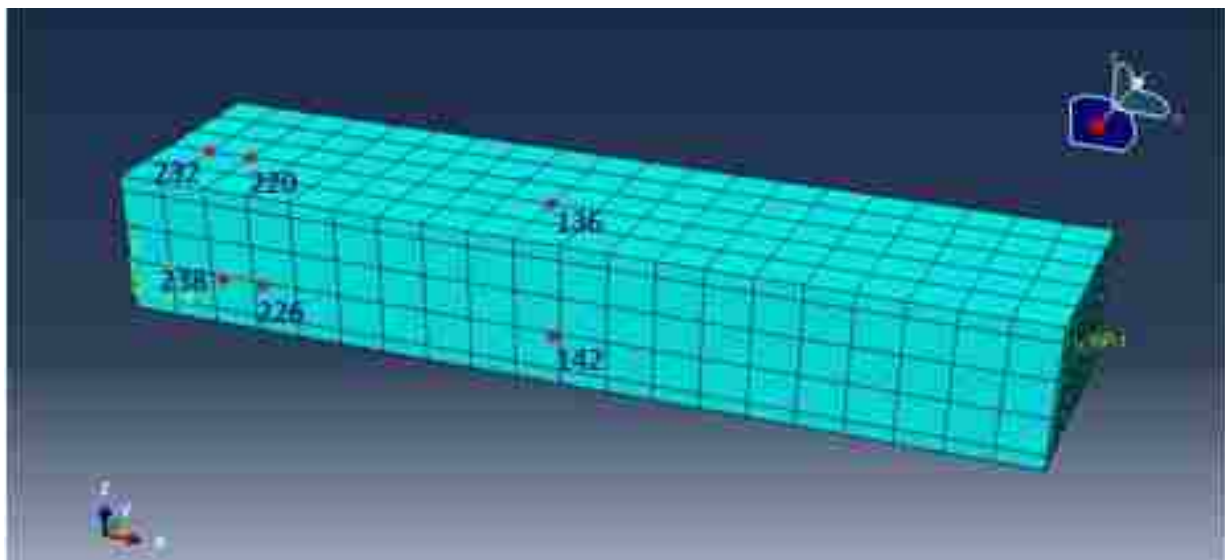

Figure 44: Identification of nodes used for output recording - piezoelectric element parts

81

From Figure 44, it can be seen that six nodes were chosen to have their outputs registered from the piezoelectric layers, top and bottom, for comparison and analysis mainly of the obtained EPOT. The points are closer to the supports, because this is observed as the region with largest strain due to the concentrated load, and, as covered before, the larger is the strain in the piezoelectric element, the larger is the Electrical Potential. The nodes chosen seen in the Figure are nodes 136, 142, 220, 226, 232 and 238. The points chosen are in the bottom and top piezoelectric layers of the beam, being placed at the same "x" coordinate. Figure 45 shows another angle of these nodes, for clarification on the positions.
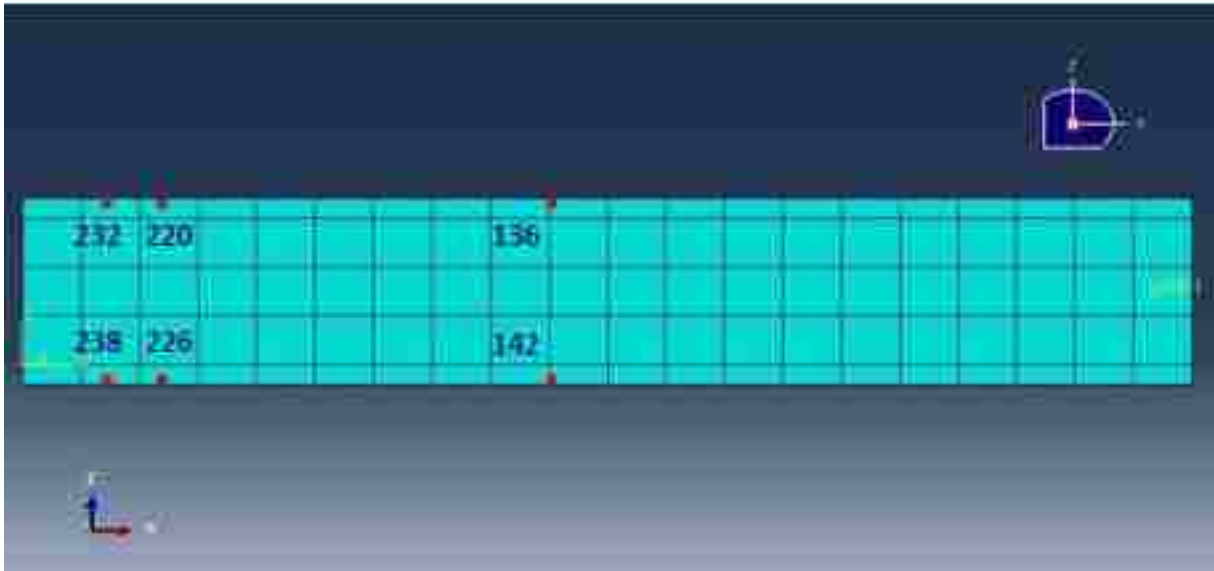

Figure 45: Identification of nodes used for output recording - piezoelectric element parts – in a different angle

Using these chosen nodes, the outputs are extracted and showed in the followings Figures 46 and 47:
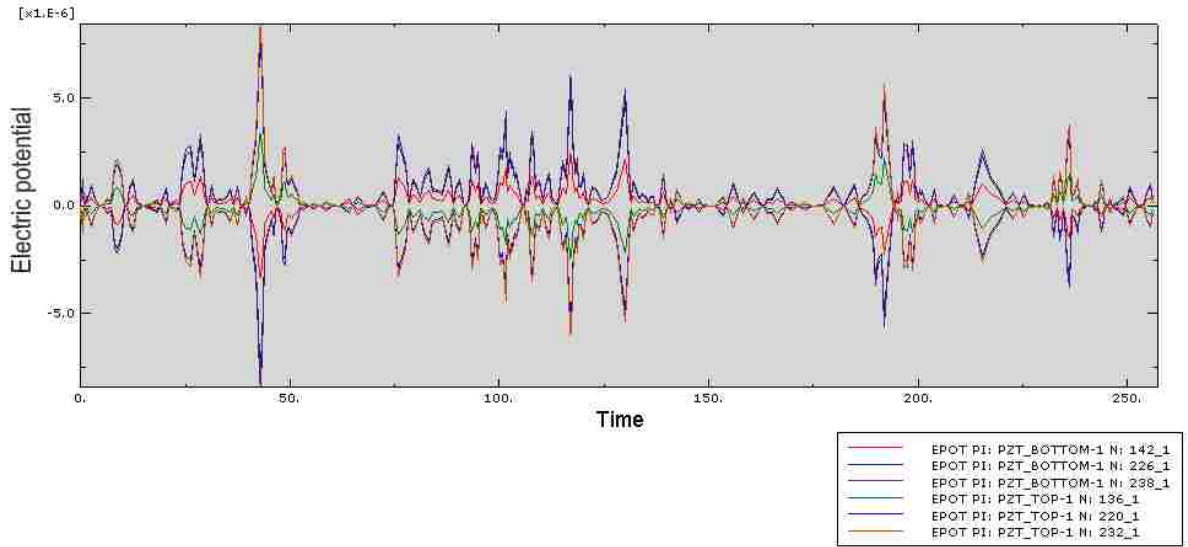
82

Figure 46: Time-history of electrical potential EPOT for the dynamic load beam model - six nodes
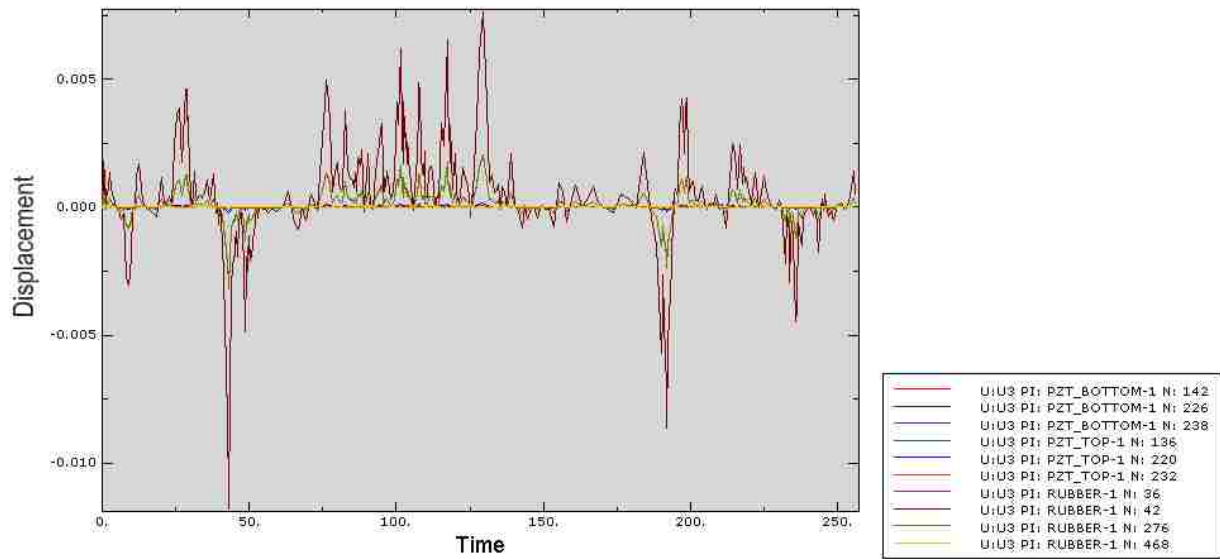

Figure 47: Time-history of displacement U3 for the dynamic load beam model - ten nodes

These graphs show consistent results with both the static analysis and with the type of load applied, following similar behavior regarding time variation.

83

6.3   Wind load application model with Matlab interaction

In this step, the same procedure explained on section 6.2 has to be executed. However, now the total quantity of loads being inputted each time in Abaqus is larger, more precisely, the load has to be inputted for 513 time steps x 590 samples, as explained in Chapter 3.

This is clearly impractical to accomplish by manual input of the loads in Abaqus and so software Matlab is used. The schematic in Figure 48 displays the steps of interaction between Abaqus and Matlab for this analysis.
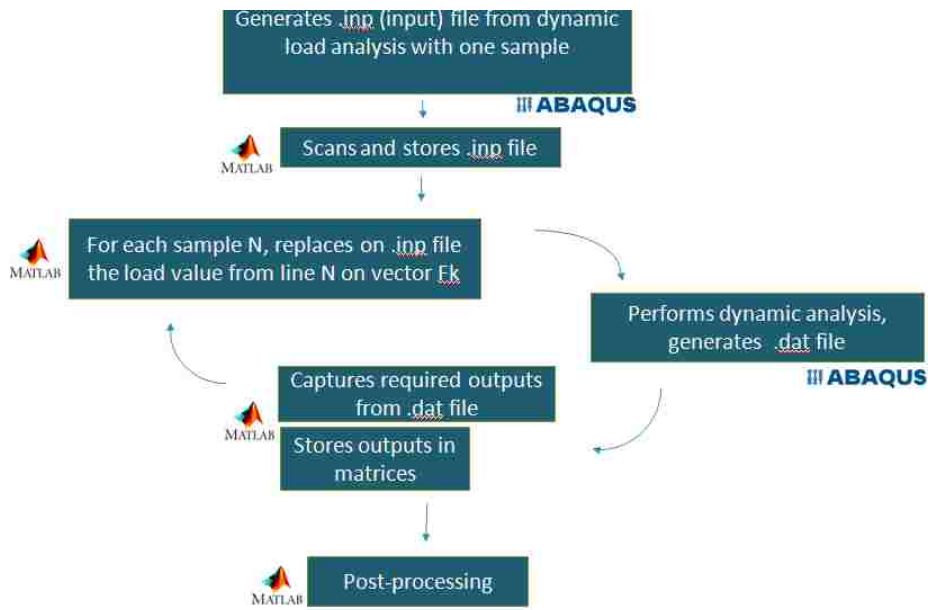

Figure 48: Schematic showing the interaction between Abaqus and Matlab

Figure 48 shows that Matlab is used to input in Abaqus the value f on the matrix 513 x 590, using Abaqus input file .inp. Matlab captures each of these input values, sends them to Abaqus, which does a structural analysis with the application of the determined load and

84

moment and releases a given output of interest (displacement at the tip U and electrical potential). Matlab then stores these outputs in a matrix, for post-processing of the user.

Due to the number of samples and interaction of this analysis, this clearly consumes a lot of processing time. For this work, server Aurora is used, from Dr. Paolo Bocchini`s reseach group at Lehigh University, due to the large numbers of core available for the analysis. Through a preliminary profiling, it was determined that eight cores of the twelve available are the optimal number of cores for this analysis, which run for 170 hours on Aurora for the 590 samples of continuous wind loads applied to the structure. The initial idea of this work was to run 10000 for the better characterization of the MCS. However, due to the large processing time this would take, 590 ended up being considered sufficient for the quality of the results.

All the same conditions for the Abaqus model showed in the previous section are kept, as well as the required outputs from the analysis. Additionaly, the time-step duration is captured in this analysis, for reasons explained later. Therefore, from the Matlab-Abaqus interaction, the required results are: Time-step, Displacement U3 and Electrical Potential EPOT. The results from this analysis are shown in the next section.

The previously mentioned outputs are stored in Matlab in 2D and 3D matrixes, considering the output from each node, in each time-step and from each sample. There are ten nodes analyzed, , for four of these nodes, one output is stored (the displacement) and for the other six two outputs are stored (i.e., displacement and electric potential). It is important to mention that, despite each sample of loads having 513 time-steps, the response of the structure has more steps than that. This happens because Abaqus automatically shortens the time-steps to values smaller than 0.5 seconds to improve the results. Therefore, the time-steps durations are flexible and vary from 0.000001 to 0.5 seconds. Hence, the outputs are obtained in a variable

85

quantity of time-steps, for example, 545, 560, 573, but they are all referring to the same time period of load application and structure response of 4.27 minutes

6.4   Finite Element Method Results

From this analysis, considering only the first sample, the following figures show the output obtained for the same nodes as in Figure 49 and 50, for comparison and validation of the Matlab analysis.
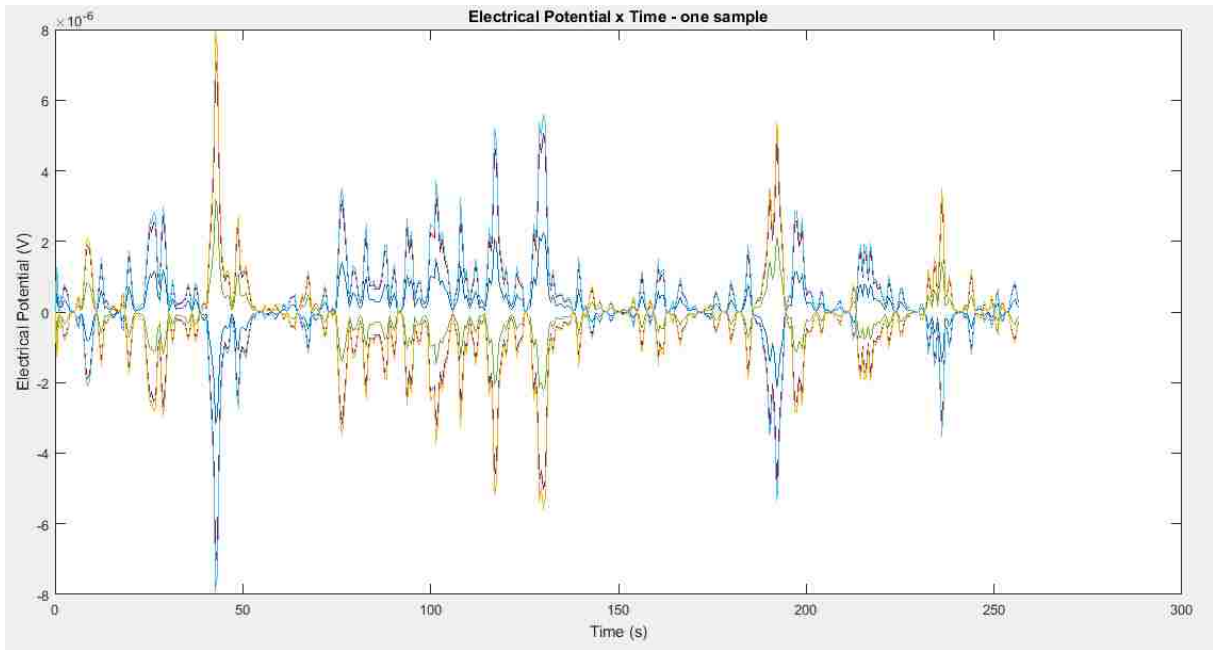

Figure 49: Time-history of electrical potential EPOT for the dynamic load beam model with Matlab interaction - six nodes
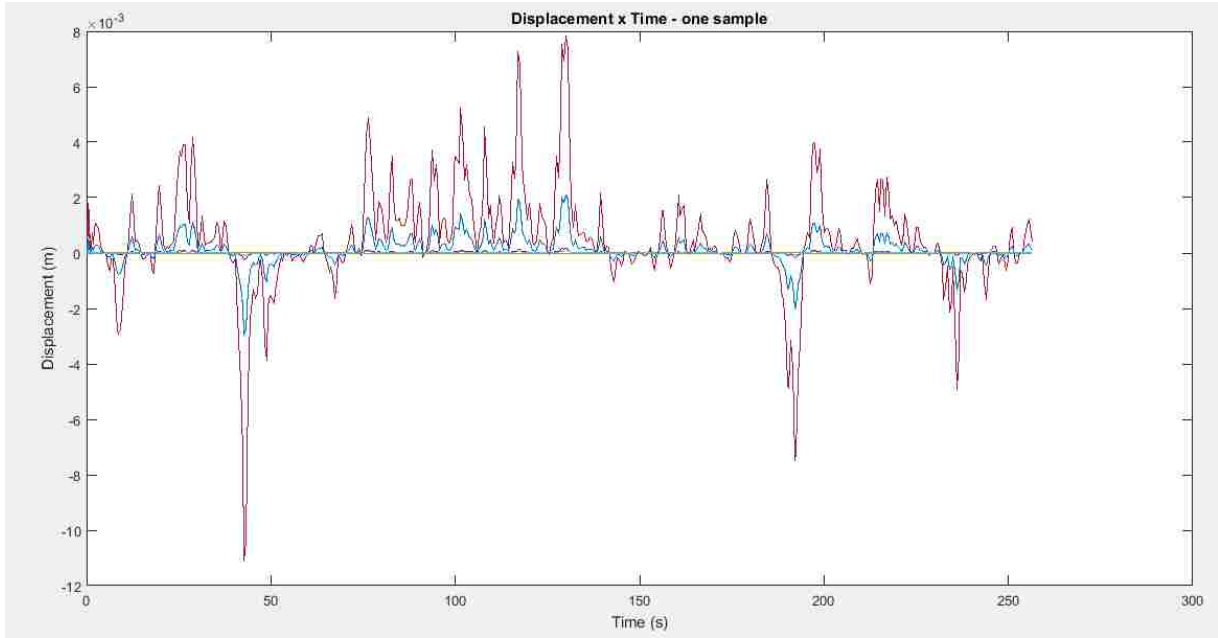
86

Figure 50: Time-history of displacement U3 for the dynamic load beam model

From these figures, it can be seen that the analysis matches the previous one using Abaqus and therefore the analysis can continue. There are some small differences observed and this can be caused by some aliasing on the data that may be happening in Abaqus plots.

Considering the first 100 samples of the analysis, a visual inspection is accomplished for in order to evaluate which nodes show the largest EPOT. Figure 51 shows the example of the EPOT distribution in sample 25, where is observed that the colors magenta and red always show larger values than the other nodes. These are the expected results, because these correspond to nodes 232 and 238, as shown in Figure 44.

87

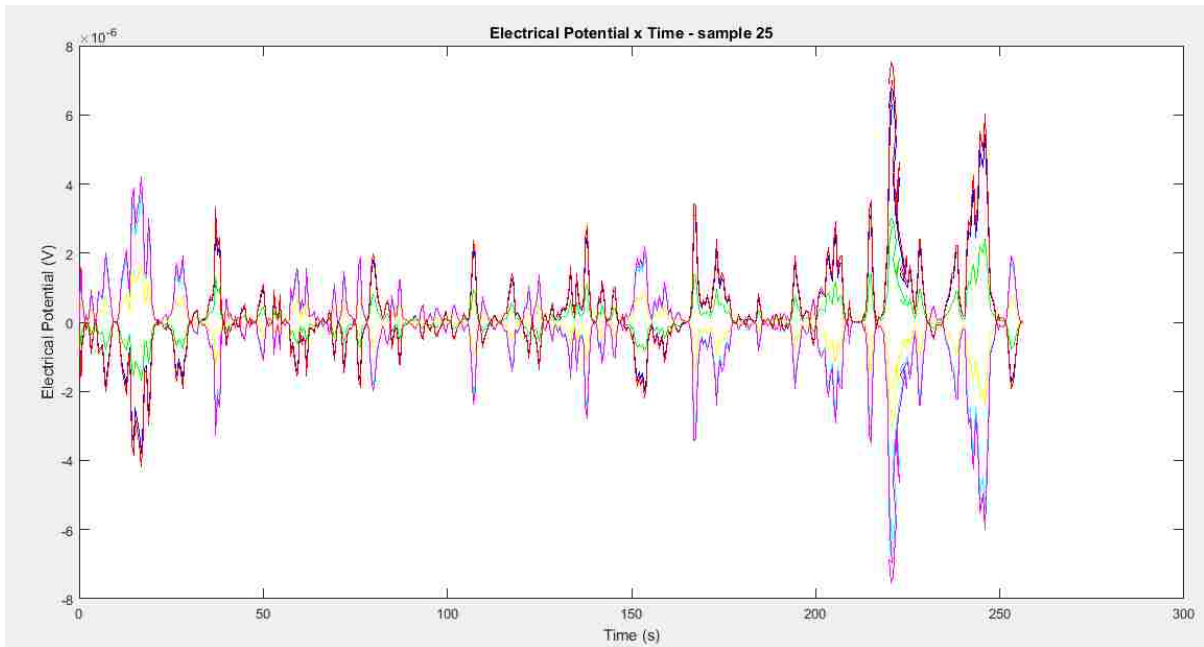*Figure 51: Time-history of electrical potential EPOT – six nodes on sample 25*

Considering that, Figure 52 displays only nodes 232 and 238 plotted separately. Figure 53 shows the plotting of 7 samples, just for visualization of the random behavior of the structural response, due to the random load.

88
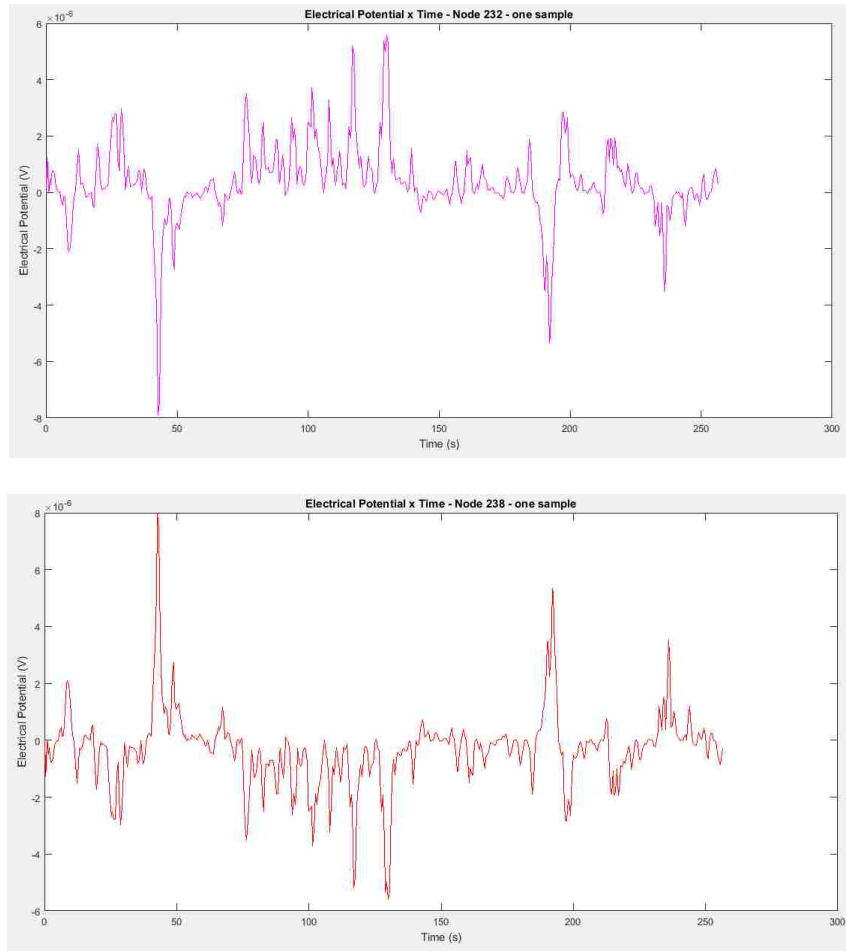
Figure 52: Time-history of electrical potential EPOT – one sample – Node 232 above and Node 238 below

89
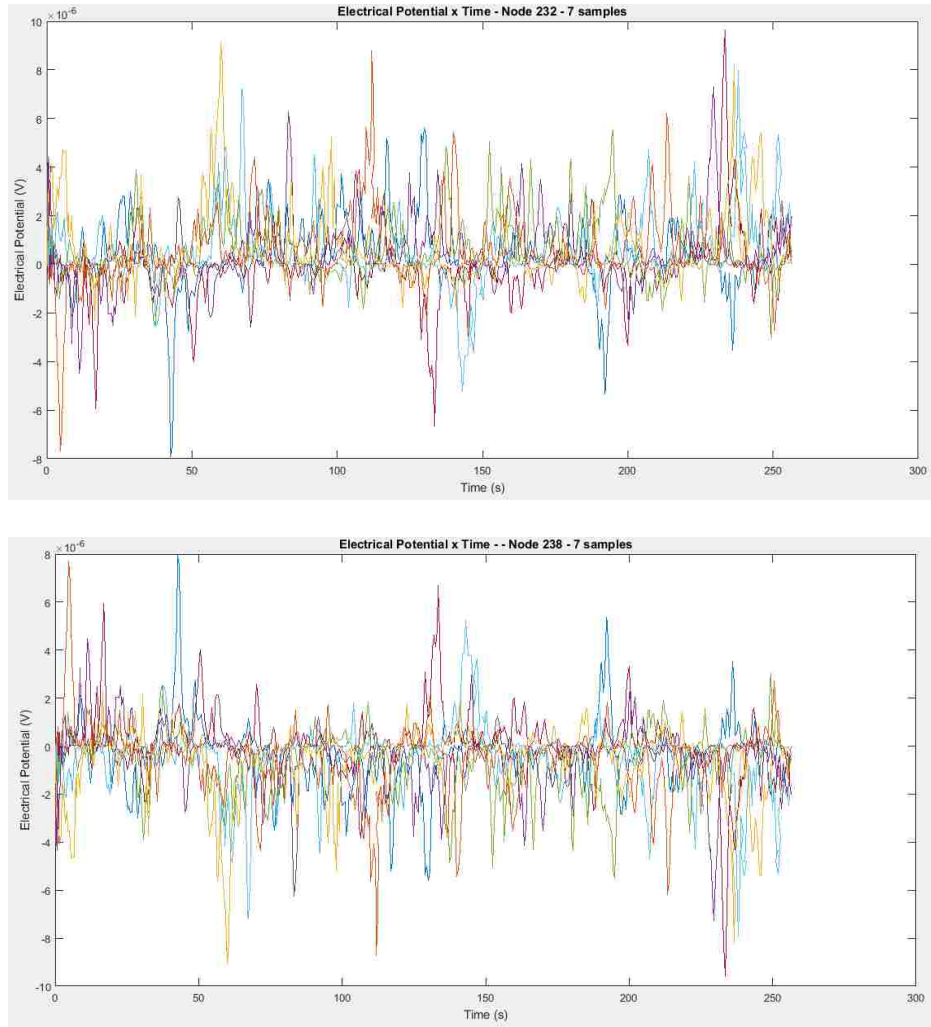
Figure 53: Time-history of electrical potential EPOT – 7 samples – Node 232 above and Node 238 below. Each color line represents one different sample

To obtain the voltage that supplies the circuit, the difference of electrical potential between nodes 232 and 238 is calculated. This value is shown for one sample in Figure 54:

90
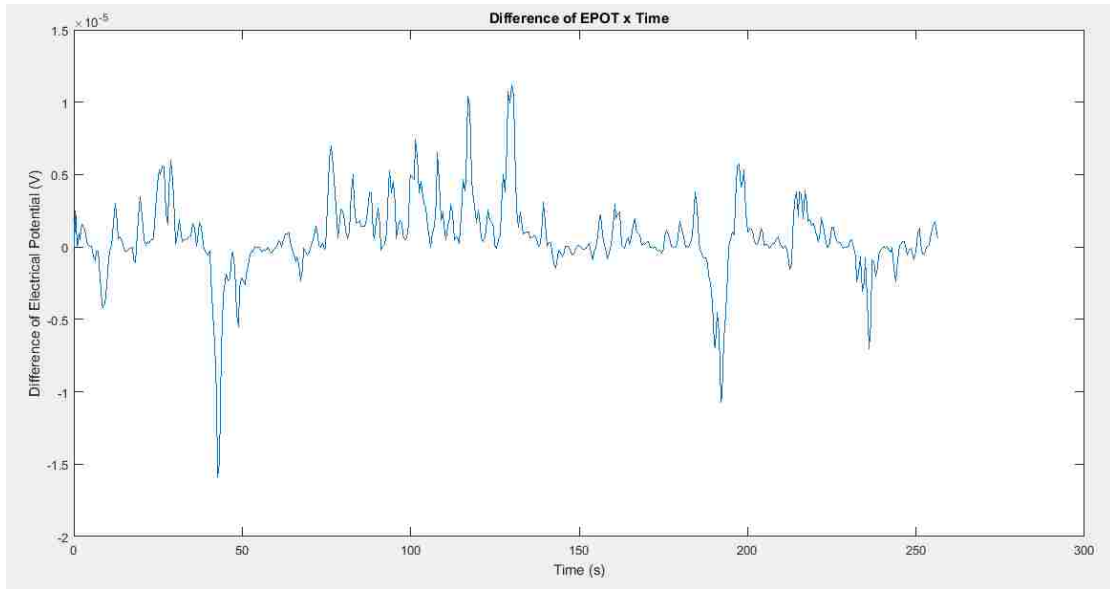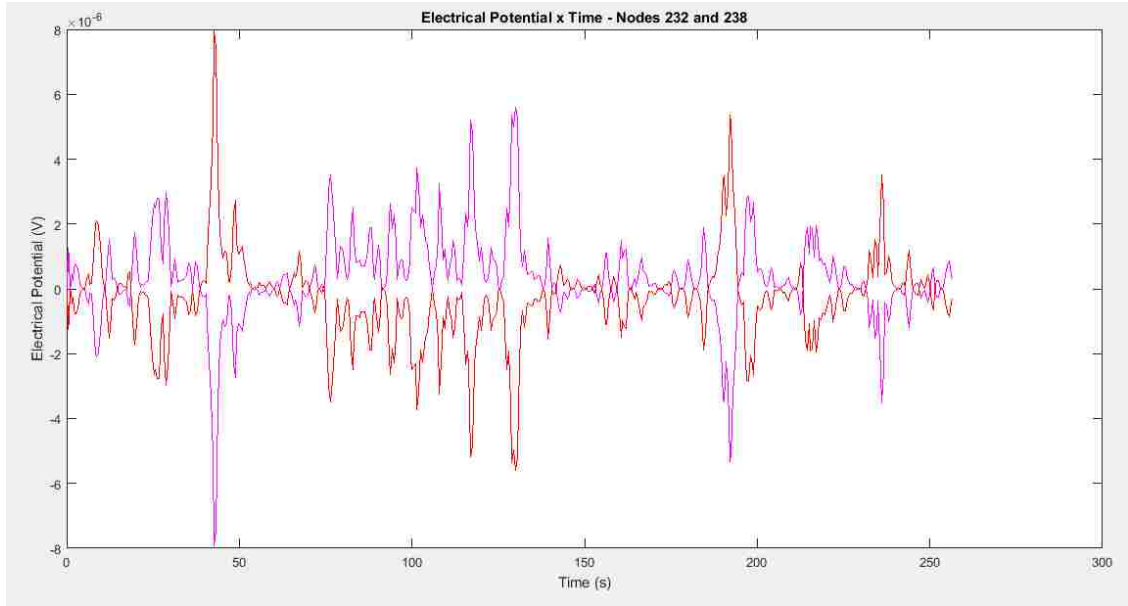
Figure 54: a) On top, the figure shows Nodes 232 and 238 plotted together – one sample b) At the bottom, the figure shows the difference between these values, which is the voltage difference generated by the harvesting device – variating with time – one sample

91

Considering all the 590 loads and structural response samples, which of them for total of 4.27 minutes of load, the Probability Density Function (PDF) of the difference of electrical potential values is plotted in Figure 55:
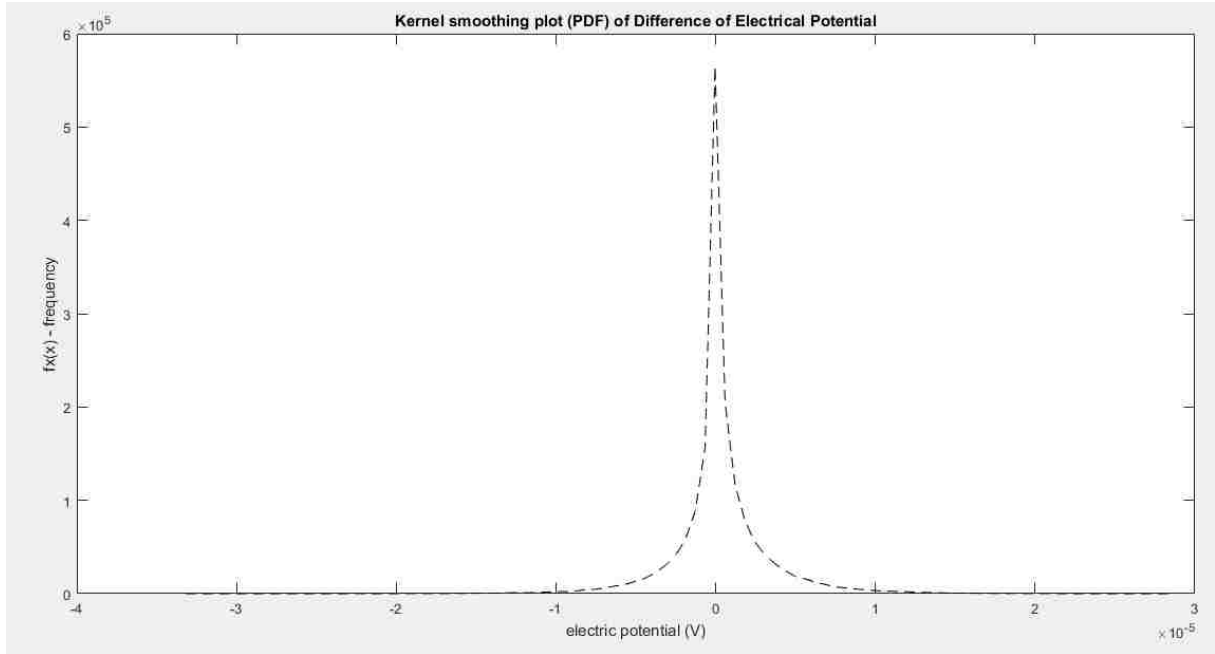
Figure 55: PDF of the difference of electrical potential

Analyzing Figure 55, it can be seen that the mean of the electrical potential is zero. This is the expected result because the beam oscillates upward as much as downward. The relevant data here is the excursion of the values, which can be seen to go further than $-3.2\ x\ 10^{-5}\ V$ and further than $2.8\ x\ 10^{-5}\ V$.

For the evaluation of the system in terms of its structural consistence, the displacement of the node at the free-end of the beam, Node 42 is also displayed. The time-history of the displacement for one sample is shown in Figure 56 and the PDF of the displacement is shown in Figure 57.

Figure 56: Time-history of displacement U3 – one sample – Node 42

93

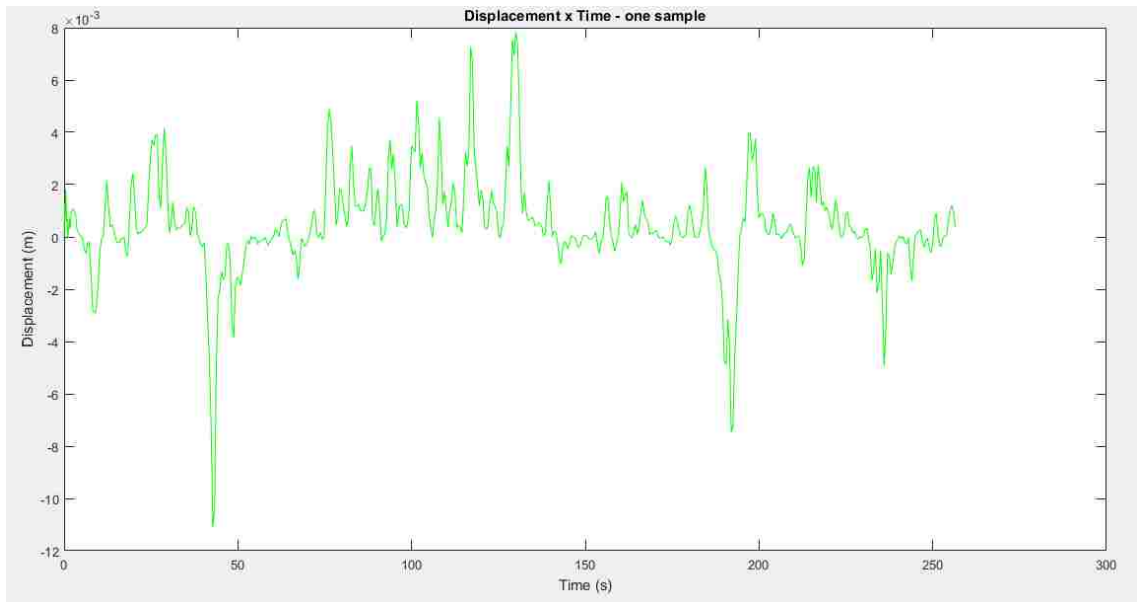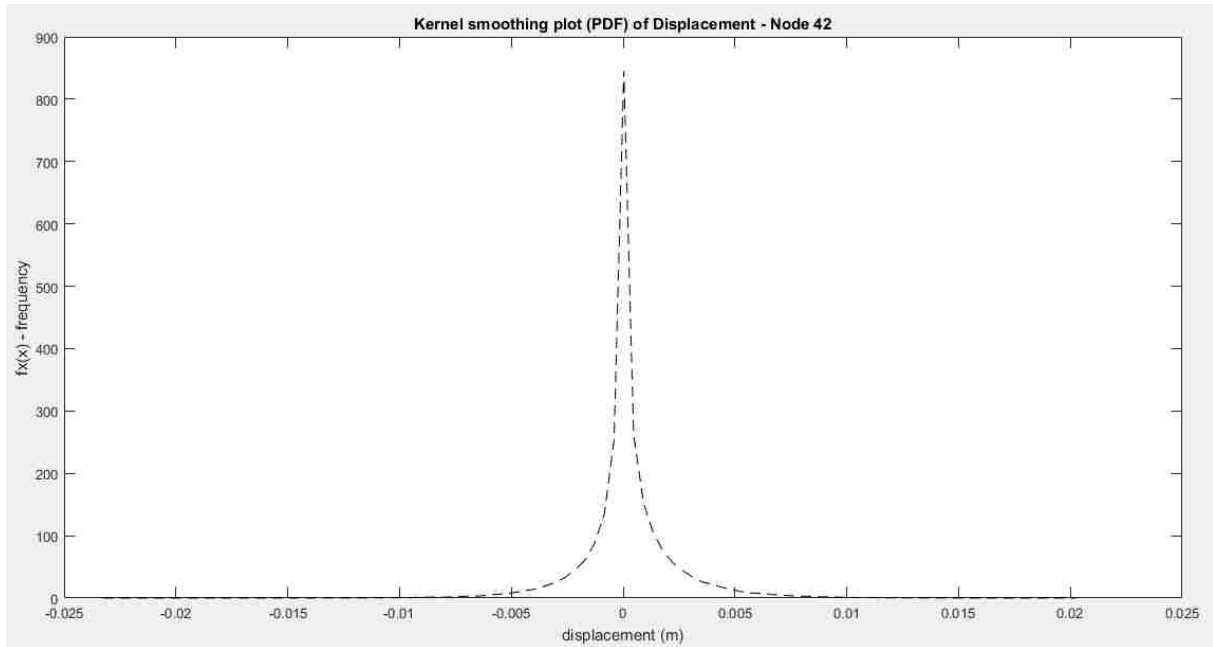*Figure 57: PDF of the displacement of Node 42*

Analyzing Figure 57, it can be seen that the mean of the displacement is zero. This is the expected result because the beam oscillates upward as much as downward. The relevant data here is the excursion of the values, which can be seen to go further than $-0.023\ m$ and further than $0.02\ m$.

94

7 Electric circuit

7.1 Electrical circuit

For the application and quantification of the electrical energy retrieved from the piezoelectric elements, it is considered here one theoretical example of a simple electrical circuit, into which the device can be connected. Figure 58 shows this circuit and the components of it are detailed.
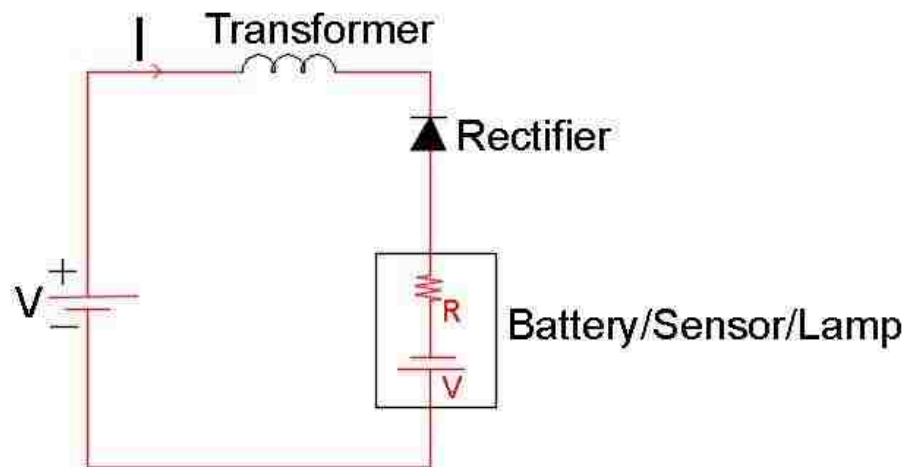
Figure 58: Basic representation of the electrical circuit

In Figure 58, there are four basic elements on a one-loop circuit. V is the voltage source, which is the piezoelectric device; a transformer is input in the circuit to boost the energy to the required voltage due to the fact that the voltage generated by the piezoelectric device is different than the resistor attached to it; after that, a rectifier can be seen, which exists because the energy generated is Alternating Current (AC) but the battery must be supplied with Direct Current

95

(DC), therefore the rectifier transform the AC current into DC. At last, the battery with its internal resistance is displayed, which is the main goal of circuit. The battery is considered to be supplied with the energy from the piezoelectric elements and after supplied, it is used for generation of clean electrical energy for diverse purposes.

7.2   Energy quantification

The end output required for the battery supply is the Energy from the piezoelectric generating device. Equation 44 shows the necessary inputs for the correct quantification [6].

$$E = \int_0^\infty \frac{V(t)^2}{R} dt \tag{44}$$

Where,

E = Energy obtained in the circuit, in Joule (J)

V = Voltage source in the circuit, in Volt (V)

t = time, in seconds (s)

R = load resistor, in Ohm (Ω)

The load resistor is part of the equation because the energy output from the harvester depends on configurations other than the achieved voltage. Generators are characterized by their voltage and power available. Therefore, as any other traditional generator, there is a maximum power that can be supplied to an electric system from the piezoelectric harvester

96

device and this value is important for the final output analysis. However, this is not a simple variable to be determined.

The analysis contained in [8] mentions that a similar study was produced as in this work, although not using FEM, but experimental data. In this scenario, the harvester was paired with a resistor to measure power output. The system was inputted to different frequencies of load and, with that, a curve of optimum load resistance testing was created and therefore, a simple power from the system could be assessed.

The load resistor considered for this work is for 1m of copper connected to the system, therefore $R = 1.68 \ x \ 10^{-8}$, according to [10]. While this load may not represent the possible systems for this harvester, it allows the device to be characterized. Investigating potential actions to measure the power with a FEM analysis where the maximum current and therefore power can be extracted from the system is a direction for future work, as well as creating an experimental environment for improvements on this research field.

Considering this value, the analysis continues with the adoption of Equation 46 for all the samples studied. Figure 59 shows the time-history of Power for one sample of wind load:
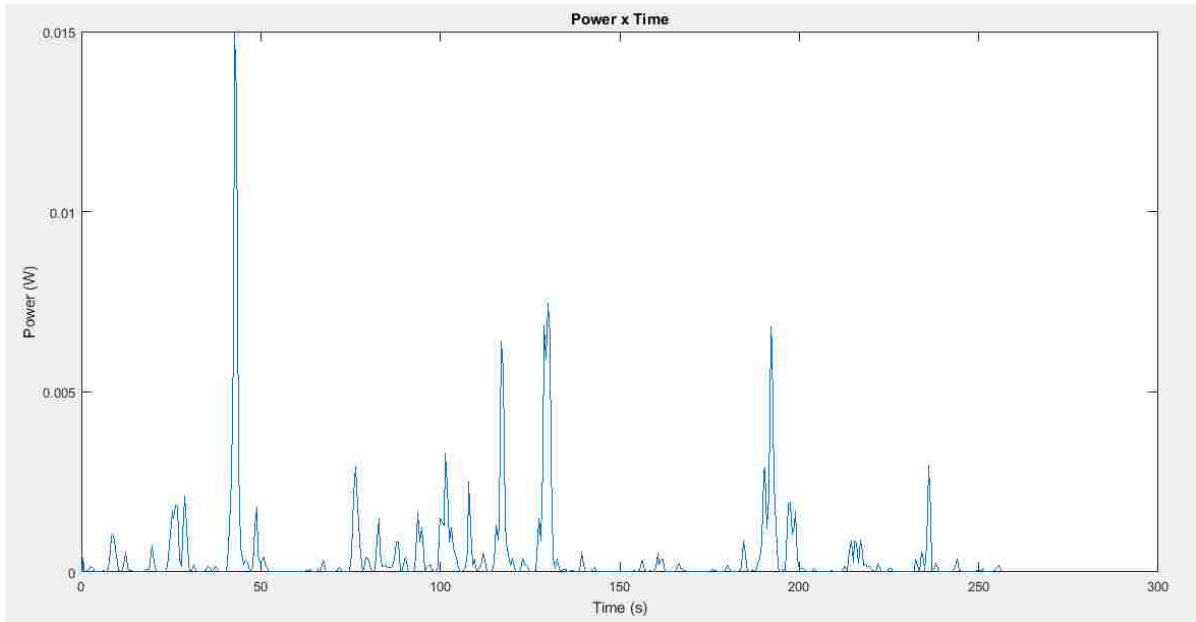
Figure 59: Time-history of power from the harvester device – one sample

Considering all 590 samples, the PDF of the power obtained from the harvester device

is plotted in Figure 60:
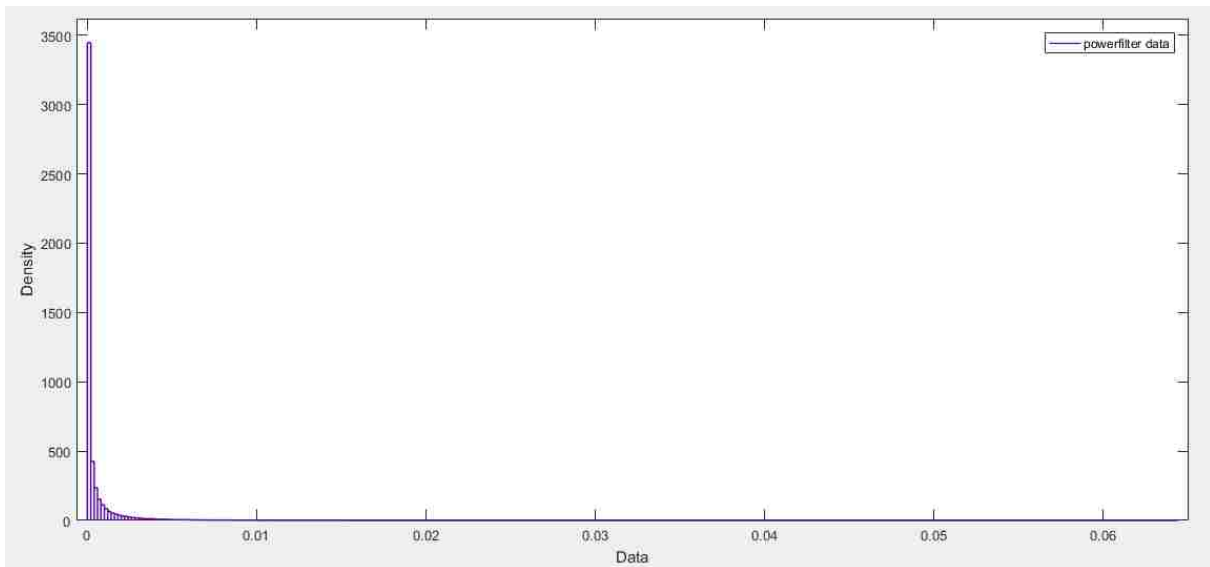
Figure 60: PDF of the power obtained from the harvester device

98

It can be seen in Figure 60 that the power does not present a typical Gaussian distribution behavior, therefore the Kernel Smoothing is not used here. Instead, the Matlab tool (dfittool) for distribution fit is used to produce this graph.

Figure 61 analyzes whether the general Weibull 3-parameter distribution is a good fit to represent the behavior of the variable Power.
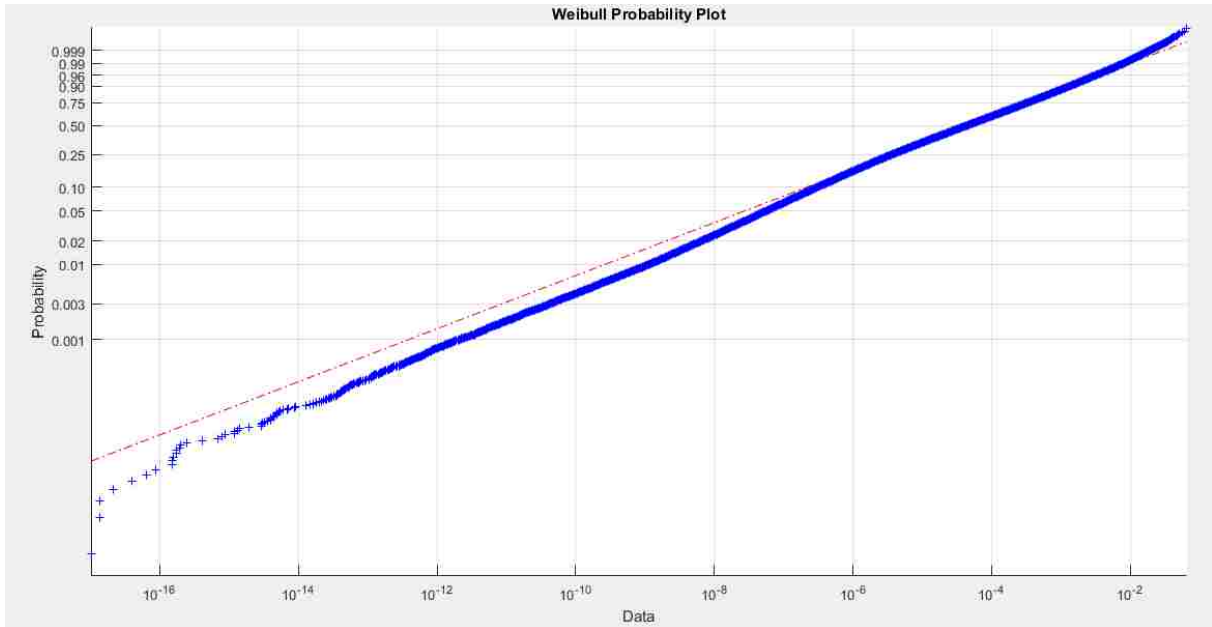
Figure 61: Verification of the data fit for Weibull distribution. Blue line is the data, red line is the normal distribution fit

Analyzing Figure 61, it seems clear that Weibull can be used to represent this data.

Applying equation 46 to the power values, energy values are obtained, which are the integration of the Power over time, from Equation 45:

$$E = P \, x \, t \tag{45}$$

99

Considering that, 590 values for energy are obtained with the time frame of 4.27 minutes.

For this scenario, the PDF of obtained energy values is plotted in Figure 62:
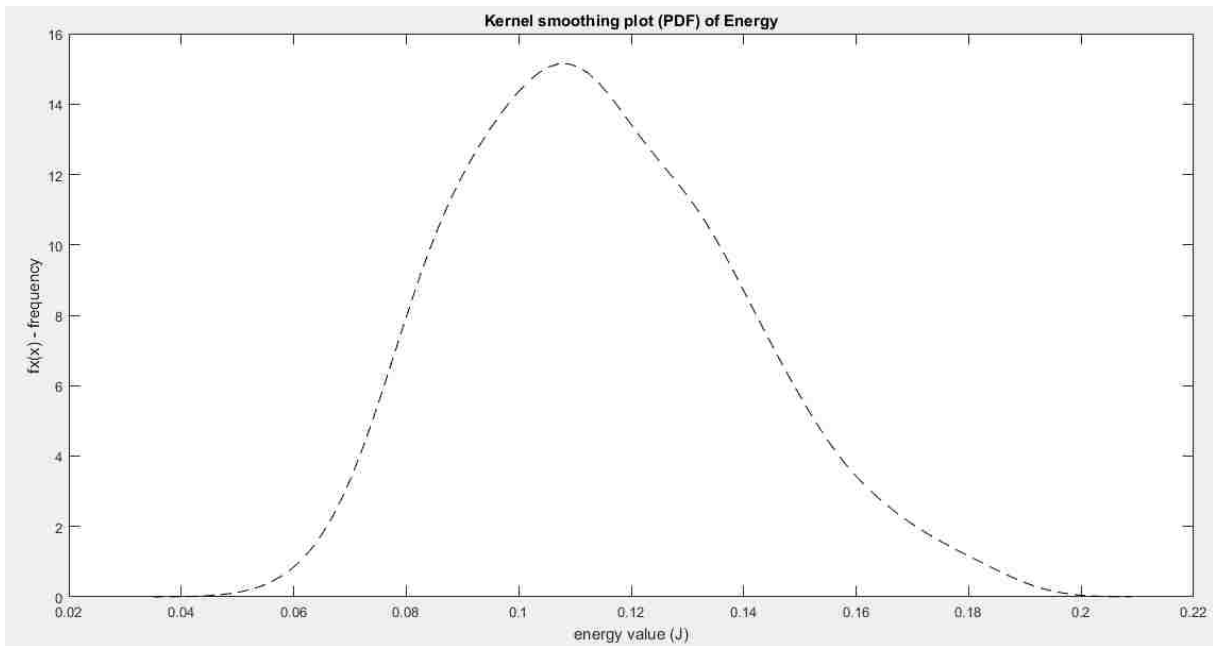
Figure 62: PDF of the energy obtained from the harvester device

Analyzing Figure 62, it can be seen that the mean of the electrical potential is approximately $0.115\,J$. Considering the excursion of the values, they vary from $0.04\,J$ and $0.2\,J$.

As an example of application of the energy obtained from the piezoelectric harvester device, Table 27 reproduces a table from [17], which presents the power and energy necessary to supply sensors available in the industry.

Table 27: Values of power and energy consumption of sensors (Reproduction from Table 1 on [17])

Operation	Commercial	Research
Microprocessor operation	350 µW (TI)	20 µW (Amirtharajah)
Receive 1 bit	200 nJ (Telos)	12 pJ (PicoRadio)
Transmit 1 bit	200 nJ (X-bow)	16 pJ (PicoRadio)
Retain volatile memory (VM) – 1 bit	100 pW (TI)	Replaced by NVM
Write 1 bit to NVM	200 nJ (Micron)	25 pJ (Cavendish)
Analogue-digital (A/D) conversion – 1 bit	2 nJ (TI)	50 pJ (PicoRadio)
Sleep	300 µW (TI)	50 nW (PicoRadio)
Digital signal processing	200 µW (LSI)	20 µW (Amirtharajah)
Pin leakage	100 nW (TI)	2.2 nW (Kao 2001)

Final statements

To finalize this work, in a few words the procedure can be summarized in the following order, if accomplished for a static load, for example: application of the load at a beam in Abaqus, extraction of the electrical potential at a few nodes, analysis of the nodes and physical properties of the beam which show larger electrical potential difference, computation of the voltage at these nodes, computation of the power at these nodes, computation of the energy at these nodes, connection to an electrical system for energy supply.

This research work has also led to other findings and observations, such as:

- The decision on use on reduced integration technique in Abaqus can lead to more flexible structure, which may help to obtain some better results, in this case

- The choice of the plate for the initial static design of the beam can be altered, so that the displacements showed could be larger and improve the total results.

- For the time history analysis of the Finite Element model, it was not trivial to obtain convergence of the results. This was adjusted with some detailed work and parameter sensitivity studies. For verification of errors of the analysis, modal analysis is very useful and practical. However, in this application it is not a good replacement for the implicit integration in, due to the longer processing time.

- In the plotting of the PDF of Electrical Potential and Electrical Energy the results shown are: Electrical Power for these load and design variates from $-3.2 \, x \, 10^{-5} \, V$ to $2.8 \, x \, 10^{-5} \, V$ and most of the probabilistic results are between $-1 \, x \, 10^{-5} \, V$ and $1 \, x \, 10^{-5} \, V$ and Electrical Energy for these load and design variates from $0.04 \, J$ to $0.2 \, J$.

102

Suggestions of Further work

As in any research work, the study of the topic treated in this thesis can be continued and improved. The following bullets list some of the suggestions for future approaches.

- Improvement of the design, adopting different dimensions, different beam materials, different direction or way that the wind load is applied

- Evaluation and comparison of the influence of different designs in the required outputs

- Evaluation of several devices working together in series/parallel for better efficiency in generating electrical energy

- Inclusion of the load receptor device in the design improvement and into the FEM analysis

- Consideration of more time for the load application than the 256 seconds

- Evaluation of the model in an experimental set up

- Experimental/FEM accurate evaluation the available power from this device, considering the obtained voltage

- Further study on the type of electrical system that the harvester can be connected to, including detailed design of the electrical system

- Study of a life-cycle economic viability for the device and system around it

- Study on the energy conversion efficiency

- Running 10000 samples, as predicted initially, for better theoretical characterization of the MCS process

Conclusion

The increasing energy demand increases the urgency to generate energy. An environmentally friendly solution is to harvest energy from natural vibrations of structures. This thesis assumes a single, two-layered piezoelectric device installed in a rubber host beam on a sample bridge structure subjected to wind load, considering the coupled problem involving random wind loads, structural vibration, electro-mechanics and energy collection.

A theoretical method is developed to assess the electrical energy generation from piezoelectric devices, showing that it is possible to evaluate piezoelectric harvesters using an approach based on the finite element method. The use of probabilistic values through Monte Carlo simulation considering a large set of wind load samples generated by spectral representation adds value to approach, by allowing to complete the analysis with the assessment of a probability density function of generated voltage and energy from the device.

Even though the values obtained for the electrical energy harvested are very small, they can be optimized and enhanced with a detailed design improvement on the plate, the piezoelectric layers and the host beam dimensions and materials, keeping the established methodology. This work can be reproduced for other characterization in different locations and therefore with different winds, by changing the parameters considered in the Kaimal Spectrum. Additionally, with the evolution of technology, new piezoceramic materials can be easily and practically adopted and evaluated by developed methodology.

References

1. Erturk, A. Inman, D. J. (2011) *Piezoelectric Energy Harvesting.* Hoboken, NJ, USA: Wiley
2. Wolfson, R. (2012) *Energy, Environment and Climate.* New York, NY, USA. :W. W. Norton & Company
3. Lu, F., Lee, H. P., & Lim, S. P. (2003). Modeling and analysis of micro piezoelectric power generators for micro-electromechanical-systems applications. Smart Materials and Structures, 13(1), 57.
4. Chen, S. M., Zhou, J. J., & Hu, J. H. (2014). Experimental study and finite element analysis for piezoelectric impact energy harvesting using a bent metal beam. International Journal of Applied Electromagnetics and Mechanics, 46(4), 895-904.
5. Karamlou, A., & Bocchini, P. (2016). Sequencing algorithm with multiple-input genetic operators: Application to disaster resilience. Engineering Structures, 117, 591-602.
6. Ali, S. F., Friswell, M., & Adhikari, S. (2011). Analysis of energy harvesters for highway bridges. *Journal of Intelligent Material Systems and Structures*, 1045389X11417650.
7. Research & Education Association (2015) *Basic Electricity.* Piscataway, NJ, USA: Research & Education Association
8. Weinstein, L. A., Cacan, M. R., So, P. M., & Wright, P. K. (2012). Vortex shedding induced energy harvesting from piezoelectric materials in heating, ventilation and air conditioning flows. *Smart Materials and Structures*, 21(4), 045003.
9. Xie, X. D., & Wang, Q. (2016). Design of a piezoelectric harvester fixed under the roof of a high-rise building. *Engineering Structures*, 117, 1-9.
10. Website http://hyperphysics.phy-astr.gsu.edu/hbase/Tables/rstiv.html
11. Simiu, E. Scanlan R.H. (1996) *Wind effects on structures.* New York, NY, USA :Wiley
12. Engineering Fundamentals, Inc. (www.efunda.com) (2016)
13. Ugural, A.C. Fenster, S.K. (2012) *Advanced mechanics of materials and applied elasticity* Westford, MA: Prentice Hall
14. Engineering Fundamentals, Inc (2016) http://www.efunda.com/materials/piezo/material_data/matdata_output.cfm?Material_ID=PZT-5A
15. Engineering Fundamentals, Inc (2016) http://www.efunda.com/materials/piezo/material_data/matdata_output.cfm?Material_ID=PZT-5H
16. ABAQUS (2014) 'ABAQUS Documentation', Dassault Systèmes, Providence, RI, USA.
17. Elvin, N. G., Lajnef, N., & Elvin, A. A. (2006). Feasibility of structural monitoring with vibration powered sensors. *Smart materials and structures*, 15(4), 977.
18. Bocchini, P. (2015). *Advanced Finite Element Method* [class notes/ word document]. Lehigh University, Bethlehem, PA, USA
19. Bocchini, P. (2015). *Random Vibrations* [class notes]. Lehigh University, Bethlehem, PA, USA
20. ASCE (2015) *ASCE Chapter 6 – Wind Loads – section 6.5.10*
21. Ang, A.H-S. Tang, W.H. (2007) *Probability concepts in Engineering.* Hoboken, NJ, USA :Wiley
22. De Jong, M., Chen, W., Geerlings, H., Asta, M., & Persson, K. A. (2015). A database to enable discovery and design of piezoelectric materials. *Scientific data*, 2.
23. Heinonen, E., Juuti, J., & Leppävuori, S. (2005). Characterization and modelling of 3D piezoelectric ceramic structures with ATILA software. Journal of the European Ceramic Society, 25(12), 2467-2470.

Curriculum vitae

Julia Tesser Tomasi was born in Porto Alegre, Brazil on October 25th, 1988 to Giancarlo Tomasi and Isabel Cristina Tesser Tomasi. She received a Bachelor degree in Civil Engineering at University of Brasilia (Unb), in Brasilia, Brazil, in 2011. During her undergrad program, she also studied Civil Engineer abroad for one semester in Czech Technical University (CVUT) in Prague, Czech Republic. She worked at Odebrecht Engineering and Construction as a Civil Engineer, in the areas of planning, budget and management of constructions, for residential, hotel and business center buildings, from 2011 to 2013. She also worked briefly in BubbleDeck, in the area of structural design before moving to the United States of America. She completes now a Masters of Science in Structural Engineering at Lehigh University, in Pennsylvania, where she attended from 2014 to 2016. During the summer of 2015 she interned at Thornton Tomasetti in the area of Forensic of structures in New York City.